THE UNIVERSITY OF WARWICK

Fundamental Understanding on The Use of Different Carbon Sources in The HIsarna Alternative Ironmaking Process

by

Darbaz Khasraw

A thesis submitted to the University of Warwick for the degree of Doctor of Philosophy

Warwick Manufacturing Group

Steels Processing Group

University of Warwick

December 2021

Contents .....

List of Figures

List of Tables

Acknowledgments

Throughout this research and writing of this thesis I have received a great deal of support and assistance from many people that I would like to give my sincere thanks for their enormous contribution.

Firstly, I would like to express my sincere gratitude to my advisor Dr. Zushu Li for the continuous support of my PhD study and related research, for his patience, motivation, and immense knowledge. Zushu continuously provided encouragement and was always willing and enthusiastic to assist throughout the research project. His guidance helped me in every part of the research and writing of this thesis. I could not have imagined having a better advisor and mentor for my PhD study. I would also like to extend my deepest gratitude to Dr. Stephen Spooner for sharing his expertise so willingly and for his support as my co supervisor for first three years of my project. I must also thank my other co supervisor Dr. Zhiming Yan for his interim supervision in the final year of my project.

Very special thanks to all HIsarna team, their participation and contribution are greatly appreciated. I am especially indebted to Dr. Hans Hage and my industrial supervisors, Ir. Koen Meijer, thank you very much for your valuable comments and suggestions.

I would also like to thank several other people who have assisted me with some of the practical aspects of this work, this including: Theint Theint Htet and Dr. Xinliang Yang from WMG Steels Processing Group for assisting with TGA and SEM use, Dr. Volkan Degirmenci from School of Engineering and Dr. Ben Breeze EPR & Diamond Group, University of Warwick for carrying out BET and Raman spectroscopy tests. I am also hugely appreciative to all my colleagues and friends at the University of Warwick, Michael Zhang, Dr. Hiren Kotadia, Akalya Raviraj, James Whiston, Dr. Ian Moore, Dr Carl Slater, Mir Hamza Khan, Sharhid Jabar, Keith Andrews, Bharath Bandi, Bharath Sampath Kumar, Stephen Hewitt, Tom Moore, and Dr Geoff West for always creating a great environment and for their continued support.

I would like to thank Tata Steel Nederland Technology BV for providing full PhD scholarship.

I must express my very profound gratitude to my parents Halawa Amin (Mum) and Khasraw Mohammed Amin (Dad) and further family and friends for providing me

with unfailing support and continuous encouragement throughout my years of study and through the process of researching and writing this thesis.

Finally, I have to thank my wife and love of my life, Begard Hamad. I am so grateful for all her support and love. This accomplishment would not have been possible without her support. The last word goes for Amez Khasraw, my baby girl, who has been the light of my life for the last three years and who has given me the extra strength and motivation to get things done. This thesis is dedicated to her.

Declaration

This thesis is submitted to the University of Warwick in support of my application for the degree of Doctor of Philosophy. It has been composed by myself and has not been submitted in any previous application for any degree. The work presented was carried out by the author.

Inclusion of Published Work:

1. Khasraw, D., Spooner, S., Hage, H., Meijer, K., and Li, Z., Devolatilisation characteristics of coal and biomass with respect to temperature and heating rate for HIsarna alternative ironmaking process. Fuel 2021; vol. 284 (July 2020). https://doi.org/10.1016/j.fuel.2020.119101
2. Khasraw, D., Spooner, S., Hage, H., Meijer, K., and Li, Z., Evaluation of devolatilization behaviour of different carbonaceous materials under rapid heating for the novel HIsarna ironmaking process, Fuel, vol. 292, (December 2020). https://doi.org/10.1016/j.fuel.2021.120329
3. Khasraw, D., Theint, T., Yang, X., Degirmenci, V., Hage, H., Meijer, K., and Li, Z., Gasification and structural behaviour of different carbon sources and resultant chars from rapid devolatilization for HIsarna alternative ironmaking process:, Fuel, vol. 309, (September 2021) https://doi.org/10.1016/j.fuel.2021.122210
4. D. Khasraw, H. Hage, K. Meijer, Z. Li, and A. Steel, “Fundamental understanding on the use of different carbon sources in the HIsarna alternative ironmaking process,” IIM ATM 2021, vol. 75th Annua, November 14-15, pp. 14–15, 2021.
5. Khasraw, D., Yan, Z., Hage, H., Meijer, K., and Li, Z., “Reduction of FeO in molten slag by solid carbonaceous materials for HIsarna alternative ironmaking process,” Metall. Mater. Trans. B, [Manuscript submitted for consideration], 1–29, 2021.

During the period of study this thesis was produced, the author also contributed to further findings:

1. Zhao, S., Li Z., Xu, R., Khasraw, D., Song, G., and Xu, D., “Dissolution Behavior of Different Inclusions in High Al Steel Reacted with Refining Slags,” Metals, vol. 11, no. 11, p. 1801, (November 2021). https://doi.org/10.3390/met11111801
2. Theint, T., Yan, Z., Khasraw, D., Hage, H., Meijer, K., Li, Z., “Kinetic study on reduction of FeO in a molten HIsarna slag by various solid carbon sources,” Metall. Mater. Trans. B, [Manuscript submitted for consideration], 1–19, 2022.

Abstract

Environmental problems such as air pollution and global warming have resulted in more stringent environmental legislations which challenges major industries to reduce carbon dioxide emissions. The most recent approach by the steel industries to address the climate challenges is the Net-Zero Steel strategy which has been initiated as a roadmap to eliminate the emissions of greenhouse gases by 2050. In 2004, the (Ultra-Low CO_2 Steelmaking) ULCOS research program lunched by major European steelmakers shortlisted HIsarna process as one of the most promising technologies to reduce CO_2 emissions from steel industry. This research conducted with the aims to provide fundamental understanding on the behaviours of renewable biomass in the HIsarna SRV and support HIsarna development in optimising carbon source selection.

Initially the slow devolatilization experiments were performed to compare coals (with low to high volatile matter content) with two biomass samples sourced from wood and grass. The results show that similar types of volatiles components were produced for all the carbonaceous materials, however the wt% of reducing gases e.g., H_2, CO, and hydrocarbons, and the temperature required for these gases to evolve were notably different. Furthermore, the off-gas analysis reveals that torrefied grass contains large amount of H_2O and CO_2 which are released at low temperatures, therefore pre-treatment to the temperature of ~ 400 °C is necessary for this material to be utilised effectively.

The study then progresses into the thermal conditions similar to HIsarna SRV using drop-tube furnace with quadrupole mass spectrometer (DTF-QMS). It was found that the gas species detected were similar for coal and biomass samples but char oxidation for charcoal (CC) was significantly faster. Despite high fixed carbon and low VM content, the weight loss (under rapid devolatilization) for charcoal (29%) was higher than that for thermal coal (23%) and Bana grass char (22%) at 1500 °C, which could lead to low solid char yield during CC injection. Furthermore, the CC char has the fastest CO_2 gasification reaction, this behaviour is likely to be governed by combination of low ash content, ash composition and char morphology in the CC material compared to thermal coal (TC) and Bana grass char (BGC).

Reactions between carbonaceous materials and molten slag under simulated HIsarna thermal conditions were carried out by injecting different carbonaceous materials (CC,

TC and BGC) into molten synthetic HIsarna slag in laboratory. The results show that the reduction process proceeds through two stages, starting with an initial rapid reduction and followed by gradual levelling off until the end of the process. The reaction rate and reduction degree of FeO in molten slag were the highest with CC chars, achieving over 60 % reduction at 1500 °C in the first 500s, compared to only ~50 % and just over 40 % with TC and BGC chars respectively for the same reaction time. The kinetic analysis suggests that the first stage reaction is controlled by chemical reactions at the carbon-slag interface, and the apparent activation energy values were 290, 229 and 267 kJ/mol for reactions with TC, CC and BGC chars respectively. On the other hand, the second stage can be described by three-dimensional diffusion model (D3) and mixed influence from gas diffusion, liquid phase mass transfer, chemical reaction and carbon diffusion is likely to control the reduction.

The results show that there are some common characteristics between coals and biomass materials selected, but the overall behaviour was different. Charcoal showed to have much higher combustibility and reactivity among the tested materials. The higher reactivity for charcoal may result in some of the solid chars to burn prematurely during HIsarna injection and this could lead to generation of higher amount of CO for CCF section on the expense of the solid chars required for SRV. Therefore, to maintain the process efficiency during CC injection it is necessary to increase the CCF productivity to utilise the extra reductive gas proportion produced to improve the balance between devolatilization/gasification and solid char yield. To build on the current findings and for efficient use of biomass or other alternative fuels, further research is suggested to consider biomass/coal blending, continuation of slag/carbon reaction (e.g., quenching), molten metal carburisation, slag chemical composition (e.g., different FeO content), effect of impurities in the raw materials and the ash content and ash chemistry.

List of Abbreviations

BET	Brunauer-Emmett-Teller
BF	Blast Furnace
BG	Bana grass
BGC	Bana grass char
BOF	Basic Oxygen Furnace
BOS	Basic Oxygen Steelmaking
CAPEX	Capital expenditure
CC	Charcoal
CCF	Cyclone Converter Furnace
CCS	Carbon Capture & Storage
CY	Char yield
DAF	Dry ash free
DB	Dry basis
DRI	Direct Reduced Iron
DTF	Drop tube furnace
DTG	Differential thermal gravimetric
EAF	Electric Arc Furnace
EU	European Union
GF	Gas furnace
HT-CSLM	High Temperature Confocal Scanning Laser Microscopy
HTF	Horizontal Tube Furnace
OHF	Open Hearth Furnace
OPEX	Operating expenditure
PCI	Pulverized coal injection
QGA	Quantitative Gas Analyser

QMS	Quadrupole Mass Spectroscopy
SCS	Single chamber system
SE	Secondary electrons
SEM	Scanning Electron Microscope
SR	Swelling ratio
SRV	Smelting Reduction Vessel
TC	Thermal coal
TBG	Torrefied Bana grass
TGA	Thermogravimetric analysis
TGR-BF	Top gas recycling blast furnace
ULCOS	Ultra low CO_2 steelmaking
VTF	Vertical tube furnace
WDXRF	Wavelength Dispersive X-Ray Fluorescence
wt%	Percentage by weight

Chapter 1

Introduction:

Steel is the most fundamental engineering and construction material in the world. In 2019 approximately 1.9 billion tonnes of crude steel were produced globally, with almost 12% increase in the steel production since 2014. Despite alternative materials and a widening product landscape, sectors such as buildings and infrastructure, oil and gas, automotive and whitegoods are still heavily reliant on the capacity and quality of output from the current steel industries. Buildings and infrastructure accounts for more than half of the steel globally produced and with the rapid increase of world's population the demand is expected to continue to grow worldwide in years to come [1].

The blast furnace-basic oxygen furnace (BF-BOF integrated) and the electric arc furnace (EAF mini-mill) are the two dominant process routes used in steel production. These two technologies combined produced more than 99% of crude steel in 2019, 71.9% of which was by the BF-BOF integrated route and 27.7 % by the EAF route [2]. The key difference between the two main routes (BF-BOF and EAF) is the type of raw materials consumed, as described in Figure 1.1 (the main steelmaking routs with row materials used). The BF-BOF route produces steel using iron ore, coking coal, and recycled steel, while the main raw material in the EAF route is recycled steel and direct reduced iron (DRI) or hot metal and electricity is the main source of energy. The direct reduced iron (DRI) is produced using natural gas/shale gas/coal and iron ore, but this requires capital investment and plant modification. Raw material availability plays a major part in choosing the predominant steelmaking route from one country to another e.g., low natural gas prices and shale gas availability in North America and the Middle East result in the EAF based steelmaking being the dominate route in those regions, whereas in Europe and China the BF-BOF is the main steelmaking route, e.g., the BF-BOF route counts for more than 90% of crude steel production in China [3-6].

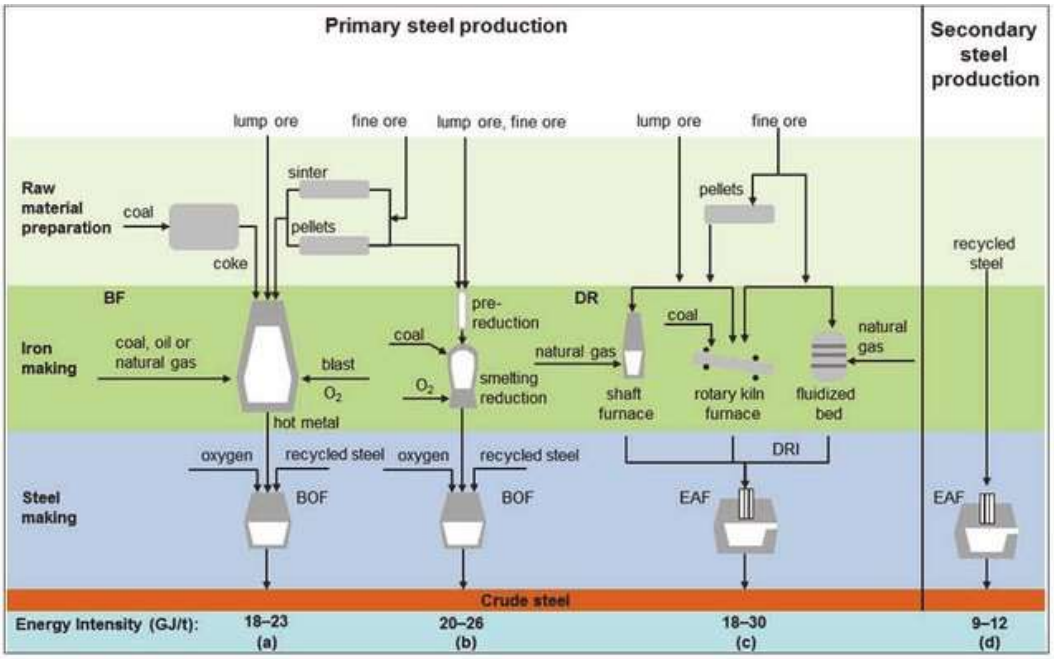

Figure 1.1: The main iron and steel production routes [7].

Lately environmental issues such as air pollution and global warming are taken on more seriously around the globe. Stringent environmental legislations such as a reduction target of between 80-95% carbon dioxide (CO_2) emissions compared to the 1990 baseline, have forced major industries into an age of innovation and refinement [8]. The iron and steelmaking is an energy intensive process which consumes about 8% of global energy and this sector is responsible for 7% global CO_2 emissions [3, 9]. Despite substantial improvements concerning environmental performance, e.g., around a 50% reduction in CO_2 since 1990, it is believed a true step change in steel manufacturing technology is required. The sintering, coke making and BF ironmaking in the BF-BOF route contributes to approximately 90% of the CO_2 output from the BF-BOF steel plant [3, 10]. Therefore, significant efforts are now being placed into alternative ironmaking technologies which promise the possibility to remove coke making, sintering and BF ironmaking. In addition, the potential of cleaner off-gas suitable for carbon capture and storage (CCS) or the possibility to be used as synthetic gas in secondary manufacturing processes presents opportunities to reduce emissions further.

In 2004 major European steelmakers launched the Ultra-Low CO_2 Steelmaking (ULCOS) research program to reduce CO_2 emissions from steel production. The program evaluated the feasibilities of about 80 different steelmaking routes in terms

of energy consumption, CO_2 emission, operation costs and sustainability. ULCOS shortlisted four routes for further investigation (laboratory and pilot scale) and commercialisation. The four main technologies identified for further research are [11-13]:

- Top gas recycling blast furnace (TGR-BF), which is expected to achieve 50% CO_2 reduction with use of CCS.
- A smelting reduction process (HIsarna technology), 20% reduction without CCS and up to 80% CO_2 reduction with CCS compared to BF.
- ULCORED with CCS, this advanced direct reduction process to achieve 55% CO_2 reduction.
- Electrolysis (ULCOWIN & ULCOLYSIS), no carbon is needed for this process.

Among the four techniques identified, HIsarna presented significant promise due to its ability for high CO_2 reduction potential, as a result it has had a widespread interest. Early HIsarna trials indicated more than 50% of CO_2 reductions can be achieved without the use of CCS technology by partially replacing coal with biomass and using scrap as part of the metallic charge [14-15]. Although, up to now the trial campaigns have been successful, there is a lack of fundamental knowledge and understanding of the mechanisms involved in the new technology. Therefore, to accelerate the development of the process, understanding of the fundamental reaction mechanisms involved are necessary.

1.1 Objectives of this Study

The main aim of this research is to explore alternative carbon sources such as renewable biomass in the HIsarna process compared to semi-anthracitic coals currently being injected as a source of energy and reductant. This study will provide fundamental knowledge for an in-depth understanding of slag-carbon reactions for different carbonaceous materials. The knowledge generated in this study will support the development of the HIsarna technology with a hope of opening the gates to the use of renewable carbon sources such as biomass.

This is achieved by investigating in comparison thermal coals that are currently used in HIsarna trials and biomass samples with various properties such as volatile matter, ash and moisture contents, and char reactivity. Using specifically designed modern

experimental techniques, the carbonaceous samples are reacted with a HIsarna type of synthetic slag to reveal the reaction kinetics for the slag-carbon reactions in the gas-slag-metal system at high temperatures using high temperature drop tube furnace. The kinetic mechanism for reduction of iron oxide provides knowledge aimed at answering the research questions and intends to obtain critical information required for understanding the process insights to support the upscaling of the promising technology.

1.2 Thesis Structure

The thesis will lead with an abstract summarising the content and key findings from the project. For easy reading the thesis is separated into 9 chapters, including introduction/background chapter to build the research landscape, experimental methods, results chapters focusing on specific findings, and conclusions and outlook. The chapters are described as follows:

Chapter 1 Introduction

This chapter gives a brief introduction on the background and status of iron and steelmaking processes, also the objectives of this study are covered.

Chapter 2 Technical background

This chapter contains the background of ironmaking technologies within the steelmaking process, concerning the environmental and economic challenges that this sector faces. This includes integral steel plant, alternative ironmaking technologies, an in-depth discussion of the HIsarna process and recent developments, relevant studies on the carbon sources used in the ironmaking processes, and the FeO reduction kinetics study in the slag-carbon reaction process.

Chapter 3 Research objectives and hypothesis

The aims of the project are formalised in this chapter with a clear focus as to why each activity has been undertaken. The research hypotheses are identified, and each hypothesis is followed by the method of investigation.

Chapter 4 Experimental Methods

All the experimental equipment as well as materials selected for each experiment are introduced and briefly described in this chapter. More in-depth experimental

procedures and methodology for material preparation are described in the relevant result chapters.

Then four result chapters (Chapter 5 to Chapter 8) follow, which are coherent and interconnected, and each chapter consists of a layout similar to academic journals, with their own introduction, experimental, results and discussions section.

Chapter 5 Devolatilization characteristics of coal and biomass with respect to temperature and heating rate for HIsarna alternative ironmaking process. Four coal samples are investigated containing different levels of volatile matter (VM), i.e., low, medium, and high, compared to biomass samples from two different sources charcoal (wood based) and torrefied Bana grass (grass based). This studies the raw material background with non-isothermal methods and specifies pre-treatment required for selected biomasses to produce chars with similar properties to coals injected in HIsarna.

Chapter 6 Evaluation of devolatilization behaviour of different carbonaceous materials under rapid heating for the novel HIsarna ironmaking process. The evolution of volatile matters, gaseous products, and char conversion for selected materials are evaluated under thermal conditions similar to HIsarna, to obtain accurate information about volatile and char yield for each material to help maintain HIsarna process efficiency during coal replacement.

Chapter 7 Gasification and structural behaviour of different carbon sources and the resultant chars from rapid devolatilization for HIsarna alternative ironmaking process. In this chapter the physical structure of chars produced from coal and biomass samples are examined using analytical and morphological methods to predict the char behaviour in the gas-slag-metal system.

Chapter 8 Reduction of FeO in molten slag by solid carbonaceous materials for HIsarna alternative ironmaking process. Finally, the reduction reaction for a synthetic FeO-containing slag (similar to HIsarna slag) with chars produced from coal and biomass samples are compared to understand the FeO reduction mechanism and evaluate the kinetic parameter for each reaction.

Chapter 9 Conclusions and suggested further study

In this chapter the main findings of the thesis are summarised and restated, to draw together the conclusions of all results chapters. The recommendations, possible impact

of the findings on industrial practice and suggestions for further work are made based on this conduction to provide greater understanding of this novel ironmaking process.

Chapter 2

Technical background

2.1 A brief history of iron and steelmaking

The history of iron and steel production can be tracked back by several thousands of years [16]. Prior to the 19th century only small quantities were produced, but development of Bessemer process in the 1850s resulted in the mass production of steel [17]. In the last century steel processing has undergone many important changes including developments of basic oxygen steelmaking and continuous casting processes in the early 1950s, which are considered as the most innovative technologies in the history of the steel industry. The integrated steel plants (i.e. the blast furnace ironmaking – basic oxygen steelmaking plants) have many advantages such as high productivity, low production cost and the ability to produce a wide variety of high quality steel products [18]. However, these integrated plants require high capital costs with complex configurations and are constructed across over large land with a limited flexibility and other disadvantages including environmental impacts from the use of fossil fuels.

Due to environmental concerns strict legislations were put in place by many governments in 1980s, as a result, major global steel manufacturers together with research institutes have launched various research programmes to address the disadvantages of the integrated steel mills. The focus has been placed on improving current technologies and developing new technologies to replace the existing BF (blast furnace ironmaking) process. As the demand for steel increases the global regulations on air pollution becomes stricter, this will force the global steel companies to reduce greenhouse gas emissions. To adjust to these changes a major restructuring of steel production facilities is required. As a result, new innovative ironmaking technologies are expected to be commercialised which are environment-friendly and have ability to use low-grade raw materials and alternative fuels [18].

Despite the recent progress made to address the climate crisis, the extreme changes to the weather conditions forced the steel industries to take more drastic action. Most recently the Net-Zero Steel has been initiated as a roadmap to eliminate the emissions of greenhouse gases by 2050 [19]. Through this strategy the balances between the carbon produced into the atmosphere, and the carbon removed from it achieved. In

2019 United Kingdom as the first major economy passed on legislation that commits the country to net zero emissions, and then consequently the global research and development in net zero steel manufacturing.

2.2 Ironmaking technologies

Metallic iron is produced by removing oxygen and other impurities from iron ore. There are several commercialised processes available, however the BF has been the most dominant route for a very long time. Because of environmental pressure, shortage in premiere raw materials and increase in demand, several new technologies have been developed to provide improvements required.

2.2.1 Raw material preparation for blast furnace

2.2.1.1 Coke making

Metallurgical coke is a solid fuel with a high strength made by heating coal to the temperature of up to 1200 °C in the absence of oxygen. This causes volatile components to be driven off while avoiding combustion resulting in the formation of a material with a high fixed carbon content. There have been several approaches at the different development stages in coke manufacturing. Process technologies such as the non-recovery coke oven, single and multi-chamber systems have been developed in the last century to provide sustainable metallurgical coke production. To start the process the oven sidewalls are heated to between 1200–1300°C and a uniform temperature is maintained, then coal blend crushed to particle size < 3mm are discharged into the oven by gravity [20]. Figure 2.1 below shows the coke making process using a single chamber system (SCS).

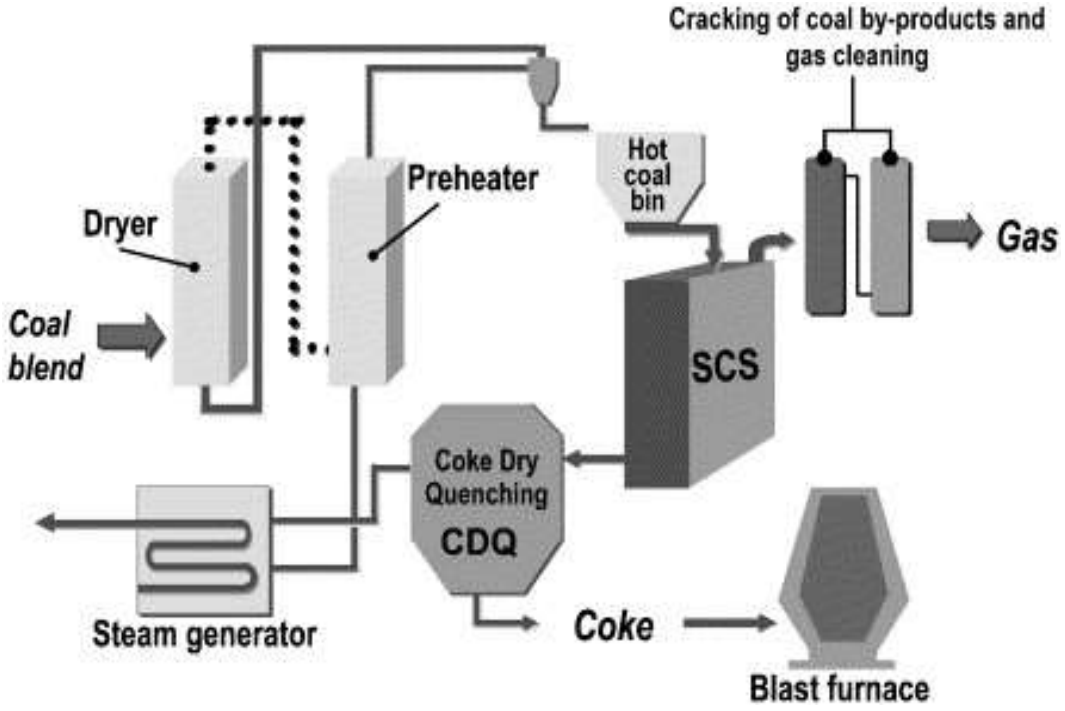

Figure 2.1: Flow diagram of coke-making through single chamber system (SCS) [20].

As the coal enters the oven, it starts to be heated due to contact with the sidewalls, the heat gradually permeates through the coal to reach the oven centre and ensures the coals are relatively evenly heated. Once the temperature of the centre reaches about 900–1000 °C the coking cycle is complete, and the coke is then discharged as a final product. This process requires a total time of around 18-20 hours [20].

Ironmaking uses about 90% of the total coke consumed in the integrated steelmaking process to maintain the productivity and for optimum reducing condition. The coke in the blast furnace has three major roles, firstly it acts as a fuel to provide heat required for chemical reactions, as well as slag and metal melting. Secondly it acts as a reducing agent by providing carbon for direct reduction and production of CO at a high temperature for FeO indirect reduction. The third and final role is to support the blast furnace burden to provide a permeable matrix for gaseous and molten products to pass through concurrently [20].

Despite all the technical advantages of coke in the BF, issues including coke shortage, high costs and high CO_2 emissions present a real problem for its use. To reduce the use of coke, supporting agents such as oil, natural gas, and pulverised coal (PC) are injected at the tuyeres at a high velocity to provide energy and act as a reductant in the blast furnace [3]. Pulverised coal injection (PCI) is the most used auxiliary fuel as it

can achieve a high injection rate to reduce the amount of coke used in the BF. Natural gas is another reducing agent that can achieve a high injection rate and is often used in the countries where natural gas is inexpensive and abundant. However, in the current BF processes use of coke is still mandatory because of the burden support function and current available materials cannot fulfil the role to fully replace it [3].

2.2.1.2 Fine ore preparation

Iron-bearing material consumed in blast furnace process is typically in form of sintered ore, lump ore, and or pellets. The fine ores are produced in a way to maintain permeability in the blast furnace and provide continuous iron ore reduction to produce reliable liquid iron for tapping [21].

2.2.1.3 Sinter ore

Sintering is the conversion process of iron ore fines into larger particles by incipient fusion to improve the ore charging. The process starts with a fixed proportion of iron ore, lime ($CaCO_3$, CaO) fluxes and coke breeze blended to form the sinter. The coke breeze and lime added through sinter can provides the permeability to the BF and increase the productivity [22].

2.2.1.4 Lump ore

Lump ore is produced directly from the mines by crushing and then screening. Lump ores usually have poorer properties, but they are cheaper raw material as the processing costs are significantly lower than sinters.

2.2.1.5 Pellets

Pellets are produced using fine iron ore with a small amount of coke breeze. The processing consists of four distinct stages (agglomerating, drying, firing, and cooling). The process starts by adding water to enable the fines to adhere to each other, followed by drying at a temperature of 300-350 °C to remove water. Then the fines are fused in the induration reaction at the temperature of 1250-1350 °C and followed by a final stage of slow cooling. Heat from stage 3 (firing) is recycled for the drying and subsequent batch firing to improve efficiency recycle [21].

2.2.2 Blast furnace ironmaking

A conventional BF is a counter current reactor which consumes iron ore in the form of sinters, lump ore and or pellets to produce liquid iron [23]. The furnace has a conical shape, and it consists of five sections as shown in Figure 2.2.

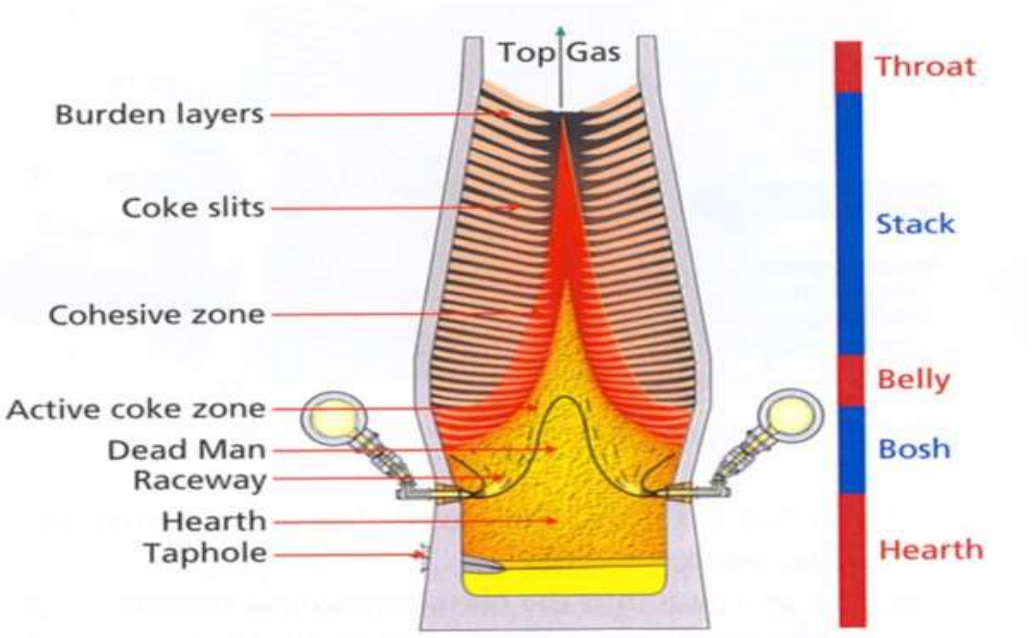

Figure 2.2: BF zones showing the layer structure of coke and ore from top downward [23].

The process starts with a charge of raw materials including pre-prepared ores, metallurgical coke and flux materials (limestone or dolomite) from the top of the furnace by either a double bell or a bell-less system distributer to spread the raw materials evenly [21]. The process heats up by blowing pre-heated air, or 'hot blast' into the furnace at temperature of 1200 °C through a series of nozzles called tuyeres. The hot blast burns auxiliary fuels such as pulverised coal (PC), natural gas or other fuels injected into the furnace through tuyeres. The auxiliary fuels are added to reduce the use of expensive coke, and their main role is to provide energy and act as a reductant for FeO. The moisture and oxides present in the BF react with the coke and auxiliary fuels to form carbon monoxide which moves upward and acts as a reductant to iron ore added from the top. The flame temperature of ascending gases are between 2000-2300 °C, which is able to melt iron ore [23].

The BF consists of alternating layers of iron ore and coke (Figure 2.2), they provide support and permeability to allow hot gases to ascend and solid/liquid materials to descend. The hot blast consumes coke and iron ore constantly to create space within

furnace for more raw materials to be added. The iron is mostly found in the form of hematite (Fe_2O_3) or magnetite (Fe_3O_4) in the ore, which goes through a series of chemical and physical changes while moving down to the hearth [24]. The main reaction of iron oxide is with reducing agents such as CO, H_2 and coke particles to remove oxygen atoms and form hot metal. Coke particles can remove about a third of the oxygen from the burden in a direct reduction equation (1) and the remaining oxygen is removed by a gas reduction (indirect reduction, equation (2)) [21]. As the hot reducing gases move upward from lower furnace, the heat is transferred to the ore burden. Then the ore burden starts softening, to the extent that it becomes molten in cohesive zone. Equations (1) to (3) are the main reactions occurring in the process: (1) is an overall FeO reduction by solid carbon/carburized iron and (2) and (3) are intermediate/alternative steps [22, 24].

$$FeO_{(l)} + [Fe–C_{(l)} \,/\, C_{(s)}] \rightarrow Fe_{(l)} + CO_{(g)} \quad (1)$$

$$CO_{(g)} + FeO_{(l)} \rightarrow Fe_{(l)} + CO_{2\,(g)} \quad (2)$$

$$CO_{2\,(g)} + C_{(s)} \rightarrow 2CO_{(g)} \quad (3)$$

The temperature of ascending gases will decrease gradually due to lose of heat to the coke and burden in the top part of the furnace. However, reduction of hematite (Fe_2O_3) to magnetite (Fe_3O_4) starts at temperature around 500 °C, and it is further reduced from magnetite (Fe_3O_4) to Wustite (FeO) in the lower zones where temperature ranges from 600 to 900 °C, but reduction of Wustite (FeO) to hot metal starts in the zones where temperature ranges from 900 to 1150 °C. The final product of pig iron is then tapped from the furnace hearth at the temperature between 1480 to 1520 °C for further processing. Equations (4) to (6) illustrate gas reduction reactions of iron oxides in the BF:

$$3Fe_2O_3 + CO \rightarrow 2Fe_3O_4 + CO_2 \quad (4)$$

$$Fe_3O_4 + CO \rightarrow 3FeO + CO_2 \quad (5)$$

$$FeO + CO \rightarrow Fe + CO_2 \quad (6)$$

2.2.3 Alternative ironmaking processes

Alternative ironmaking represents all the ironmaking routes other than the BF; this includes the processes using coal, natural gas, biomass, and hydrogen to produce solid and liquid iron. Smelting and direct reduction are seen as keyways to improve

ironmaking as they are able to use a wider range of raw materials to cut carbon emission and costs. The following smelting technologies show a great potential to replace or limit the reliance of steel industries on the BF.

2.2.3.1 HIsarna® Technology

HIsarna represents a new route of smelting reduction process. It has been developed by combining two well-known technologies, the cyclone converter furnace (CCF) and the smelting reduction vessel (SRV), into a single highly integrated smelting furnace [8, 25]. The process is a result of the European ULCOS program, to find an innovative solution to reducing CO_2 emission in steel manufacturing. The pilot plant located at Tata Steel in IJmuiden, the Netherlands was constructed in 2010 with a capacity of 60,000 t hot metal/year. The process is flexible in raw materials, which can utilize low-cost thermal coal instead of coking coal, low-quality iron ore, and complex iron ore (e.g., titanomagnetite). By removing the sintering and blast furnace (BF) ironmaking steps, it reduces energy usage and CO_2 emissions compared to traditional BF process [26, 27]. There have been many attempts to substitute coking coal and thermal coal (e.g., pulverised coal injection) with renewable biomass and natural gas in the BF, to reduce the environmental impacts and help improve sustainability. However, the necessity for burden support by coke has set limitations on using renewable biomass in the BF, which is not required in the HIsarna process. The flexibility that HIsarna process poses creates the potential to substitute current thermal coal with low dense, low strength but environmentally friendly biomass and still maintain the process efficiency and productivity [29]. The main advantages of HIsarna technology in comparison to the traditional blast furnace ironmaking are [14, 25]:

- Reduced OPEX and CAPEX (30%) compared to the greenfield BF
- Clean off-gases make it more suitable for carbon capture, usage, and storage (CCUS)
- High energy efficiency leading to 20% less energy consumed
- CO_2 emissions cut by up to 50% without CCS (proved by trials), and 80% with CCUS
- Flexible with raw materials, as it can operate with low-cost coal and low-grade iron ores

- Elimination of coke-making and agglomeration plants help reducing costs and NO_x, SO_x, dust and CO_2 emissions
- High quality hot metal with low silicon, manganese, phosphorous and titanium impurities

Since the construction of the HIsarna pilot plant several successful trial campaigns have been conducted. The first four campaigns focused on technical feasibility of the process, production rate to achieve the design capacity of 8 thm/h, demonstration of raw materials flexibility, ability to use scrap steel, dusts and sludges that are by-products of other processes, and supplying the first hot metal to the BOF plant [14]. Then in the follow-up campaigns the process potential for CO_2 reduction and long runs with stable production were demonstrated. The pilot plant underwent a major upgrade between 2014 and 2017, which resulted in the change or major upgrade to large sections of the existing plant, while the raw material handling and the preparation area were built on the HIsarna site. During 2018 trials were conducted to partially replacing coal injection with sustainable biomass, and metallic charge with the scrap steel to achieve further CO_2 emission reductions without use of CCS [14]. These trials were granted as part of the European Union's Horizon 2020 program (H2020) to demonstrate the capability of the HIsarna technology to achieve at least 35% reduction in CO_2 emission compared to the conventional BF-BOF route [30]. These trials showed that it was possible to replace up to 42% of injected coal with renewable carbon, while between 35% to 37% of the hot metal produced was from scrap steel. As shown in Fig. 2.3, the CO_2 emission can be reduced by further 55% if partial use of renewable carbon is combined with the scrap charging. However, the results showed the process was less efficient when biomass was injected as partial replacement for thermal coal at low production rate without scrap charging, achieving about 30% reduction of the CO_2 emission, despite 45% carbon replacement with renewable biomass. This suggests that the reduction mechanism was greatly affected by coal replacement with biomass, which resulted in a less efficient process [14]

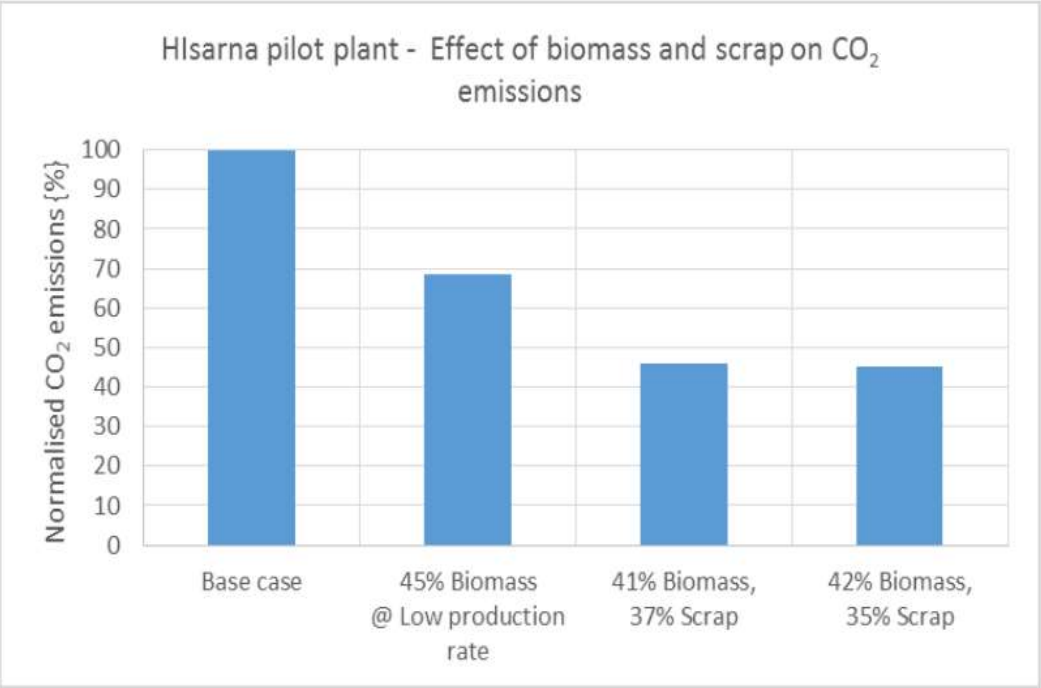

Figure 2.3: Effect of combined use of biomass and scrap on the specific CO_2 emissions of the HIsarna process [14].

The HIsarna process starts with raw materials (i.e., iron ore and fluxing agents) and oxygen injected into the CCF, where CO rich off-gas evolved from SRV is burned and reacts with the iron ore. It is not possible to measure the exact temperature of cyclone gases, but using the heat balance modelling the temperature range is predicted to bebetween 1400 - 2000 °C, at which the iron ore melts and is partially reduced by up to 20 % [30, 31]. The gas temperature is expected to be very high where the combustion takes place in lower section of CCF, but it will gradually decrease as the gases moving upward and contact with the charging materials. The molten iron ore forms a liquid film along the cyclone wall and falls under gravity into the slag layer in the SRV where the temperature is between 1400-1500 °C. The granular thermal coal (or other carbonaceous materials) is injected into the slag layer in the SRV bath using nitrogen as a carrier to reduce iron oxide in the slag to liquid metal and carburise the hot metal bath [14]. This injection process causes an intense metal-slag mixing and creates a large amount of splash of both metal and slag that circulates through the upper section of the vessel as droplets, where oxygen is introduced to generate heat by combustion of the upward gas stream. These droplets create a large metal-slag interfacial area and transfer heat from the post combustion zone to the slag bath to maintain the temperature of the slag and metal. Coal temperature is critical to the

process as the bath runs at 1400-1500 °C, to maintain the temperature injected coals are preheated. Impurities are present at very low level in the pig iron as most of the phosphorous and titanium are rejected to slag phase, as a comparatively more basic and oxidising ironmaking slag is formed [28, 32]. Fig. 2.4 shows the combination of the CCF and the SRV to form HIsarna.

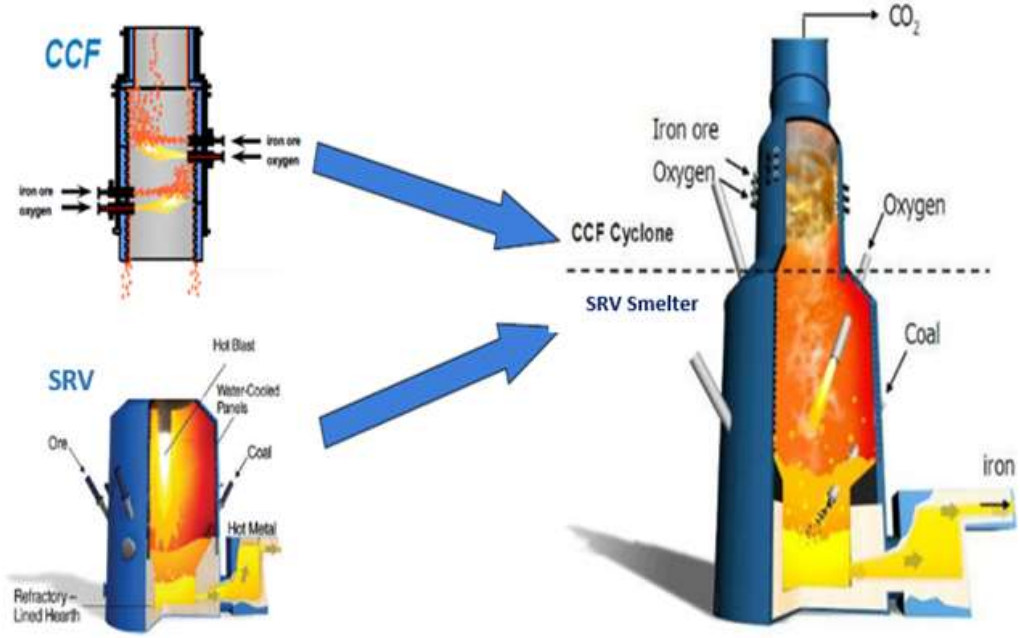

Figure 2.4: A schematic of HIsarna technology combines cyclone converter furnace and smelting reduction vessel [34].

Molten ore drops down into the SRV from the CCF and dissolves in the slag bath containing 5-6% FeO, while injected coal creates a large slag/metal interface for smelting. The FeO-containing slag reacts with the injected coal and creates a significant amount of CO. This reaction is endothermic, so a large amount of heat is required to maintain reaction temperature. Liberated CO along with carrier gases and volatile matter removed from coal provide a hot gas stream moving upward, this along with ejected metal (due to coal injection) and slag creates large amount of splashing through the upper section of the vessel. This results in significant numbers of Fe-C droplets creating a large liquid metal interfacial area which transfer heat from the post combustion zone to the slag bath and reduce dissolved iron oxides in slag [33].

2.2.3.2 COREX®

COREX is the first industrially and commercially proven smelting process that allows hot metal to be produced directly from metallurgical coal and iron ore. COREX consists of two main parts, the melter-gasifier and the reduction shaft furnace which is a counter-current reactor mounted above the melter-gasifier (Figure 2.5). Lump ore or pellets along with fluxes, namely limestone and dolomite, are directly charged into the shaft furnace, also small amount of coke is added to avoid clustering. The iron bearings are reduced to over 70-90% in the shaft by reducing gases, this is known as Direct Reduced Iron (DRI). Using a feeding screw system, DRI and fluxes are discharged into the melter-gasifier at the temperature around 700-800 °C, where more coal and coke is added to maintain the process and melt DRI. The rate of FeO reduction in the shaft depends on the amount of gas flow injected, temperature of the gas, and reducibility and particle sizes of iron bearings [35]. Oxygen is continuously injected via tuyeres to maintain the process temperature and generate CO which acts as reducing gas in the reduction shaft. Finally, the hot metal and excess slag are tapped from the hearth zone [8]. Moreover, the performance of the melter-gasifier depends on the CO_2 present in reduction gas, oxygen distribution, char bed permeability and system pressure [35].

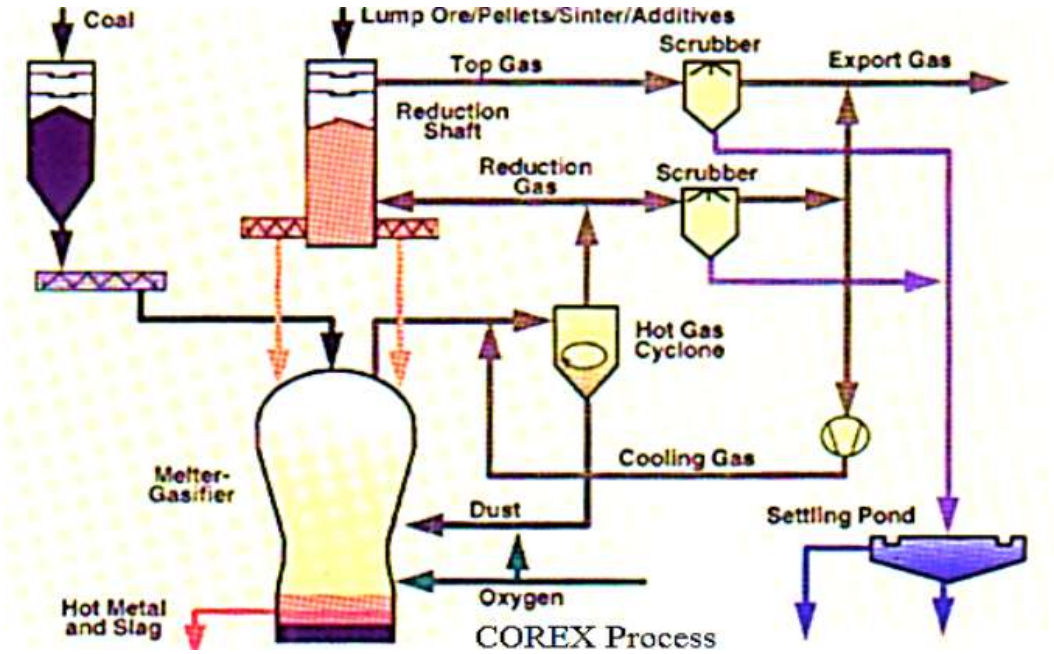

Figure 2.5: A flow diagram of COREX process [36].

Like the other ironmaking processes the performance of COREX is dependent on the raw materials, and for the process to work efficiently and effectively the iron ore and coal are required to have certain physical and chemical properties [37]. The main parameters affecting the productivity and reaction rate are mean particle size, coal moisture, volatile matter content, char strength, reduction disintegration of pellets and slagging rate. Therefore, to achieve an effective operation process the above parameters need to be considered for optimisation [37].

COREX has many economic and environmental advantages including abilities to use non-coking coal, reducing energy usage and CO_2 emission by up to 20% as well as Lower CAPEX and OPEX to help on saving costs. Yet, the inability to use ore fines directly, restrictions on the thermal coal and necessity for export gas utilizations suggest that further improvements are required to meet the demands.

2.2.3.3 FINEX®

FINEX is another smelting process that produces hot metal using fine ore and non-coking coals. The process operates using similar plant configurations to COREX but FINEX consists of a series of successive counter-flow fluidised bed reactors as shown in Figure 2.6. Fine ores are reduced to DRI in three or four stages, in the upper reactor stage ores are preheated then reduced to DRI in the subsequent stages. DRI is compacted and charged into the melter-gasifier where it becomes molten and reduced to hot metal using reducing gases and heat generated through coal gasification with oxygen. Hot metal and slag are frequently tapped from the hearth zone. Like COREX process the reducing gases are generated by coal gasification and used in the DRI production in the fluidised bed reactors.

FINEX's elimination of iron bearing agglomeration and flexibility with raw materials makes the process attractive economically and environmentally by saving costs on ore preparations and reduces CO_2 emission [8].

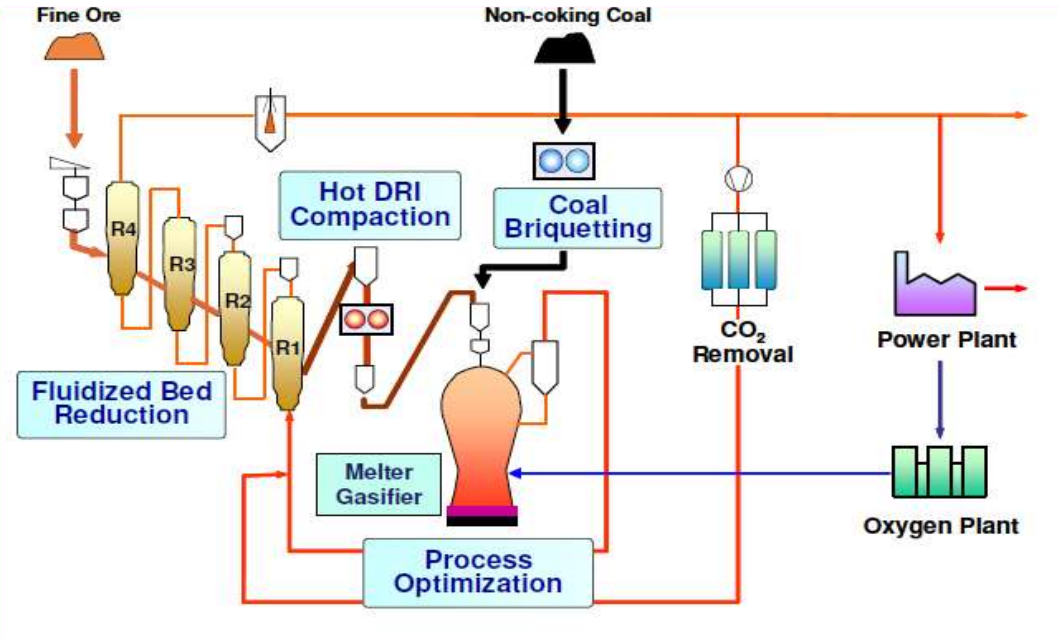

Figure 2.6: A flow diagram FINEX process [36]

2.2.2.4 Other emerging alternative ironmaking technologies

As well as these mentioned technologies, the makers put significant efforts into other alternative ironmaking technologies including direct reduction processes. The development stage of these processes varies considerably with some of them being already commercialised but some needing further development to be commercialised. In general, these technologies are strongly dependant on the raw material availability and costs [8]. The most promising DRI processes are, ITmk3, paired straight hearth furnace, Coal based HYL process (a syngas based DRI plant), fluidised bed (Circored and circofer), Midrex and MXCOL. Coal-based HYL process, a syngas based DRI plant is the only truly established gas based direct reduction processes, and Tenova HYL have orders to build 4 units, each with 2.75 million-t/year production [8].

2.3 Biomass production and application

Biomass refers to materials that are biologically produced and have the ability to be converted into char through pyrolysis. This includes wood, agricultural crops and their waste products. Plants generate C through photosynthesis when CO_2 is absorbed from the atmosphere with the presence of water and sunlight; carbon is formed and stored in plants as glucose ($C_6H_{12}O_6$). Biomass is considered a renewable energy source because of its short life cycle. The life cycle of wood which is considered as the most sustainable source is typically between 5 to 10 years in a tropical forest, while the life

cycle of Bana grass (grass-based biomass) is between 4 to 6 months. Despite all the economic and environmental benefits from utilization of biomass, due to high moisture content, low calorific value, low density, and high volatile matter, use of raw biomass is inconvenient and inefficient in many applications. As a result, pre-treatment processes are required for the material to be a viable raw material. The processes consist of mechanical, chemical, and thermal treatments to reduce volume, dry, and densify raw biomass before the conversion process. The conversion of biomass is typically achieved through two main routes: biochemical and thermochemical conversion [38].

Solid, liquid and gas biofuels are produced through the thermochemical route, using pyrolysis/torrefaction, liquefaction, and gasification respectively. The industrial use of biomass primarily focused on solid biofuel which is mainly made up of torrefied wood pellets and charcoal [39]. The demand for solid biofuel is the highest, which is mainly made up of torrefied wood pellets and charcoal. Their properties include a high fixed carbon and calorific value making charcoal and torrefied wood pellets a potential replacement for injected coal in ironmaking. The properties of solid biofuels are highly dependent on processing conditions. Charcoal and torrefied wood pellets are converted into biofuel through similar processes, both require relatively slow heating, but they work under different process conditions. Torrefaction takes place in the temperature range of 200-300 °C, in the absence of oxygen to avoid combustion. However, the pyrolysis takes places in the temperature range of 300-600 °C with a specific amount of oxygen present to allow partial combustion to supply heat [38]. Biomass produced through pyrolysis will have a higher fixed carbon and calorific value, but lower volatile matter and energy yield compared to torrefied wood pellets. Table 2.1 below compares the chemical and physical properties of torrefied wood pallets, charcoal, and thermal coal on the dry basis.

Table 2.1: Solid fuels property comparison [38].

Properties	Torrefied wood pellets	Charcoal	Coal
Moisture content (wt%)	1-5	1-5	10-15
Calorific Value (MJ/kg)	20-24	30-32	23-38
Volatile Matter (wt%)	55-65	10-12	15-30

Fixed carbon (wt%)	28-35	85-87	50-55
Bulk Density (kg/l)	0.75-0.85	~0.2	0.8-0.85
Energy Density (GJ/M^3)	15-18.7	6-6.4	18.4-23.8
Sulphur content	Low	Low	High
Reactivity	Higher	Higher	Lower
Dust	Limited	High	Limited
Grindability	Good	Good	Good

Biomass feedstock may also be converted into liquid and gaseous biofuels through fast pyrolysis and gasification respectively, to produce bio-oil, syngas, and synthetic natural gas (SNG). Liquid biofuel is produced through fast pyrolysis with a high heating rate and short vapour time, as a result the water content can be as high as 51% depending on the feedstock's moisture content. Due to high water content, liquid biofuel tends to have a very low heating value compared to heavy oils. As the BF performance is largely dependent on the fuel energy content and ability to create a reductive atmosphere, liquid fuels are less suitable to be used as a reducing agent [40].

Gaseous biofuels which could be used as a reducing gas in ironmaking is generated from partial oxidation. For gaseous biofuel to be used in current ironmaking and maintain process efficiency and productivity, CO and H_2 gases need to be made around 90% of the total gas mixture. Like the other forms of biofuels, gaseous phase properties are influenced by different variables including feedstock moisture content and calorific value. In addition, the final product performance can be influenced by ash content and the reactors temperature. Several technologies have been developed to utilise syngas from biomass. A temperature range of 600–1000 °C is required for biomass gasification to be processed. Based on the heat supply the technologies are divided between allothermal (indirect) and autothermal (direct) classifications. For syngas to be used as a reductant in ironmaking applications, it needs specific qualities, including a low CO_2 content and CH_4 content around 3% as higher levels of hydrocarbon require extra heat to split the bonds. Synthetic natural gas (SNG) is also produced from biomass feedstock. During this process the materials are first converted into syngas and then is passed through a series of stages including gas cooling and cleaning, as well as the use of a methanation unit to convert the CO and H_2 gases produced in the first step into CO_2, CH_4 and water. Finally, H_2O and CO_2 are removed to create SNG as a final product [40].

Previous studies have indicated that biomass-based fuels have a potential to replace current carbon sources in iron and steel making applications [3]. Considering the technical and economic aspects, the solid biofuel is the more likely source to be used as an alternative to thermal coal for the HIsarna process. The price of the biofuels is greatly affected by factors such as feedstock costs, conversion technologies and energy consumption [3]. Currently HIsarna uses an injection system to add powdered coal into the SRV. Solid charcoal has similar properties to injected coal which makes the coal replacement rather straightforward with lower cost required for plant modifications.

Historically charcoal has been used as a fuel to provide heat and act as a reductant in metallurgical processes. However, in the current BF charcoal cannot be used as the only source of carbon due to insufficient strength compared to lump coke to support the burden which is necessary for BF. Charcoal has a very good reducibility and low volatiles but due to low dense and strength, the use of charcoal often associated with some mini-BFs in Brazil as the mini-BFs do not require as much strength and support for burden [41]. Based on previous studies solid biomass has a potential to fully replace current fossil fuel in smelting processes, as smelting does not require the strength to support the burden.

HIsarna operates with specific low calorific value coal as the SRV provides hot fuel gas for the CCF. To provide enough hot fuel gas for CCF, the SRV needs to slow down to perform less smelting and more coal gasification which is achieved by using specific low calorific value coals. The SRV slow-down creates an opportunity for higher volatile coals to be used in HIsarna, also use of higher volatile coal means higher fuel gas generation which is needed to optimise the process [33]. HIsarna's ability to use high volatile and low calorific value coals could mean potential for use of low calorific value and high volatile torrefied wood which require less processing and is cheaper in price compared to charcoal. In the current integrated steel plant, charcoal has been used for partial substitution of coal and coke which means HIsarna may be able to break out of the traditional limitations of ironmaking routes.

2.4 Mechanism of FeO reduction in smelting slag by solid carbon

Bath smelting processes produce metallic iron by reduction of FeO in the molten slag through reducing gases, solid char, and dissolved carbon in the hot metal. It has been

reported that the rate of reduction of iron oxide in the molten slag is controlled by dissolved carbon in hot metal (Fe-C) droplets and solid carbon [42]. Therefore, the knowledge and understanding of slag-carbon, carbon-metal reaction kinetics are critical aspects of the smelting process. The reduction of FeO containing slag by solid carbon is expressed by Equation (7), which is considered as the overall reaction between FeO in the slag and solid carbon:

$$FeO_{(in\ slag)} + C_{(s)} \rightarrow Fe_{(s)} + CO_{(g)} \quad <1535\ °C \tag{7}$$

The reaction proceeds with the help of gaseous intermediates, as shown in Figure 2.7, when the reaction begins a gas film is formed around the solid carbon which separates the molten slag from the carbon. The reduction process consists of five individual steps as described below [41-43]:

- Chemical reactions at the slag-gas interface expressed by Equation (2)
- Chemical reactions at the gas-carbon interface expressed by Equation (3)
- Mass transfer of FeO from the bulk slag to the slag-gas interface
- Rate of carbon diffusion into liquid metal to form Fe-C
- CO and CO_2 gas diffusion through the gas halo

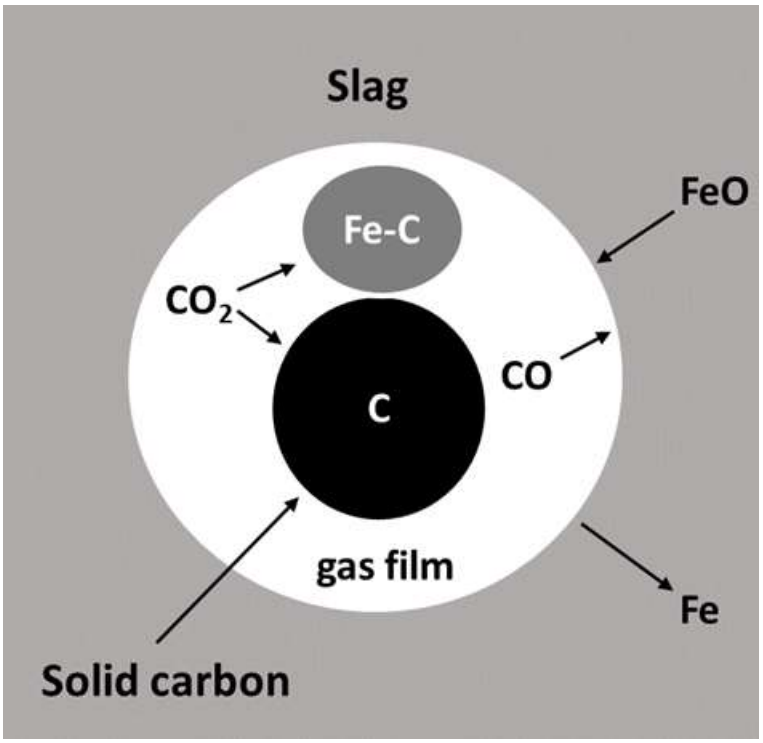

Figure 2.7: Schematic diagram of reduction of FeO in the slag by solid carbon with the aid of gas intermediates.

These steps are known to have an important effect on the reduction mechanism which controls the smelting performance. To understand the influence of each of the above steps in the reduction kinetics, several studies have been performed. The role of gas-carbon reaction (Equation (3)) is studied by selecting different carbonaceous materials (graphite, coke, and coal char), and it is noted that different carbonaceous materials have different reactivity level toward CO_2, which can be crucial in the CO generation [40-52]. In the same studies, the effect of chemical reaction at slag-gas interface, rate of mass transfer of FeO in the liquid slag to slag-gas interface, and gas diffusion in the halo were analysed to determine the rate controlling step(s).

Sarma et al. [42] investigated the rate of carbon monoxide evolution from the reaction of slag containing 2 to 10 wt% FeO with solid carbon (such as graphite, coke, and coal char) using stationary and rotating carbon rods, stationary horizontal carbon surfaces, and pinned stationary spheres as the reductants to determine the rate controlling step. It was found that the rate is controlled by liquid phase mass transfer, gas diffusion and chemical reaction at the slag-gas interface, therefore the overall reduction rate is governed by a mixed control mechanism. Seo and Fruehan [43] studied the reduction kinetics of blast furnace slags containing 1 to 3 wt % FeO with solid char remaining from pulverised coal injection at 1450 °C. The finding indicates that the mixed control mechanism is rate limiting but for low FeO content liquid phase mass transfer is the primary controlling step. The mass spectrometer technique was used by Min et al. [44] to measure CO and CO_2 evolving from the reaction of graphite rod with slag containing a wide range of FeO contents. It was observed that an increase in the FeO content has a positive effect on the rate of reduction. At low FeO (<5 wt %) content the mass transfer of FeO in the liquid slag is rate limiting but at a high FeO content (>30 wt %) chemical reaction at the gas-carbon interface is the rate controlling step. Story et al. [45] re-examined the work done by Sarma et al. [42] for carbon gasification reaction using mixed control model, and found that the carbon type has a great influence on the reduction rate. Depending on the reaction conditions i.e., agitation and carbon type, the overall rate is controlled by a mixed mechanism.

To determine the role of solid carbonaceous materials on the reduction of FeO in the slag, Teasdale and Hayes [47] reacted slag with graphite, coke and two types of coal at the temperature range of 1400-1600 °C, using online mass spectrometry for real-time gas analysis and EPMA to analyse quenched samples. The results suggest that

the carbon type significantly affects the reaction rates, and carbon gasification takes place at the char surface; however, the slag phase mass transfer is defined as a rate limiting step. In another study, Fruehan [49] studied the rate of reduction of iron oxide by chars produced from different biomass sources, coke and coal at low temperature range between 900-1200 °C. Huang et al. [54] studied the interaction between slag containing iron oxide and a wide range of carbonaceous materials. It was found that the reaction takes place through a gaseous intermediate formed between solid char and iron oxide. The findings suggested that the carbon type has a significant influence on the reduction rate due to their interaction with the slag; therefore, carbon oxidation step is defined as a controlling mechanism. Various other factors have been studied which may affect FeO reduction rate including particle size and quality of solid coal by Ozawa et al. [48]. The results indicate that the rate is controlled by chemical reaction for high volatile matter coals, but for the low volatile coals liquid phase mass transfer controls the rate. The findings by Ji et al. [55] for coal injection into electric arc furnace (EAF) slags reveals that the rate is controlled by chemical reactions at the slag and carbon interface. For high basicity slag greater than 3.2 the gas-carbon is the rate limiting step but for slag basity between 1.8 and 3.2 the reaction at both slag-gas and gas-carbon interfaces is likely to control the rate. However, for low slag basicity (<1.8) gas-slag reaction becomes slower therefore it becomes the rate limiting step. In aonther study, Ji et al. [56] used injection method to find the optimum conditions for coal injection into EAF slags for stablising slag foaming. The study found that the carbon gasification is the main rate-limiting step, but slag-gas reaction also has significant contribution during long injection runs. The findings by Ji et al. [51] for coal injection into electric arc furnace (EAF) slags reveals that the rate is controlled by chemical reactions at the slag and carbon interface. For high slag basicity gas-carbon is the rate limiting step but for low slag basicity (<2.7) gas-slag reaction becomes slower therefore it becomes the rate limiting step. Also results by Bafghi et al. [53] indicate that the slag basicity controls the reduction mechanism, for the slag with a basicity of 2 the liquid phase mass transfer is the rate limiting but for the lower basicity slag the mixed-control model is applied. In another work by Bafghi et al. [52] the effect of slag foaming on reduction of FeO in the slag is studied. It was found that the rate is affected by slag foaming and liquid phase mass transfer is the rate limiting step.

Additionally, other aspects including Fe-C droplets interaction with slag have been studied relavent to iron smelting process[55-59]. Molloseau and Fruehan [62] studied the reaction behavior of Fe-C-S droplets containing 2.9% C and 0.01% S with the slag containing 3~35 wt.% FeO in the temperature range of 1370 to 1490 C°. The study shows that the FeO content has significant effect on the droplet behavour and the droplets remained intact when the FeO content is less than 10% and the rate is controlled by chemical reaction on the metal surface. However, the increase in the FeO in slag causes the droplet to become emulsified within the slag which help increase the rate of reaction. Smith and Fruehan [58] investigated the rate of reduction of FeO in the slag by carbon in the metal with different sulfur contents from moderate to high at 1450 °C. it was found that at the high sulfur content the rate was controlled by metal-gas reaction but mixed controlled mechanism from FeO mass transfer and metal-gas are likely to control the rate for reaction with low sulfur content. In another study by Min and Fruehan [59], it was confirmed that sulfur content has an important effect on the rate and at high sulfur content the rate was controlled by kinetics at the metal-gas interface but for low sulfur content the rate was controlled by liquid and gas mass transfer steps. The study by Biswas et al. [60] for Fe-C droplets with oxiding slag suggests that the reaction is controlled by oxygen supply to the droplets, therefore FeO liquid phase mass transfer is the rate limiting step. In another study conducted for dephosphorization by Gu et al. [61] the carbon free iron droplets and droplets contain carbon reacted with FeO containing slag and it was concluded that carbon content leads to faster dephosphorization rate due to the stirring effect from CO bubbles formed from reduction of FeO. A series of studies conducted by Barati and Coley [61-63] investigated the kinetics of the CO-CO_2 reaction with iron oxide containg slags. Through these studies the authors developed a kinetic model to measure the rate of the CO-CO_2 reaction with slag melt, which relates the apparent rate constant to temperature, and both pre-exponential and activation energy are functions of slag chemistry.

2.5 Literature review findings and unresolved issues

This study outlines the challenges conventional ironmaking processes are facing. The demand for steel is expected to continue to grow worldwide and stringent environmental legislation on the CO_2 emissions and lack of flexibility in the raw materials increase the pressure on the steel producers. Despite substantial

improvements concerning environmental performance in the last three decades, a true step change in steel manufacturing technologies is required to sustain the productivity and meet the environmental legislation requirements.

The traditional integrated route (i.e., the BF-BOF route) is limited in terms of raw material consumption, therefore significant effort has been put into developing alternative technologies which promise to be more flexible with raw materials. HIsarna is one of the newly developed processes that has shown potential with an ability to cut CO_2 emission by more than 50% without CCUS and 85% with CCUS. In addition, it has a high flexibility in raw materials. Due to its flexibility with raw materials the coke-making and agglomeration plants are not required, this will help reduce costs and CO_2 emission. HIsarna has the potential to substitute thermal coal with alternative renewable carbon sources such as biomass; a development which has not been possible with the use of the BF due to its innate requirements of high strength material for supporting the burden.

HIsarna has undergone a series of successful trials using thermal coal as a reductant. It has shown potential to meet the expectations and requirements of the steel industry to move with the times. HIsarna can operate with a specific low calorific value and higher volatile coals to allow more coal gasification in the SRV to provide hot gas for the CCF. Since the high volatile coals are more widely available, this will help cut costs and could mean potential for use of low calorific value and high volatile torrefied wood which again may help in cost saving.

Although extensive research has been conducted on carbonaceous materials characterization for metallurgical processes, the research and development for the carbonaceous materials (coal and biomass) for HIsarna technology is scarce, and there is very limited information on direct comparison between coal and biomass for HIsarna applications. The performance of both CCF and SRV sections are very heavily reliant on the carbonaceous materials injected. The amount and the nature of volatile components released during injection into an extreme high temperature (up to 1500 °C) together with the CO produced from carbon-slag reaction controls the partial reduction of the iron ore and maintain the temperature in the post-combustion zone in the CCF. While the remaining chars will dissolve into the hot metal and react with the iron oxide in the slag to produce metallic iron in the SRV. Therefore, a full understanding of the devolatilization behaviour and characteristics of the chars

received in the SRV bath from thermal coal and biomass injection under HIsarna's thermal conditions is necessary to select the right mixture of carbonaceous materials (e.g., substitution of coal with certain biomasses). Although there have been numerous studies on the slag-carbon reaction using thermal coal as a reductant, no direct research has been conducted on the slag-biomass reaction relevant to the bath smelting HIsarna process. Also, there is some discrepancy in the literature findings for rate controlling steps and reaction mechanisms for iron oxide containing slag with carbon. Furthermore, no studies have been conducted on the reaction kinetics for smelting reduction by solid carbon injection into FeO containing slag concerning HIsarna technology, which are key aspects in understanding the reduction rate of FeO in the slag.

Chapter 3

Formulating the Research Approach

This project will study the thermal behaviour and the reactions of different carbonaceous materials with the slag and metal at the high temperature through different experimental techniques. The project will use a hypothesis driven approach to direct the research and ensure focused research findings are clearly delivered. The hypotheses are drawn based on the knowledge gaps in the available literature along with the industrial requirements, followed by an investigation plan for each chosen question.

Hypothesis 1 – Once a biomass or thermal coal particle is injected into the vicinity of the slag-metal interface in the SRV, devolatilization happens first.

Objective 1 – The volatile matter (i.e., hydrocarbons, mainly CH_4) may crack to C and H_2 or react with the environment to form CO and H_2 or H_2O. The gases generated in the SRV will flow up to CCF and partially reduce iron ore particles injected in the CCF. The amount of volatile matter (VM), moisture and ash contents, which directly affects the amount of fixed carbon content, will be critically important to maintain the balance between smelting reduction and gasification in the SRV and the balance in performance between SRV and CCF.

The amount of VM, the moisture and ash contents in the biomass are determined in comparison with thermal coals in laboratory under argon atmosphere to understand the difference in behaviour and reveal the ideal preparation condition required for biomass materials to produce chars with similar properties to HIsarna injected coal.

Approach to Hypothesis 1 – To investigate this hypothesis four thermal coal samples containing different levels of volatile matter (VM) from low through medium to high and two biomass samples sourced from wood and grass are heated to 1500 °C under slow heating conditions to give out volatiles. The experiments are performed under N5 Ar atmosphere using thermogravimetric analysis (TGA) to measure the weight loss and in a vertical tube-furnace (VTF) for off-gas analysis to determine the volatiles characteristics for selected materials. The off-gas will be continuously monitored with a gas mass spectrometer to attribute the volatile species released with the maximum weight loss peaks produced in the TGA at each stage of the devolatilization.

Hypothesis 2 – The devolatilization behaviour and solid char yield for carbonaceous materials can be measured using DTF-QMS techniques for injection and off-gas measuring under similar thermal condition (e.g., rapid heating and high temperature) to HIsarna SRV.

Objective 2 – It is known that the post combustion ratio (PCR, Eq. 18) value of the reducing gases affects the pre-reduction degree of the iron ore in the HIsarna's cyclone (CCF). On the other hand, the final reduction of the iron oxide in the SRV is controlled by the amount of solid char particles received in the smelting bath. Therefore, it is critical to know the devolatilization behaviour of carbonaceous materials under thermal conditions similar to SRV to help select the right mixture of carbonaceous materials, to ensure effective reduction (indirect reduction in SRV and pre-reduction in CCF) and heat balance (via post combustion) achieved.

Approach to Hypothesis 2 – A DTF-QMS is used to heat the carbonaceous materials in the environment close to HIsarna SRV thermal condition to predict the nature of volatiles, the proportion of each components produced and the solid char yield efficiency during carbonaceous materials injection. Using injection method, the carbon particles from each source are rapidly heated to 1000, 1250 and 1500 °C in the DTF under high purity Ar atmosphere. The volatiles released during the heat treatment are measured using QMS and the char yield calculated from the sample weight before

and after injection to determine the temperature effect on the devolatilization rate, the variation in the gas species produced and the maximum weight loss.

Hypothesis 3 – The rate of carbonaceous materials gasification is controlled by physical structure and chemical composition of the materials.

Objective 3 – The HIsarna SRV is responsible for up to 80% of iron oxide reduction through direct/indirect reactions between iron oxide with solid carbon. The char reactivity of carbon particles is influenced by physical parameters such as particle size, surface roughness, shape, porosity, and char chemical composition including ash content and ash chemistry. These parameters will affect the char interaction with the slag containing FeO, the hot metal and the oxidation atmosphere, and these together control the rate of FeO reduction in the slag.

Approach to Hypothesis 3 – The high temperature conditions similar to HIsarna SRV are simulated by using DTF injection method. This allows to produce chars with a true representation of the char particles received in the SRV bath. The reactivity tests for resultant chars and their parent materials are performed using TGA method. The reactivity index of the chars calculated from the weight loss measured in the TGA under CO_2 atmosphere at 1500 °C isothermal condition. These results will provide the information needed to understand the characteristics of the chars received in the SRV bath, and the adaptations required to replace thermal coal with biomass.

Hypothesis 4 – The thermal coal particles are expected to go through higher degree of structural transformation under rapid devolatilization compared to biomass materials.

Objective 4 – When the carbon particles are injected into the HIsarna SRV, they will instantly encounter an extreme high temperature condition. This sudden high temperature and heating rate that the particles experience will result in the sever structural changes, which will influence the overall particle behaviour in the smelting bath. Previous study by Moore [66] have shown variables such as density, porosity and thermoplasticity control the coal particle swelling behaviour under thermal conditions. The study used HT-CSLM as a suitable technique to investigate the swelling behaviour of different coal grades, but no research has been conducted concerning biomass materials. The structural behaviour study for coal and biomass materials using the in-situ HT-CSLM technique can provide information about the

real-time changes in the particles structure during rapid heating. This can help to determine the effect of the morphological changes on the char reactivity, and potential impacts on the performance of the HIsarna process during coal substitution.

Approach to Hypothesis 4 – To explore this hypothesis, the morphology of the solid carbon particles from each carbonaceous material and their resultant chars produced in the DTF are examined under SEM. This reveals the extent of the structural transformation from the effect of rapid devolatilization. The real-time structural changes were observed using HT-CSLM to calculate the particle swelling ratio, while the BET is used to measure the particles surface area, the pore volumes and type of pore present in each raw material and their chars.

Hypothesis 5 – Biomass chars will react differently with FeO-containing molten slag in comparison to thermal coal chars.

Objective 5 – After reaction initiates a gas film will form around the carbon particles which separates the molten slag from the solid carbon. Therefore, the reduction reaction continues through the aid of the gaseous intermediates. The reaction mechanisms for slag reduction by solid carbon consists of five steps, and it proceeds by the chemical reactions at the slag-gas and gas-carbon interfaces. The reaction behaviour of the HIsarna slag with biomass chars is studied and compared with the slag reaction with thermal coal chars under the same experimental conditions.

Approach to Hypothesis 5 – Since the reducing reaction kinetics are the possible rate limiting factor in the smelting process, the role of each step involved in slag-char reduction kinetics will be examined for chars produced from biomass and thermal coal materials. A DTF-QMS is employed to study the injection of char particles into pre-melted slag under simulated HIsarna thermal conditions (High temperature and heating rate). The experiments are conducted under the temperature range from 1450 °C to 1525 °C (with 25 °C increments), to measure the temperature impact on the reduction rate and determine the reaction mechanism and kinetic parameters. The extent of FeO reduction in the reacted slag is quantitatively measured by Wavelength Dispersive X-Ray Fluorescence (WDXRF), while the SEM is used to determine the change in morphology of the reacted slag compared to unreacted slag.

Chapter 4

Experimental Apparatus and Analysis Methods

4.1 Introduction

HIsarna's SRV is a critical section where a series of complicated chemical reactions take place. The SRV is responsible for final reduction and provides off-gas for the CCF section. Therefore, an in-depth understanding of the thermodynamic and kinetic behaviour of the gas-slag-metal system is needed to understand the overall process. To complete this study a series of laboratory scale experiments were carried out using a suite of equipment, to study different aspects of the reactions. The focus is on the physicochemical behaviours of the carbon source injected into the SRV such as its devolatilization, and reactions with the slag and metal. The conditions to study are slow and rapid devolatilization of the carbon sources, structural characteristics of chars in SRV, and slag/carbon reactions. In addition, the influence of Fe-C droplets is expected to have a large impact on the reduction rate and process efficiency.

The studies in the literature indicate that physical and chemical properties of the carbonaceous materials will control the chemical reactions between carbon sources and the slag in the gas-slag-metal system. However, most of these laboratory experiments and kinetic studies are conducted under conditions similar to industrial process which operates differently to the HIsarna technology. The HT-DTF combined

with a gas analyser is extensively used to study iron oxide reduction by solid carbonaceous materials [40, 48, 50] and to simulate the carbonaceous materials combustion behaviour and solid char formation which occurs at high temperature [65-68]. The DTF allows conditions such as temperature, residence times, and atmosphere to be closely controlled to simulate the conditions of the ironmaking processes (e.g., rapid heating and high temperature). In the HIsarna SRV the carbonaceous materials are penetrated into the smelting bath using injection method at high temperature. Therefore, in this study the DTF-QMS is adopted as the laboratory experimental set-up to simulating the SRV reactor. This set-up allows the synthetic slag to be melted under temperature range similar to SRV temperature and then solid chars to be injected using specifically designed injection set-up, while the off-gas is continuously measured using QMS to calculate the real-time reduction rate. In addition to DTF-QMS, various other equipment and methods including VTF, HT-CSLM, TGA, BET, Raman spectroscopy, SEM and Origin are used to perform experiments and analyse the data collected. This chapter describes all experimental equipment as well as materials selected for each experiment. Experimental procedures and methodology for material preparation and standard testing will also be included for reference.

The results chapters will follow a layout similar to academic journals, with their own introduction, experimental, results and discussions sections. This ensures a clear and rounded evaluation of each directed activities producing high quality results accessible to the reader.

4.2 High temperature drop tube furnace (HT-DTF)

Drop tube furnace (DTF) has been used in the past to investigate the behaviour of carbonaceous materials in different ironmaking processes [67, 69-76]. The DTF allows to simulate the high heating rate and temperature as well as atmospheric conditions carbonaceous materials experience during charging. Some researchers used DTF to produce char particles under rapid heating to determine the combustion characteristics and kinetics of the rapid heating chars [69-74], while others used it to inject carbon into iron oxide containing molten slag to study the reaction mechanisms under well controlled conditions [75, 76]. The specific design of the DTFs used in these studies may vary, however the main features are the same, e.g., the furnace is a vertical heated tube, a gas flow is laminar flow and designed to enable making additions during reaction.

The DTF used in this study is constructed using an electric resistance heating high temperature vertical tube furnace (VTF) with a recrystallized alumina tube (VTF-1700/50, internal diameter 88 mm x length 1000 mm) and an isothermal reaction zone (±5 °C) of 250 mm. To measure the real temperature for the samples tested, a type B thermocouple located directly underneath the reaction stage within the reaction zone. An illustration of cross-section image of the DTF used is shown in Figure 4.1.

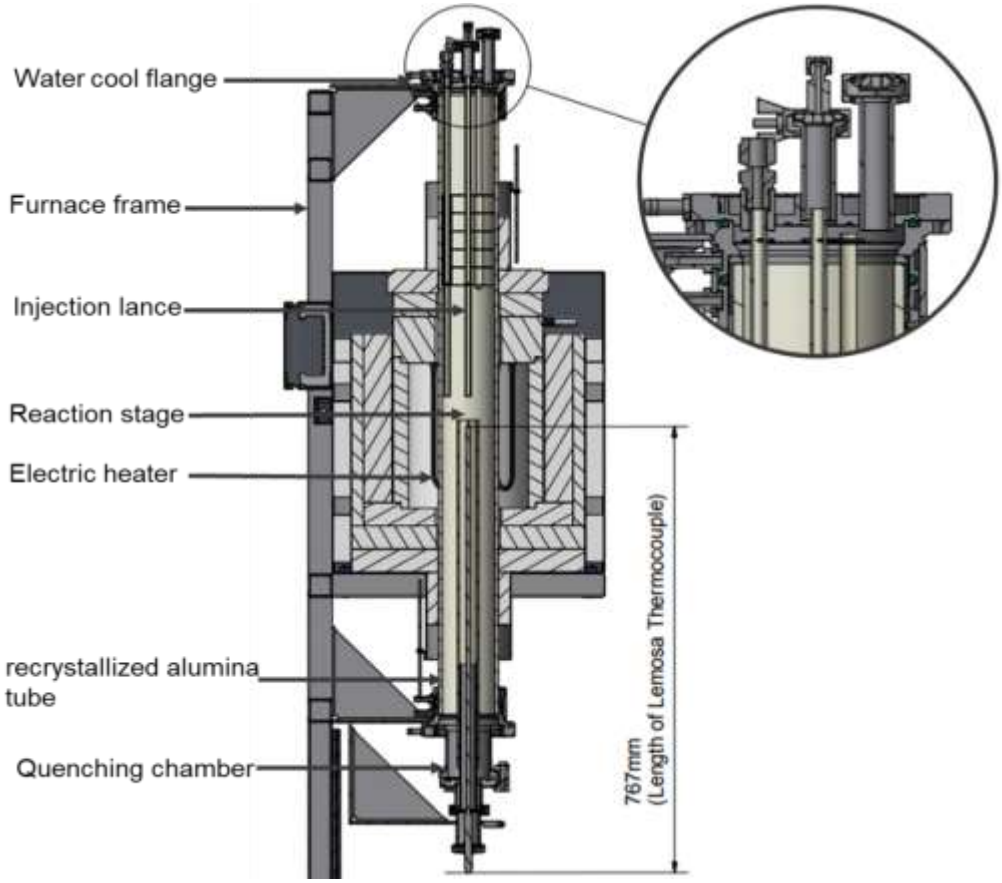

Figure 4.1: A cross-section illustration of the drop tube furnace [79].

The design of the DTF allows to perform experiments under both non-isothermal and isothermal conditions in the controlled gas atmosphere. The samples can be loaded into the furnace and then the furnace heated from atmospheric to desired temperature under low heating rate for non-isothermal experiments. This will help to understand the decomposition stages of the coal and biomass samples under continues heating, also the nature of volatiles released at each stage. These experiments will reveal the biomass pre-treatment temperature required to produce chars with similar properties to coal injected in HIsarna. On the other hand, the isothermal experiments are conducted by pre-heating the furnace to desired temperature and then the samples are

added to the high temperature zone for reactions to take place. These experiments provide information required to understand the reaction controlling mechanism and kinetic parameter under similar thermal condition to HIsarna process.

The DTF is applied to all the experimental chapters, however the experimental set-up for each chapter is different and the set-up for each experiment is described within the relevant chapters.

4.3 Quadrupole mass spectrometer

Mass spectrometry is a highly sensitive analytical technique which ionises atoms to separate and detects mass ions (mass to charge ratio). The Hiden HPR 20 QMS used for this study can only analyse gas phase samples, and the equipment itself is depicted in Figure 4.2. The end of the inlet capillary from the MS is connected to the exhaust of the DTF where the gas samples are taken from. The MS capillary which connects the MS to DTF exhaust is continuously heated to 150 °C to prevent condensation of vapours or adsorption of active sample gas species during the sampling process which could ultimately cause blockages and effect the experimental results [80].

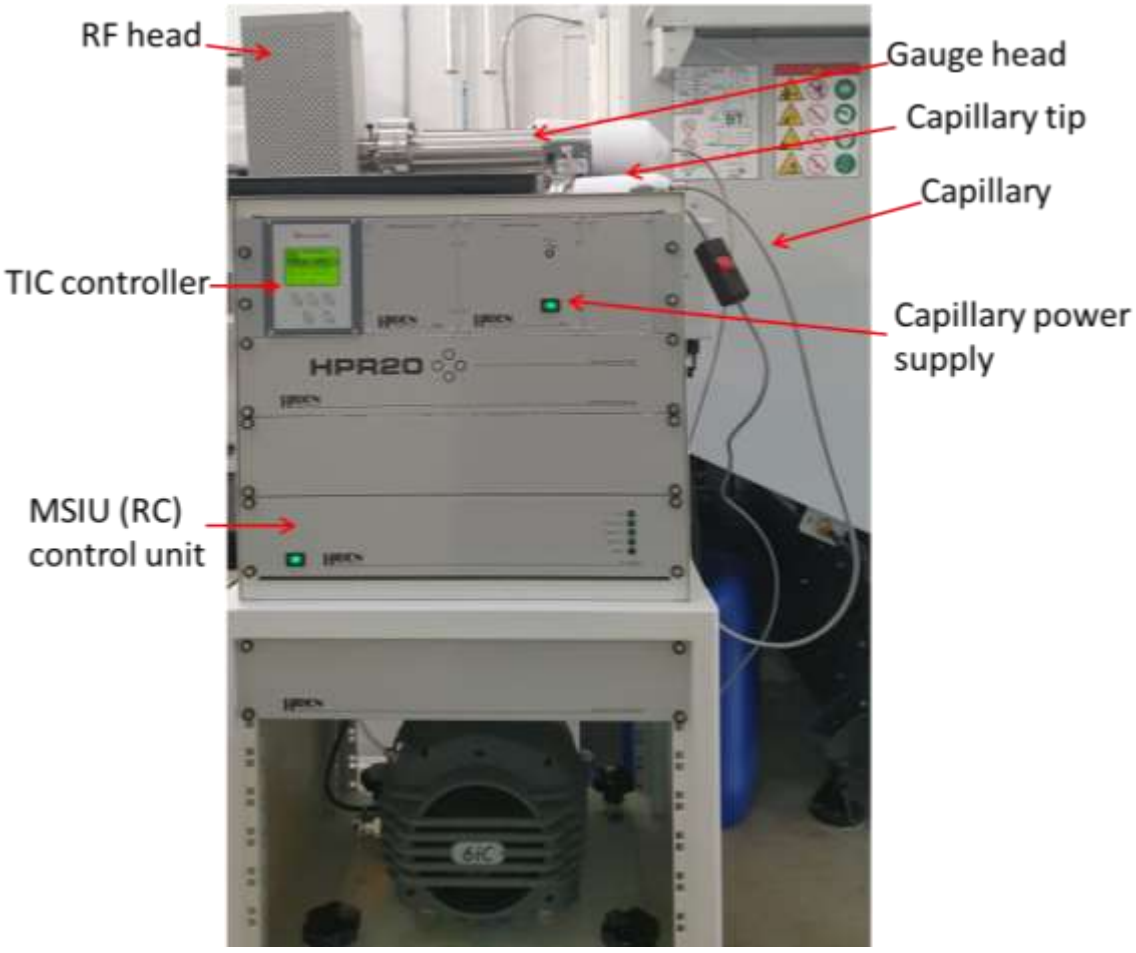

Figure 4.2: A schematic diagram of the Quadrupole Mass Spectrometer.

The Hiden QGA software is used for quantitative gas analysis of vapours and gas species. This equipment is used for devolatilization experiments to measure the rate and the amount of each gas species evolved during slow and rapid heating. Furthermore, the real-time FeO concentration in the molten slag during the carbon-slag reactions is calculated from the QMS measurements, which subsequently is used to obtain relevant kinetic parameter under similar temperature condition to HIsarna process.

4.4 Thermogravimetric analysis (TGA)

The mass loss due to devolatilization under non-isothermal conditions and char reactivity tests under isothermal conditions were conducted using thermogravimetric analysis (TGA) with a NETZSCH STA 449 instrument shown in Figure 4.3 that has an analytical balance sensitivity of 20 ± 0.01 mg. The below procedures are followed to complete the TGA experiments:

1. The devolatilization experiments are performed for raw carbonaceous materials under dynamic heating from 20 to 1500 °C at the heating rates of 10, 20 and 30 °C/min. These experiments are carried out under high impurity (99.9999%) argon atmosphere at the flow rate of 50 ml/min. The sample mass loss measured during these experiments is used for devolatilization kinetic study of the materials selected.
2. The gasification experiments are performed for chars produced under rapid heating in the DTF and under slow heating in the TGA. These experiments are carried out through three steps. The first step is dynamic heating from ambient to 1500 °C at a rate of 30 °C/min under high impurity (99.9999%) argon atmosphere. When the desired temperature was reached the sample was kept at that temperature for 10 minutes under Ar and then the gas atmosphere was switched to high purity (99.999%) CO_2 at the flow rate of 50 ml/min for 30 minutes to measure the reactivity of chars towards CO_2.

The detailed description of each experimental set-up and the method of analysis is described within the relevant chapters.

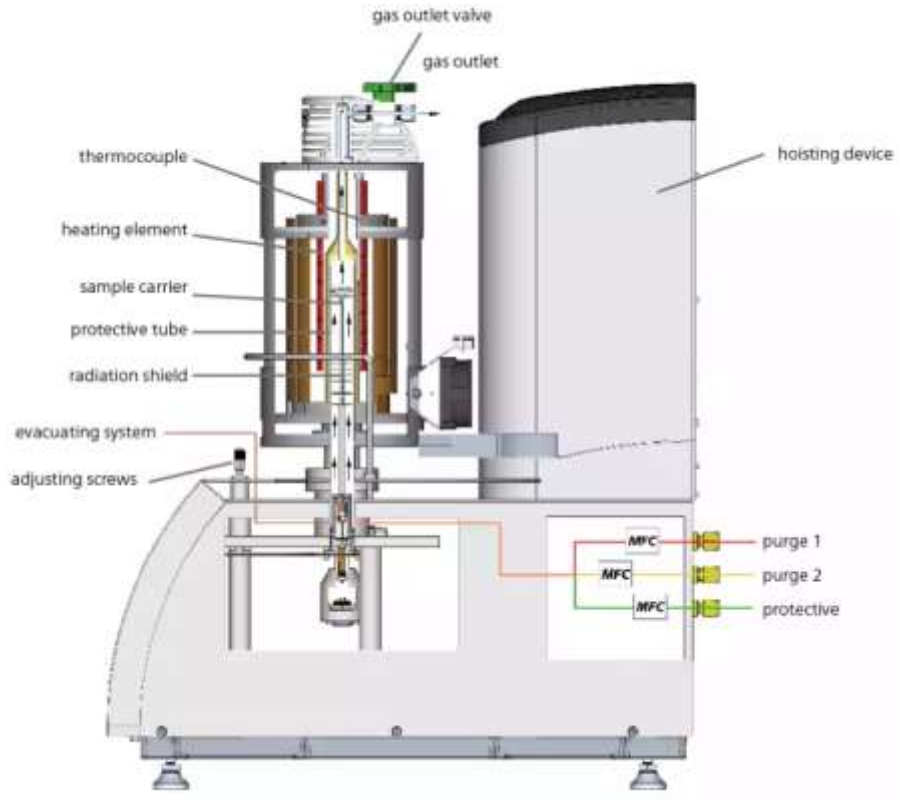

Figure 4.3: A schematic diagram of the TGA experiment set up of NETZSCH STA 449[81]

4.5 High temperature confocal scanning laser microscope (HT- CSLM)

The schematic of the HT-CSLM microscope is shown in Figure 4.4. The inner body of the chamber is a gold-coated, elliptical shape, to provide reflection for the IR radiation produced by the halogen lamp at the lower focus point to heat the small sample at the upper focus point. This results in possible heating rate of up to 1000 °C/min and temperature up to 1600 °C. The platinum sample holder is positioned in the centre of the upper focal point through the extension of an alumina rod from the side of the chamber. A R-type thermocouple wire is fused into the bottom of the platinum sample holder at the free end of the alumina rod to provide real temperature of the samples tested. The HiTOS software package is used for video capturing and to control the temperature programme.

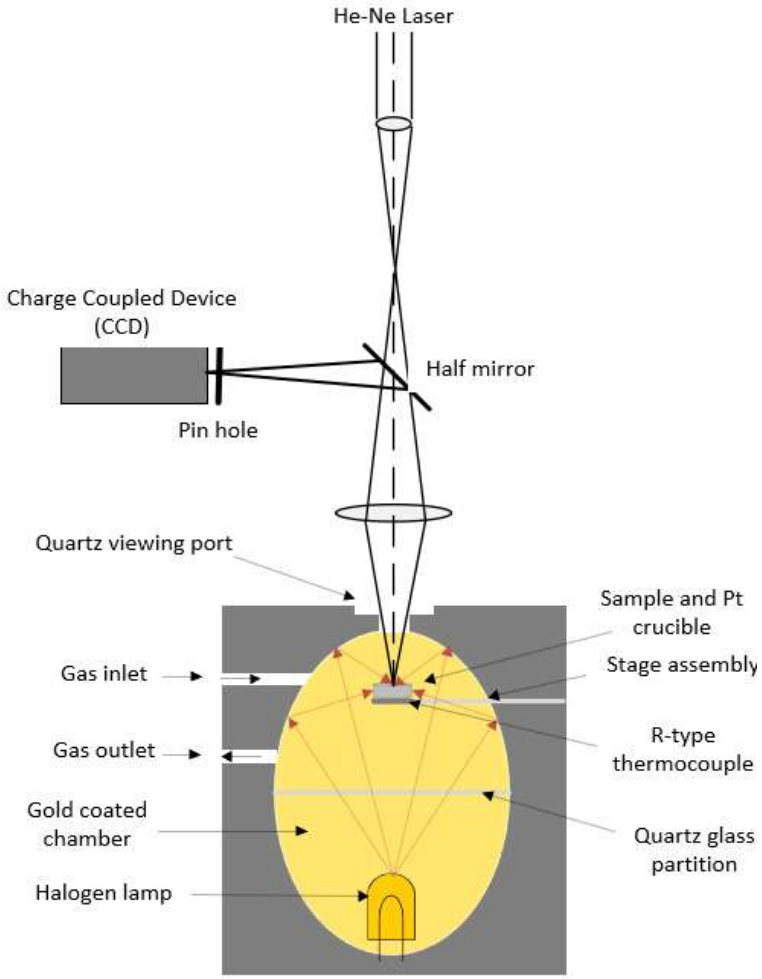

Figure 4.4: Schematic of the HT-CSLM to study real-time changes in the shape of carbon particles.

4.6 Additional Analytical Techniques

Scanning electron microscopy (Sigma Zeiss SEM) images were obtained for each carbonaceous material sample before and after rapid heat treatment to investigate changes in shape and structure. SEM imaging is also used to study the surface morphology (texture), and chemical composition of reacted slag. While N2 (77K) adsorption was applied to determine the carbonaceous material specific surface area, pore volume, and average pore diameter based on the multipoint Brunauer-Emmett-Teller (BET) method. The wavelength dispersive X-ray fluorescence (Rigaku Primus IV WDXRF with a Fluxana RAW package) was used as a quantitative method for chemical composition analysis of the reduced slags to determine the total iron content to measure the extent of reduction.

4.7 Materials

4.7.1 Carbonaceous materials selection

Four coals and two biomass samples were tested in this study. Their proximate and ultimate analysis (conducted by the HIsarna team at Tata Steel in IJmuiden) are listed in Table 4.1. The four coal samples contain different levels of volatile matter (VM) from low (8.63%, Coal C) through medium (16.00% Coal B and 22.18% Coal A) to high (36.00%, Coal D), while the two biomass samples are charcoal CC with 12.10% VM (a Birch wood based pre-treated biomass) and torrefied Bana grass TG with 63.60% VM (a grass-based torrefied material provided by OrangeGreen BV through the pilot plant located at Tata Steel in IJmuiden). Coal A and charcoal CC have already been used in HIsarna process during the pilot plant trials and torrefied Bana grass TBG is another renewable source which may be considered for future trials. The samples were dried at 80 °C for 12 h to ensure the removal of the free moisture and then crushed into small particles with the size range from 90 to 300 μm. The coal samples selected have different sulphur and ash contents that directly affect their reaction performance at high temperatures while biomass samples are generally much lower in sulphur and lower in ash contents.

Table 4.1: Proximate and ultimate values of the used carbonaceous materials using ISO 17246:2010 standards. Statement on who did analsysi

	Coal A	Coal B	Coal C	Coal D	Charcoal CC	Torrefied Bana Grass TBG
Proximate Analysis wt% (db)						
Moisture/ % (ad)	8.87	7.11	1.24	1.30	4.56	4.40
Volatile Matter	22.18	16.00	8.63	33.00	12.10	63.60
Ash	8.80	10.00	4.41	7.20	1.80	4.40
Fixed Carbon (by difference)	69.02	74.00	86.96	59.80	86.10	32.00
Ultimate Analysis wt% (db)						
Carbon	81.91	83.60	86.97	80.30	89.4	57.60
Hydrogen	4.27	3.93	3.43	5.09	3.11	5.60
Nitrogen	2.19	1.07	1.20	1.50	0.57	0.29

Sulphur	0.24	0.78	0.86	0.89	0.06	0.09
Oxygen by (difference)	2.59	0.62	3.13	5.02	5.06	32.02

db - on a dry basis; ad - on an air dried.

4.7.2. Bana grass char preparation

The torrefied Bana grass contains large amount of oxygen which can cause temperature drop in the HIsarna furnace as a result heat compensation is necessary. To avoid these problems and utilise torrefied Bana grass efficiently, a pyrolysis is necessary to reduce the oxygen content and produce chars with similar chemical properties to thermal coal currently used in HIsarna plot scale trials.

In order to produce char particles with desired properties, 15g of torrefied grass was pyrolysed under inert environment to three temperatures (400, 500 and 600) °C using horizontal tube furnace coupled with quadrupole mass spectrometry (HTF-QMS) shown in Figure 4.5. The gas analysis was performed for evolved volatiles while the residual chars were weighed after the treatment completed to determine the char yield. The type k thermocouple was connected to the crucible to measure the samples' real temperature and when the pre-setup pyrolysis temperature was reached the samples with the crucible was pulled from the reaction zone to one side of the furnace where the temperature is close to ambient. This was done to prevent further reactions and the atmosphere was kept under Ar to prevent further char oxidation.

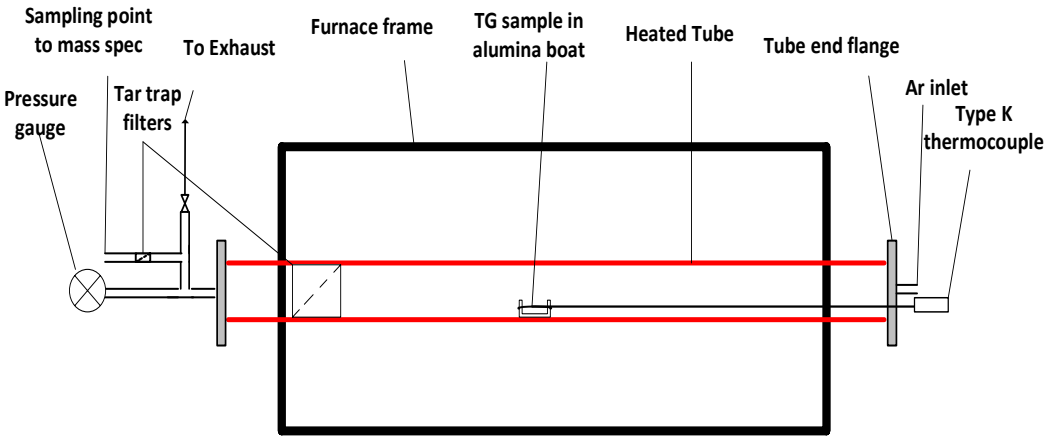

Figure 4.5: Horizontal tube furnace setup with a quadrupole mass spectrometry for Bana grass pyrolysis study.

Figure 4.6 shows the volume of each gas species generated from pyrolysis process at different temperatures. As expected, the results in Figure 4.6 show similarity in the curves produced for each gas species under these selected treatments, except (Figure

4.6d) the water peaks are not matching with each other, this could be due to condensation and gas trap by tar trap filter. Despite filtering the condensable gases and tar to protect QMS, large amount of H_2O measured at temperature of > 300 °C. The decomposition of oxygen containing groups mainly starts at temperature of < 300 °C, although small amount of CO_2 was detected at 250 °C. The gas analysis shows all the oxygen containing components (H_2O, O_2, CO and CO_2) almost reached their peak values at 400 °C, and the trough level almost reached at 500 °C. On the other hand, the hydrocarbons reached their peak value at 600 °C, and hydrogen is also close to its peak.

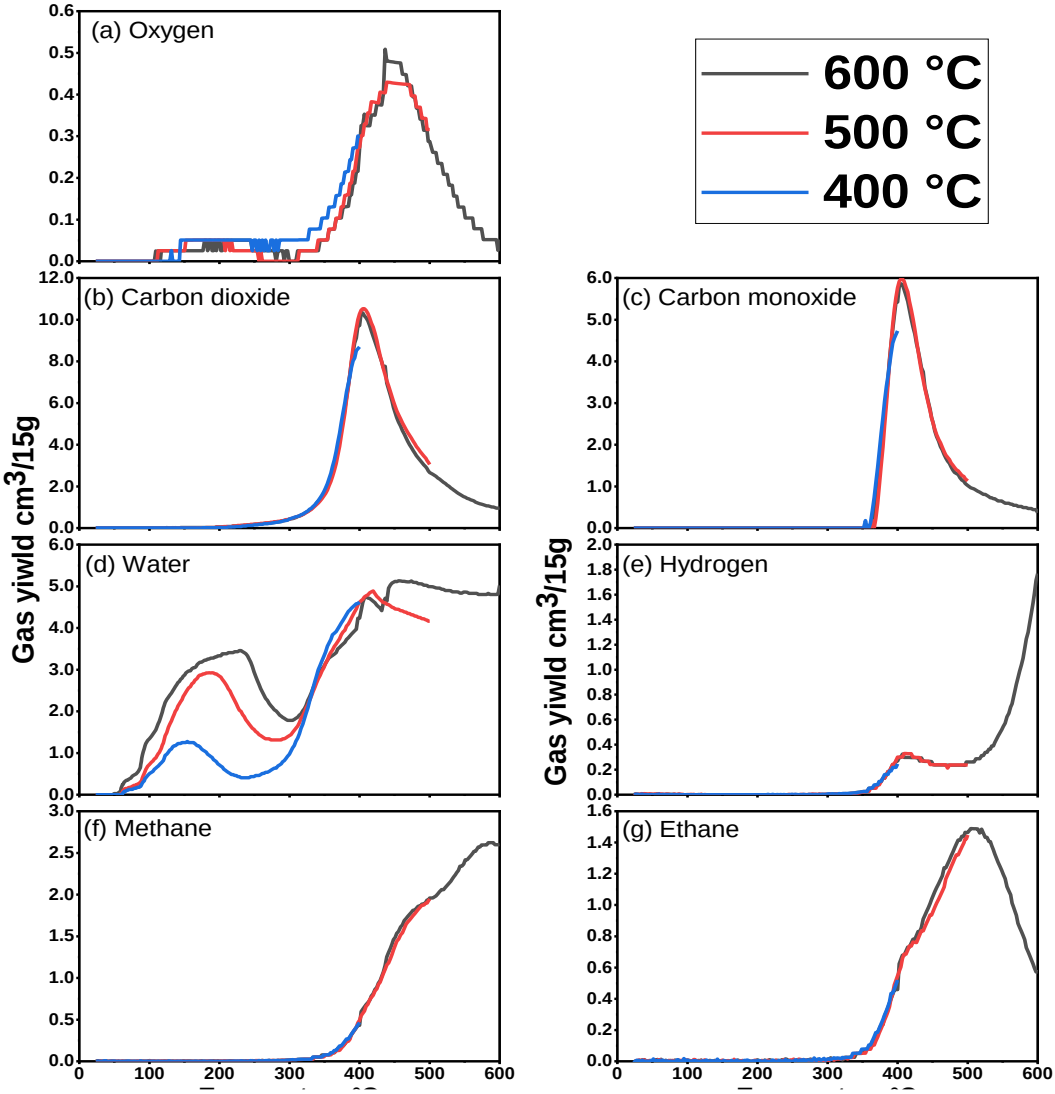

Figure 4.6: An off-gas analysis of (a) O_2; (b) CO_2; (c) CO; (d) H_2O; (e) H_2; (f) CH_4; and (g) C_2H_6 evolved during HTF-QMS experiments.

The solid char yield calculated from weighing the samples before and after the pyrolysis was 56.6% (400 °C), 48.3% (500 °C) and 44.7 % (600 °C). Regardless of

the pre-treatment temperature used, large amount of the material is converted into gases and condensable tar during char preparation process. To keep the "green" credentials of biomass, in the actual HIsarna process the pyrolysis process can be completed using heat sources from other parts of the steel plant, and the gases and tars released in the pre-treatment of torrefied Bana grass can be used to generate heat and power for HIsarna process.

The proximate and ultimate analysis were performed for the resultant Bana grass chars (BGC) which are presented in Table 4.2. The results show that the volatile matter and oxygen content are reduced significantly under all treatments, however the char particles heated to maximum temperature of 400 °C still contain significantly amount of oxygen compared to coal A. The char particles produced under pyrolysis temperature of 600 °C contain the lowest amount of oxygen, but the volatile content is also reduced significantly. These results are confirmed by the gas analysis curves in Figure 4.6. When the samples are heated to 600 °C large amount of reducing gases e.g., H_2 and hydrocarbons are also removed.

Table 4.2: Proximate and ultimate values of the Bana grass char (BGC) produced from pyrolysis process using ISO 17246:2010 standards.

Proximate Analysis wt% (db)	BGC 400°C	BGC 500°C	BGC 600°C
Moisture/ % (ad)			
Volatile Matter	28.8	19	13.2
Ash	8.19	9.6	10.38
Fixed Carbon (by difference)	63.01	71.4	76.42
Ultimate Analysis wt% (db)			
Carbon	74	78.6	82.4
Hydrogen	3.83	3.28	2.87
Nitrogen	0.52	0.46	0.45
Sulphur	0.14	0.14	0.14
Oxygen by (difference)	13.32	7.92	3.76

db - on a dry basis; ad - on an air dried.

Based on the combination of findings from gas analysis for pyrolysis and analysis of the solid residuals, the BGC particles produced under pyrolysis temperature of 500 °C

appear to have more comparable chemical properties to coal A (HIsarna injected coal). Therefore, approximately 300g torrefied grass is pyrolysed to 500 °C following the procedures described previously and then the resultant chars crushed into small particles with the size range from 90 to 300 μm.

Chapter 5

Devolatilization Characteristics of Coal and Biomass with Respect to Temperature and Heating Rate for HIsarna Alternative Ironmaking Process

5.1 Hypothesis to be investigated

Hypothesis 1 – Once a biomass or thermal coal particle is injected into the vicinity of the slag-metal interface in the SRV, devolatilization happens first.

5.2 Introduction

The granular thermal coal (or other carbonaceous materials) is injected into the slag layer in the SRV bath to reduce iron oxide to liquid metal and carburize the liquid metal [28, 32]. The smelting reactions are shown in equations (1) to (3), (1) is an overall FeO reduction by carbon dissolved in the metal or solid char and (2) and (3) are intermediate/alternative steps [25].

Replacement of coal with a carbon-neutral biomass in ironmaking offers great potential to reduce reliance on non-renewable carbon sources in this major contributor to carbon dioxide emissions from the steel industry. However, to maintain HIsarna's performance while substituting coal, carbonisation of raw biomass is necessary to increase fixed carbon (C_{fix}) content and remove moisture, oxygen and part of the volatile components, since existence of these components decrease the energy content [14]. Different thermochemical conversion technologies can be used for pre-treatment of the raw biomass to obtain chars with suitable properties for HIsarna. The pre-treatment conditions as well as the type of raw biomass determine the chemical, physical, and mechanical properties of the chars. These characteristics are the necessary properties to produce chars which qualities most closely resembles the thermal coal currently used in the HIsarna process to maintain process efficiency and enable the technological shift in raw material use [33].

Once being injected into the smelting reduction vessel, the carbonaceous materials go through complex reactions, two of which are devolatilization and burning out of the carbon. Devolatilization happens first, and it continues to influence the solid carbon particles to the point when it is burnout [82]. The gaseous products evolved during the heating process are light hydrocarbons (mainly CH_4 and C_2H_6) which may crack into

C and H_2 or react with the environment to form CO and H_2 or a mixture of H_2, H_2O, CO, and CO_2, the balance of which will change the reducing environment and control other parameters such as ignition, temperature, and flame stability in the post combustion zone. As such devolatilization of carbonaceous materials used in HIsarna technology is a key phenomenon which needs to be considered to achieve high efficiency [83]. While volatile matter is released the char structure goes through significant changes e.g. particle break-up, softening and swelling, which is strongly dependant on the chemical properties and reaction conditions such as heating rate, temperature and pressure [82].

Biomass devolatilization usually involves the thermal decomposition of three components namely hemicellulose, cellulose, and lignin [84]. The process of decomposition for these components proceeds in three stages: moisture desorption, active decay and passive decay. Moisture desorption occurs at temperature < 150 °C. This is followed by active decay in which most of the volatile matter is released at temperature between 200-500 °C, during this stage decomposition of hemicellulose and cellulose takes place. Decomposition of lignin starts in active decay and continues to passive decay at a very slow rate through the full temperature range of treatment [85]. Coal devolatilization proceeds through a similar thermal degradation process, starting with moisture desorption at temperature < 150 °C and then degradation mobile and immobile phases occur at the temperatures between 150-600 °C. This results in the formation of the aliphatic and aromatic tar components and a number of light gases (e.g., H_2O, CO, CH_4 and CO_2). The final stage of thermal coal decomposition is the breakup of heterocyclic compounds at temperature higher than 600 °C [86].

The literature contains studies on coal and biomass pyrolysis by using TGA [85-87], fixed-bed reactors [88-90] and fluidized-bed reactors [91, 92]. TGA is the most common technique used to study thermal decomposition and kinetic analysis of coal and biomass. Combining this equipment with different analytic techniques, e.g. Fourier transform infrared spectrometry (FTIR) [93-96], gas chromatography (GC) [94] and mass spectrometry (MS) [97-103] is quite common. Using these techniques, the gaseous products evolved during heat treatment can be investigated simultaneously or afterwards to establish the mechanism for coal and biomass decomposition. TG-MS technique has been applied because of its main advantage of being the on-line monitoring of evolving gases, which can be used simultaneously with TG equipment

to monitor the gas atmosphere during sample decomposition. The effect of important parameters such as particle size, heating rate, holding time and gas atmosphere have been studied using TGA. In addition, there are numerous studies which used simultaneous thermal/gas analysis to analyse evolved gases.

Much of the pyrolysis work done on gas evolution analysis has focused on determining the effect of coal rank on the off-gas generated during thermal processing. Chinese coals with different grades and different H/C atomic ratios have been studied using simultaneous gas analysis under an inert atmosphere [97-99], and it was found that thermal decomposition and gas evaluation behaviour of coals are strongly dependent on temperature and the coal rank. This method has also been used to study the effect of temperature and time interval [102] with regards to devolatilisation kinetics for different types of biomass and coal/biomass blends [101, 102]. These researchers found that devolatilisation of biomass is dependent on chemical properties including ash and volatile contents, temperature and thermal treatment time. Additionally, the off-gas of chitin biomass with various molecular structures in an inert atmosphere was studied to determine the influence of zeolite catalysts on the utilization of chitin biomass [105].

Although extensive research has been carried out on the devolatilization behaviours for a number of different coals and biomass, the research and development for the carbonaceous materials (coal and biomass) for HIsarna technology is scarce, and also there is very limited information on direct comparison between coal and biomass in term of devolatilization. Much of the research done on devolatilization or gas evolution focused on the pyrolysis of coals and biomass using simultaneous TGA-MS carried out with small sample size between (10-20) mg. Despite all the advantages of simultaneously measurement such as real time analysis, qualitative and quantitative analysis but small sample size may mean high level of uncertainty in the off-gas analysis due to side reactions. An increase in the sample size in TGA can cause a temperature distribution problem and on the other hand, TGA may struggle to handle heavy tar products if sample size increased. In this study a high temperature vertical tube furnace coupled with a mass spectrometer is utilised to reliably study larger samples with regards to their devolatilization characteristics with an aim of attaining a more accurate representation of gaseous product evolution from each sample under

novel alternative ironmaking technologies. This research aims to enable the selection of suitable fuel mix for the HIsarna alternative ironmaking process.

5.3 Experimental

5.3.1 Sample preparation

This chapter investigates six carbonaceous materials (four coals and two biomasses) listed in Table 4.1. using the preparation procedures described in section 4.7.1.

5.3.2 Thermogravimetric analysis

The mass loss due to devolatilization under non-isothermal conditions was determined by using thermogravimetric analysis (TGA). A 20 mg ± 0.01 sample was placed in an alumina crucible (height 4 mm x diameter 6.8 mm). Considering it is suggested to use samples weighing between 2 and 50 mg for most TGA measurements, the sample mass of 20 mg was selected for this study to obtain accurate measurements. Chen et al [97] studied the effect of samples mass on the mass and heat transfer and found 20 mg samples to produce better results than smaller sample weights. The alumina crucible with test sample was placed on a platinum stage, which has a thermocouple located directly underneath to provide real temperature of the sample tested. All the samples were heated in a high impurity (99.9999%) argon atmosphere at the flow rate of 50 ml/min. The mass loss due to volatile matter evolving was recorded from ambient temperature to 1500 °C, at the heating rates of 10, 20 and 30 °C/min respectively. To ensure the reliability and reproducibility of the tests, preliminary tests have been carried out to define experimental conditions, and the test for the same sample has been repeated three times to produce concordant results.

5.3.3 VTF-QMS gas analysis

The gas analysis during devolatilization was carried out using a Carbolite-Gero high temperature vertical tube furnace described in section 4.2 shown in Figure 5.1. The furnace was coupled with a Quadrupole Mass Spectrometer (QMS) to monitor gaseous products evolving from the samples. The VTF-QMS combination allowed an increase in the sample weight to produce more representative volatile measurements of the bulk material and reduce measurement uncertainties. The samples were heated to 1500 °C in a high purity (99.999%) argon atmosphere at the heating rate of 10 °C/min while the furnace exhaust was connected to the QMS through a heated capillary (150 ^{o}C) to monitor gaseous products evolving from the samples and ensure no condensations

occurred before the ionization chamber. Each sample was weighed to be approximately 1.0 g and placed in an alumina crucible on the alumina pedestal and lifted to the hot zone of the vertical tube furnace (VTF). The tube was sealed, vacuumed using a standard rotary pump and then back filled with argon gas at a flow rate of 300 ml/min that carried gaseous products to the mass spectrometer (QMS). The argon concentration was measured to be 99.7% before the furnace heating cycle started. The QMS was set to measure readings of the following gases evolving from devolatilization: N_2, O_2, CO, CO_2, Ar, H_2O, H_2, CH_4 and C_2H_6. After the desired temperature was reached, the furnace cooled down at 5 °C/min to room temperature in Ar atmosphere. Then the samples were taken out to weigh and analyse.

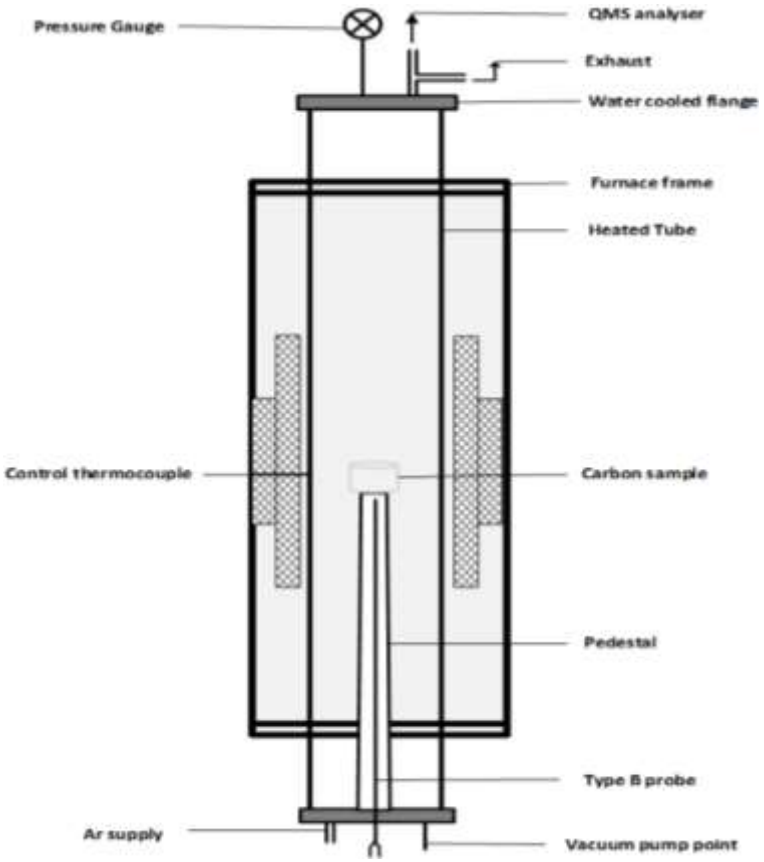

Figure 5.1: Vertical tube furnace (VTF) setup with a mass spectrometry for slow devolatilization study. The quadrupole mass spectrometer (QMS) is connected to the gas sampling port.

5.4 Results and discussion

5.4.1 TG-DTG analysis

The weight loss curves, and derivative thermogravimetric (DTG) curves produced from the TGA tests for the materials in Table 4.1, are shown in Figures 5.2a and 5.2b respectively. Figure 5.2a shows the weight loss due to devolatilization of the samples at the heating rate of 10 °C/min under argon atmosphere.

Slow weight loss begins for all four coal samples at the temperature of ~100 °C and continues to ~180 °C, which is mainly associated with surface moisture loss. This is followed by rapid weight loss due to the release of organic volatile matter, and the starting temperature of the release of organic volatile matter depends on the volatile matter content of the coal sample. The weight loss curve starts at lower temperature for coals with higher volatile matter, but all the curves stabilise at the temperature of around 650 °C regardless of the volatile matter contents. However, slow weight loss to the temperature of 1500 °C was still notable, this could be from decomposition of materials with a higher activation energy e.g., carbonyl and heterocyclic compounds, which subsequently leads to CO and H_2 formation [83].

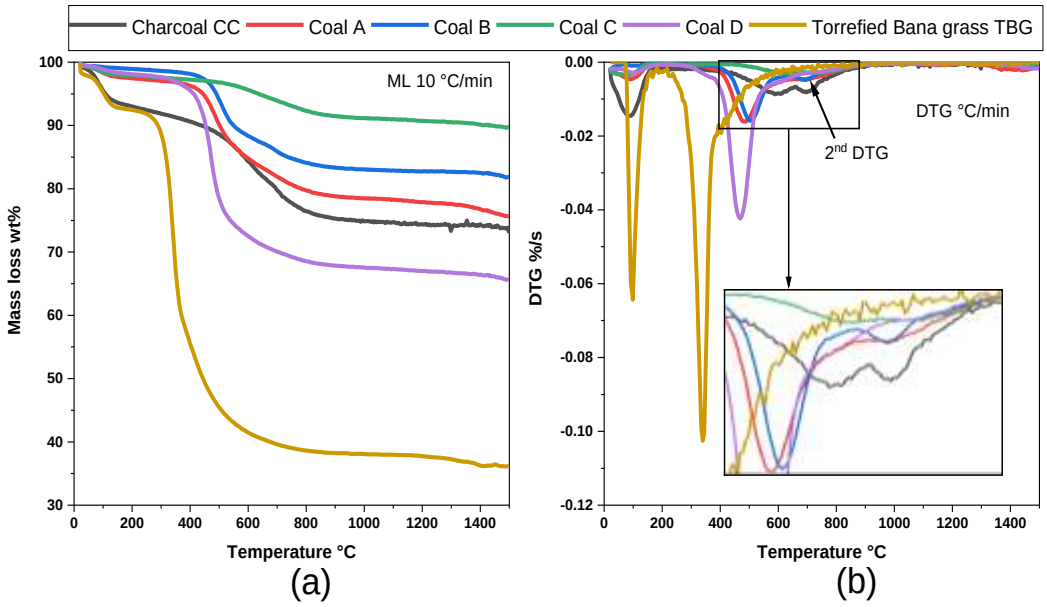

Figure 5.2: (a) Mass loss curves and (b) DTG curves of the carbonaceous materials tested in the argon atmosphere at the heating rate of 10 °C/min from room temperature to 1500 °C.

These thermal decomposition results for coal samples can be explained with the reported mechanisms of coal devolatilization [106], such as the devolatilization process proposed by van Heek and Hodek (Figure 5.3) [86]. Coal decomposition starts with desorption of moisture and some light gasses at the temperatures of ~100 °C. On

continued heating to ~250 °C the mobile phase degradation occurs which leads to tar formation, in particular the aliphatic tar component. Then at the temperatures of 300 °C and higher, degradation of the immobile phase occurs which results in formation of the aromatic tar components and a number of light gases (e.g., H_2O, CO, CH_4 and CO_2) as shown in Figure 5.3 [86], which is evidenced by the experimental results shown in Figure 5.4 (section 5.4.2). This is followed by decomposition of heterocyclic compounds at temperatures higher than 600 °C producing N_2, CO and H_2 gases.

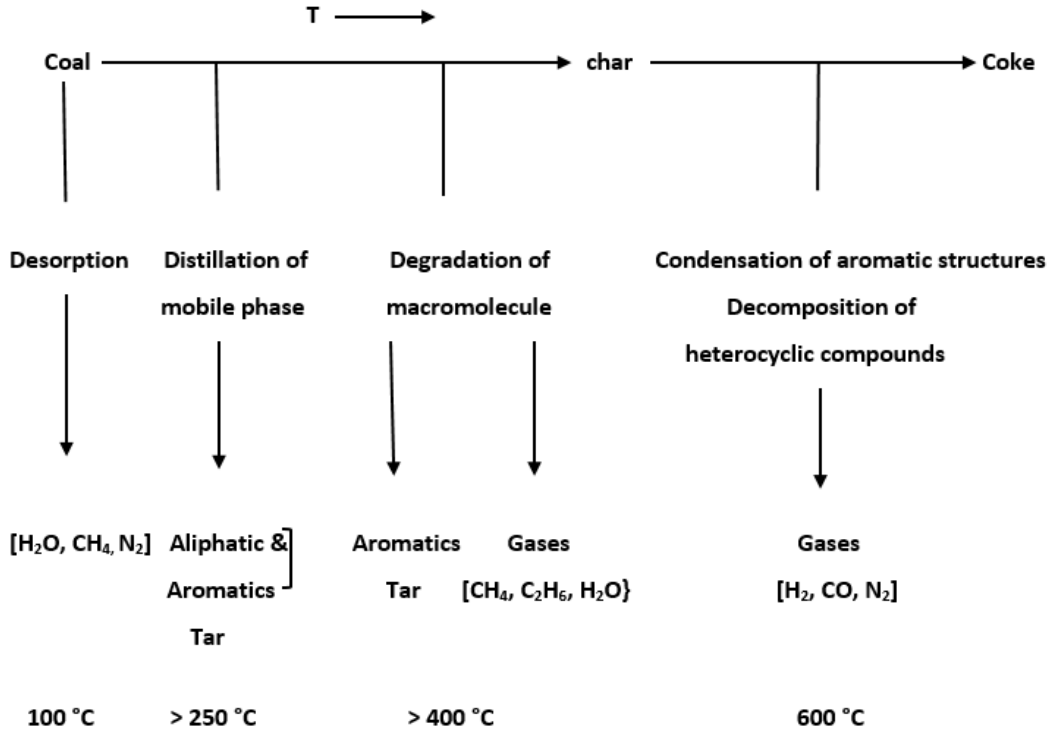

Figure 5.3: The main reactions occurring during the coal devolatilization process [86].

As shown in Figure 5.2, the decomposition behaviour of biomass samples is different from the four coals tested. The initial weight loss for both torrefied grass and charcoal starts at slightly lower temperatures of ~80 °C and continues steadily to the temperature of 200 °C. After this a sharp weight loss curve for torrefied grass occurs at temperatures from ~250 °C to 400 °C and the weight loss continues slowly to 1500 °C. However, the second step of weight loss for charcoal starts at much higher temperature of ~500 °C and continues to 1500 °C with a flatter weight loss curve that is because of the pre-treatment of the starting material. Decomposition of hemicellulose is expected to occur at the lower temperature range due to its random

amorphous structure. The subsequent decomposition of cellulose and lignin follows at higher temperatures as the materials are more ordered and stronger bonded respectively. Biomass has a porous structure providing higher adsorption potential than thermal coal, which is likely to allow large amounts of moisture and carbon dioxide to be absorbed from the atmosphere. These absorbed components are weakly bonded and evolve at the very low temperatures [107]. Cellulose is the main component responsible for the second DTG peak, while lignin is the main component responsible for char formation. However thermal degradation of lignin can start at low temperature at a very slow rate and increases with the increase in temperature [108].

Figure 5.2b shows similar behaviour for coal samples, starting with the small peak at low temperature due to desorption followed by a large single peak due to devolatilization. The exception for this is with coal B which has produced a clear secondary peak for devolatilization, meaning coal B goes through extra phase of decomposition. However torrefied grass and charcoal both produced larger initial DTG peaks due to moisture loss followed by two devolatilization peaks. There is one sharp peak which starts at the temperature of ~250 °C and the second peak which is partially superimposed on the late phase of the first peak for torrefied grass. This behaviour is linked to decomposition of cellulose and lignin respectively, while charcoal produces two peaks at much higher temperatures compared to torrefied grass which are from decomposition of lignin and agrees with other researchers' findings on similar materials [87, 106].

5.4.2 Comparison of devolatilization behaviours for different carbonaceous materials

Various reactions occur simultaneously during devolatilization upon heating, including break-up of chemical bonds, vaporisation, and condensation or recombination [95]. Using a quadrupole mass spectrometer (QMS) gaseous species evolved during heating process were measured continuously up to the temperature of 1500 °C. Figure 5.4 shows the mass loss due to devolatilization measured in TGA tests against the normalized off-gas species measured in the VTF-QMS tests at the heating rate of 10 °C/min for the two biomass and four coal samples.

Similar behaviour has been observed for all the samples that gas species detected at low temperature of 100~200 °C were mainly H_2O, as the weight loss at low

temperature is associated with the loss of surface moisture. However, at this low temperature range, the weight loss of the biomass samples was significantly higher than that of the coal samples measured, which is confirmed by the amount of these gases detected. Devolatilization continued with increasing temperature, generating large amount of H_2O and CO_2 gas by biomass samples at temperature of >300 °C while none or very small amount of CO_2 from coal samples was measured but still significant amount of H_2O was produced. The amount of H_2O and CO_2 produced from torrefied grass during heating was much higher than charcoal, as charcoal has already been pre-treated. However, the amount of gas species generated by charcoal was still significantly higher than that from any of the coal samples tested at similar temperatures, which could be due to higher oxygen content in the charcoal, resulting in the oxidation of carbon and contributing to higher mass loss in charcoal.

The second region of weight loss is associated with the release of organic volatile matter, which started at similar temperatures for all the samples, but the gas species generated were different. Both biomass samples started to generate H_2O and CO_2 at temperature > 300 °C, followed by the release of hydrocarbons at temperature > 400 °C, and H_2 and CO at > 500 °C. The peaks for gases generated in VTF-QMS tests spread over larger temperature range than those observed in TGA tests. This is caused by the gas mixing in the VTF, and the time require for evolved gases travelling from the sample location to the detection of mass spectrometer. This travelling distance in the VTF tube gives rise to the comparatively consistent delay for all devolatilization peaks compared to the TGA results. All the four coal samples tested were found to produce H_2O, CO_2, CH_4, C_2H_6 and H_2 at temperatures > 500 °C which corresponds to the region of mass loss in the TGA test results. The H_2O released at temperature >150 °C is associated with the release of inherent moisture which presents in the pore/capillaries of the carbonaceous materials and H_2O produced from decomposition of organic components. It is also known that some H_2O exist as part of the crystal structure of inorganic minerals which can contribute to H_2O formation at higher temperatures [109].

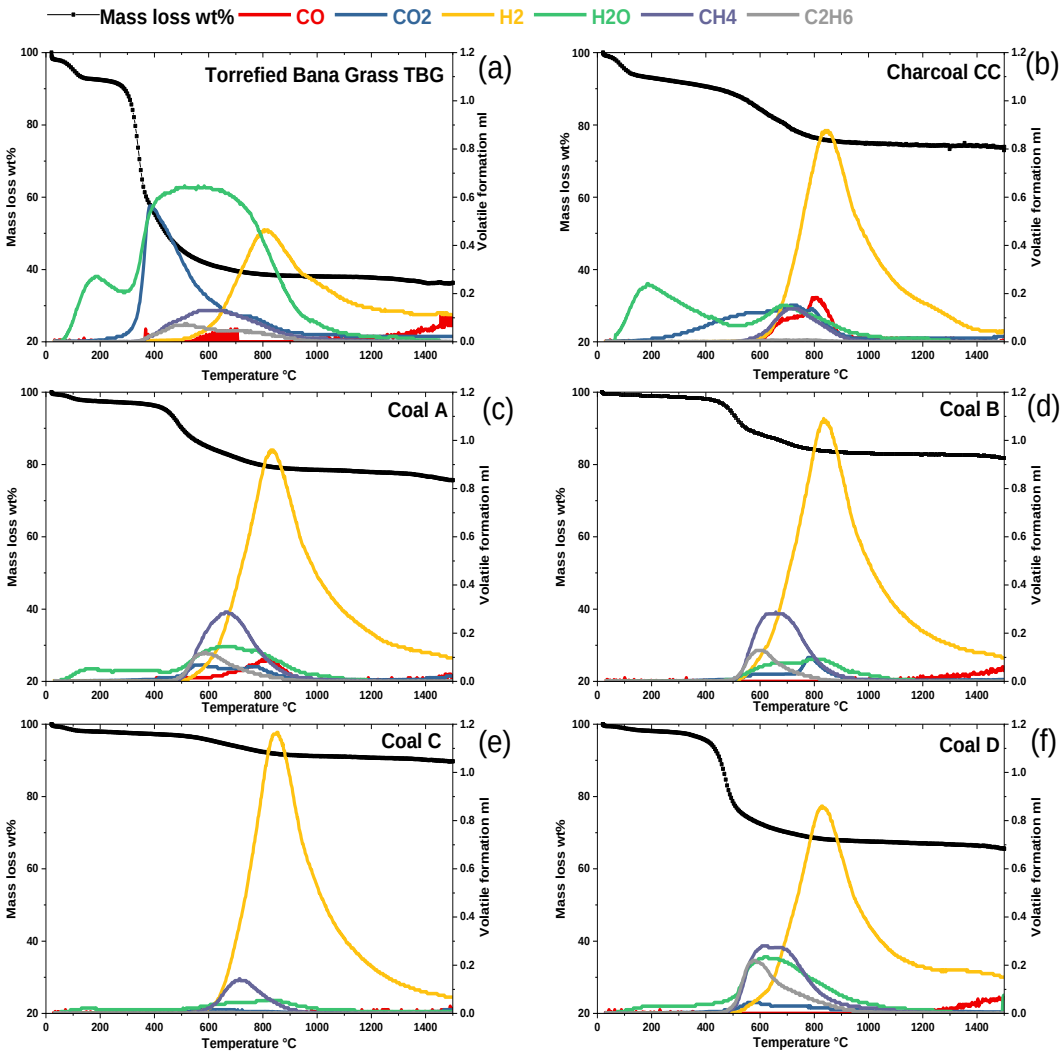

Figure 5.4: VTF-QMS for normalised gas species (CO, CO_2, H_2, H_2O, CH_4, and C_2H_6) evolved against TGA mass loss during heating at the heating rate of 10 °C/min under argon atmosphere for (a) Torrefied Bana grass (TBG); (b) charcoal (CC), (c) coal A; (d) coal B; (e) coal C; (f) coal D.

The gas products evolved during the heating process are plotted in Figure 5.5, and some common phenomena can be observed for the biomass and coal samples. As it can be seen both charcoal and torrified grass samples produced larger amounts of H_2O at low temperature (100 to 200 ̊C) than that of all coal samples. Each sample produced a peak for H_2O and CO_2 gas during the heating within the temperature range of 300 - 800 °C, but the peak for both biomass samples was significantly larger than those for the four coal samples. The sharp H_2O and CO_2 peaks for torrefied grass at the temperature of 300-400 °C links well with the second sharp DTG peak for torrefied grass (shown in Figure 5.2b) and presents the case that this is due to the release of H_2O and CO_2 from decomposition of hemicellulose and cellulose at that temperature.

Charcoal produced a flatter but wide peak of H_2O and CO_2 which may be because of the sample already being pre-treated to similar temperatures during the charcoal formation. Previous studies linked the amount and the temperature required for the gas species to be produced to the chemical structure of the biomass component used for the investigation [110]. Hemicellulose is higher in carboxyl content which results in higher CO_2 yield, while cellulose contains carbonyl and carboxyl species which results in CO and CO_2 product yield, and Lignin releases much more H_2 and CH_4 from cracking of aromatic rings and methoxyl [87, 108].

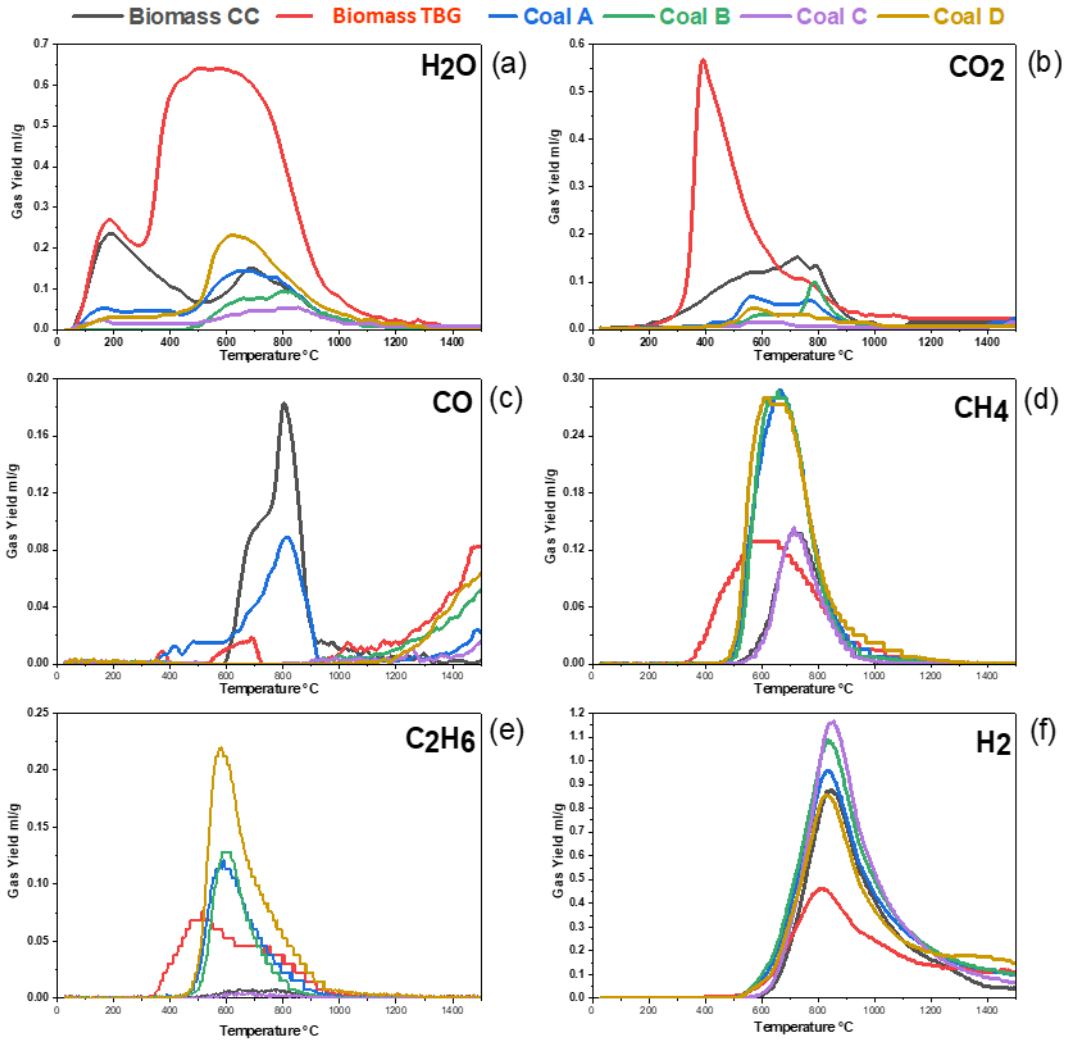

Figure 5.5: An off-gas analysis of (a) H_2O; (b) CO_2; (c) CO; (d) CH4; (e) C_2H_6; and (f) H_2 evolved during VTF-QMS experiments.

Torrefied grass was the only material which started to produce CH_4 and C_2H_6 at the temperatures under 400 °C, while all the other samples produced these gases at the temperature > 500 °C. Finally H_2 and CO formation happened in the higher

temperature range which is linked to reactions that take place at higher activation energy [80, 109]. In addition, the thermal cracking of hydrocarbons is possible at temperature > 600 °C. The formation of CO and H_2 at high temperature is also linked to CH_4 reaction with CO_2 to form CO and H_2 [112]. Also hydrocarbons evolved at higher temperatures may react with H_2O to form H_2 and some CO [101, 111] through the reaction schemes presented in equations (8) and (9).

$$CO_{2\,(g)} + CH_{4\,(g)} \rightarrow 2CO_{\,(g)} + 2H_{2\,(g)} \quad (8)$$

$$H_2O_{\,(g)} + CH_{4\,(g)} \rightarrow CO_{\,(g)} + 3H_{2\,(g)} \quad (9)$$

5.5 Kinetic analysis

5.5.1 The Kissinger–Akahira–Sunose method

The devolatilization for carbonaceous materials is a complex process as several reactions occur during thermal decomposition, which includes carbonizing and gas evolution simultaneously during the heating process. For a better understanding of the devolatilization process, many researchers studied thermal decomposition of carbonaceous materials using TGA technique (which is the most common technique) to measure the weight loss for kinetic analysis. The kinetic parameter obtain are used to understand the complexity of the reaction and in modelling devolatilization process to predict the mass and energy balances. The devolatilization mechanism can be described as following: [96]

Raw carbonaceous materials $\longrightarrow$ Volatile + Char

The devolatilization conversion and apparent rate of reaction is calculated through equation (10):

$$\frac{da}{dt} = k(T)f(a) \quad (10)$$

The temperature dependent reaction rate constant k (T) can be expressed by equation (11):

$$k(T) = A\, e^{\left(\frac{-E_a}{RT}\right)} \quad (11)$$

By combining equations (10) and (11) the overall reaction conversion rate can be expressed by equation (12):

$$\frac{da}{dt} = A\, e^{\left(\frac{-E_a}{RT}\right)} f(a) \quad (12)$$

where a, $\frac{da}{dt}$, A, Ea, R, T, and f (a) denote the devolatilization conversion degree, reaction conversion rate, pre-exponential factor, activation energy, universal gas constant, temperature, and reaction function respectively.

The devolatilization conversion degree (a) is defined by equation (13):

$$a = \frac{mi - mt}{mi - mf} \tag{13}$$

where mi is the initial weight of the sample, mt is the instant weight of the sample at time t, and mf is the final weight of the sample after the reaction.

The experiments are carried out using non-isothermal heating with a constant linear heating rate, β :

$$\beta_i = \frac{dT}{dt} \tag{14}$$

where i represents the given heating rate being considered.

The following equation for reaction conversion rate can be obtained by equations (12) and (14):

$$\frac{da}{dT} = \frac{A}{\beta} e^{\left(\frac{-E_a}{RT}\right)} f(a) \tag{15}$$

Equation (16) can be obtained by integrating equation (15) to represent the cumulative reaction rate:

$$g(a) = \int_0^a (f(a))^{-1} = \frac{A}{\beta} \int_0^T e^{\left(\frac{-E_a}{RT}\right)} dT \tag{16}$$

where $g(a) = \int_0^a (f(a))^{-1}$ is the integral form of the reaction model [105]. There are several integral methods available which can be used to accurately estimate kinetic parameter. Among them Kissinger–Akahira–Sunose (KAS) model is used by many researchers as a proven model, since the kinetic parameters of a solid-state reaction can be obtained without knowing the reaction mechanism and also it is known to have high accuracy in estimating kinetic parameter [82, 102]. The apparent activation energy (Ea) obtained by plotting natural logarithm of heating rate over temperature square at a given value of conversion $\ln(\frac{\beta_i}{T_{ai}^2})$ versus $\frac{1000}{T_{ai}}$, which is represented by a linear equation (17) for the KAS model for a given value of conversion, a, where the gradient is equal to $-\frac{E_a}{R}$ [114].

$$\mathrm{In}\left(\frac{\beta \mathrm{i}}{\mathrm{T}a\mathrm{i}^{2}}\right) = \mathrm{l\,n}\left(\frac{\mathrm{A}a\ \mathrm{R}a}{\mathrm{E}_{a}\mathrm{g}a)}\right) - \frac{\mathrm{E}_{a}}{\mathrm{RT}_{a\mathrm{i}}} \quad (17)$$

5.5.2 Kinetic analysis

The results obtained from the TGA tests at three heating rates (10, 20, and 30 °C/min) are inputted to a calculation according to the KAS method in order to calculate the activation energy (E_a) [84]. This method allows an overall activation energy to be calculated by averaging the activation energy at each conversion point. There are other models which use temperature at the maximum DTG peak (maximum rate of mass loss) for each heating rate to calculate overall activation energy rather than at each conversion. The maximum DTG peak method assumes that the reaction mechanism is the same throughout the decomposition reaction. However, a single point reaction at peak temperature is not the same as what is observed during the reaction earlier or later than that point. Therefore, alternative kinetic models such as Kissinger–Akahira–Sunose (KAS) and Flynn–Wall–Ozawa methods (FWO) have been developed to determine activation energy at different conversion points to overcome the difference in the reaction mechanism and use average activation energy for the whole reaction. The Kissinger–Akahira–Sunose (KAS) iso-conversional model is commonly used by researchers for kinetic analysis of carbonaceous materials as a proven model due to its high accuracy in predicting kinetic parameters [104]. As can be seen from off-gas analysis plots in Figure 5.5, at the temperature of < 200 °C the weight loss is mostly related to surface moisture, with the devolatilization process related to reducing gases beginning at > 200 °C and then proceeding rapidly to 900 °C. So, the devolatilization conversion degree (a) was calculated according to equation (13) for weight loss in the temperature range of 200-900 °C for all carbonaceous materials tested. Figure 5.6 shows the devolatilization conversion degree (a) for torrefied grass (TG) as a function of temperature in TGA tests at the heating rates of 10, 20, and 30 °C/min.

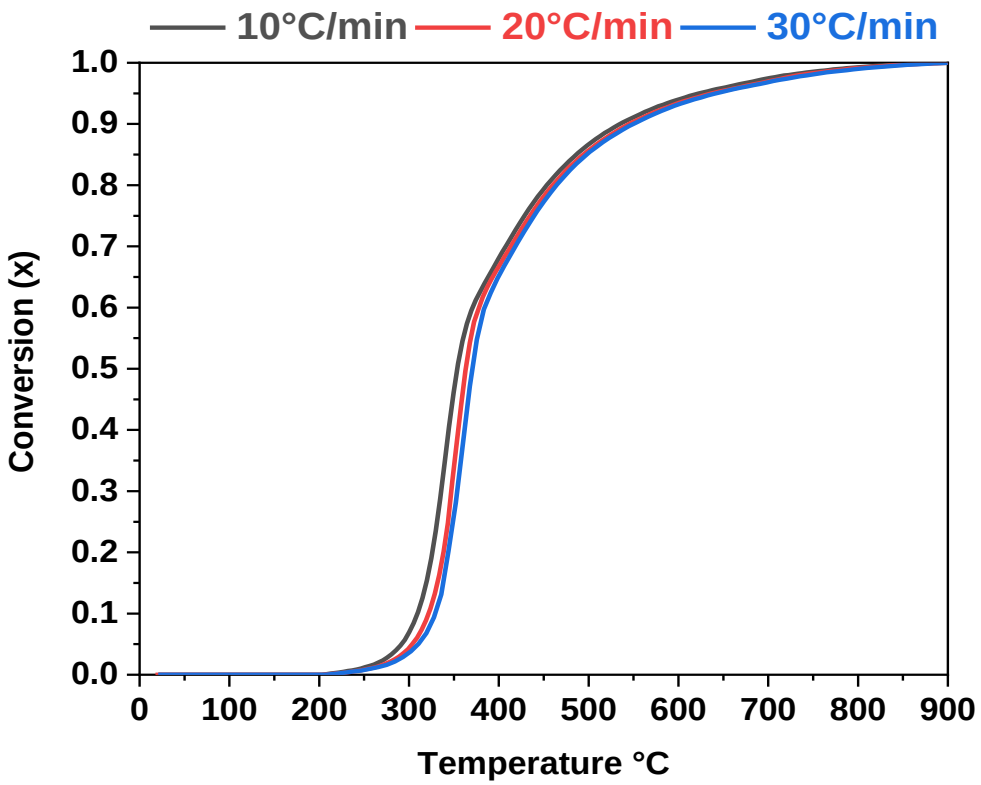

Figure 5.6: Extent of conversion curves for the devolatilization process of torrefied Bana grass (TBG) as a function of temperature in TGA tests at different heating rates.

The apparent activation energy from a plot of $\ln(\frac{\beta i}{T_{ai}^{\ 2}})$ versus $\frac{1000}{T_{ai}}$, for a given value of conversion (a) in the range of 0.2 to 0.8 is shown in Figure 5.7 for torrefied Bana grass (TBG). The average activation energy is calculated from the gradient equal to $-\frac{E_a}{R}$ and the correlation coefficients. R^2 values corresponding to the linear lines of best fit were in the range of 0.91 to 1.00 [106] showing good agreement.

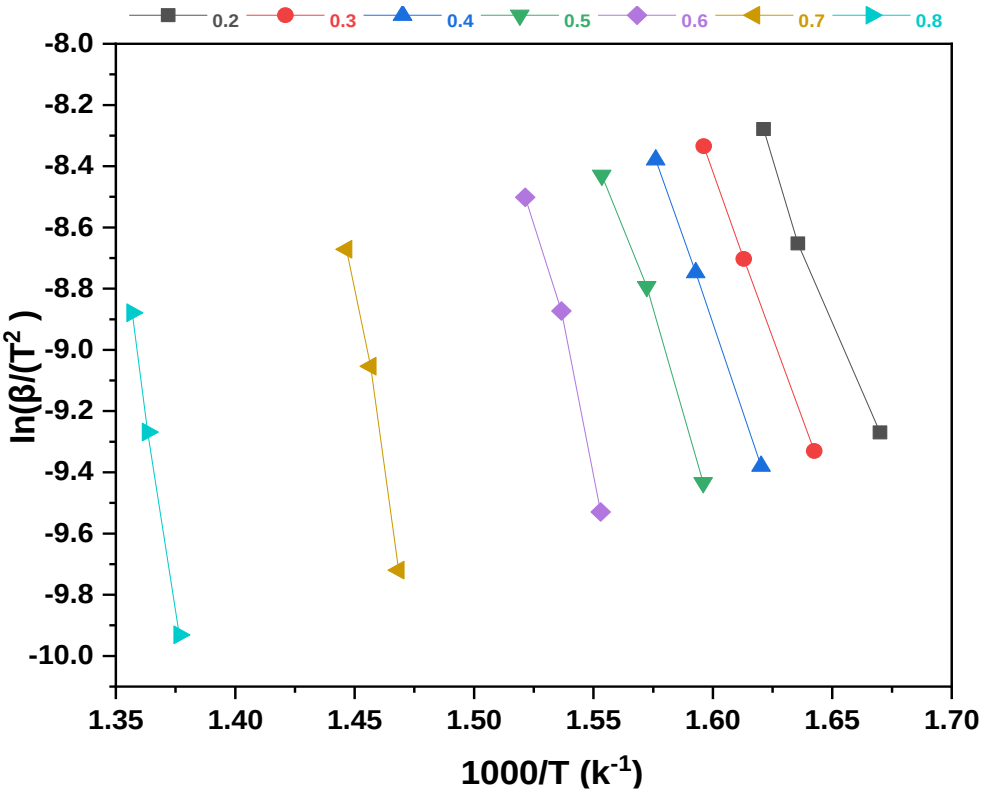

Figure 5.7: KAS plot of torrefied Bana grass (TBG) for different values of conversion to calculate the activation energy at different heating rates.

Table 5.1 contains the calculated variables for all carbonaceous materials tested in this study. It is seen that the apparent activation energy was not the same for all conversion degrees, which confirms the occurrence of different reactions at different temperatures during the experiment. Charcoal has quite high and stable E_a values throughout, and the value does not change a lot with the change in conversion degree probably because of the effects of pre-treatment on this material. Torrefied grass behaved differently, starting with a low E_a value at a low conversion degree and increasing linearly with an increase of conversion. This may correspond to low E_a values for decomposition of the remaining hemicellulose and cellulose but higher E_a values for lignin decomposition. Coal A shows a similar behaviour to charcoal with quite stable high E_a values, while coal B which contains medium volatile matter content has low stable E_a values. Coal C has low E_a value at low conversion degree and increases linearly with an increase in conversion. Coal D starts with low E_a value at low conversion degree and increases linearly with an increase in conversion degrees up to 0.6 conversion, and then there is a significant increase in the values at conversion degrees of 0.7 and 0.8. This behaviour may be influenced by error in the method since the

difference for conversion degrees at different heating rates are not very large, which is seen in Figure 5.6.

Table 5.1: Activation energy E_a values in kJ/mol obtained for different carbon sources by using KAS, R^2 corresponding to linear fittings

	CC		TBG		A		B		C		D	
Conversion (x)	E_a	R^2	E_a	R^2	E_a	R^2	E_a	R^2	E_a	R^2	E_a	R^2
0.2	201	0.99	165	0.99	215	1.00	183	0.96	77	0.95	192	0.99
0.3	224	1.00	179	1.00	246	1.00	194	0.97	120	0.93	242	0.99
0.4	293	1.00	189	1.00	247	1.00	197	0.97	154	0.93	278	1.00
0.5	313	1.00	198	0.99	268	1.00	193	0.96	185	0.95	311	1.00
0.6	341	1.00	271	0.98	304	1.00	180	0.91	219	0.94	390	0.99
0.7	366	1.00	400	0.99	294	1.00	169	0.92	264	0.95	650	0.98
0.8	294	1.00	440	1.00	323	1.00	173	0.95	335	0.95	1897	95.00
Average E_a	290		263		271		184		194		566	

These kinetic models assume the same reactions occurring at a specific conversion degree for different materials but as it can be observed from Figure 5.4 multiple reactions take place at different temperatures. Therefore, it is difficult to make accurate comparison between different carbon materials. This means the reaction mechanism can change during the devolatilization process, therefore E_a is dependent on conversion and the average value of E_a can be estimated as a function of conversion. Kinetic analysis showed charcoal, torrefied grass, and coal A (already injected in HIsarna trials) have similar average activation energy values (290, 263 and 271 kJ/mol respectively). Since decomposition of the carbon materials consists of multiple chemical reactions, the E_a value may change depending on the reactions taking place at specific conversion degree. It can be noticed in Figure 5.8 that the value of E_a increases with an increase in conversion.

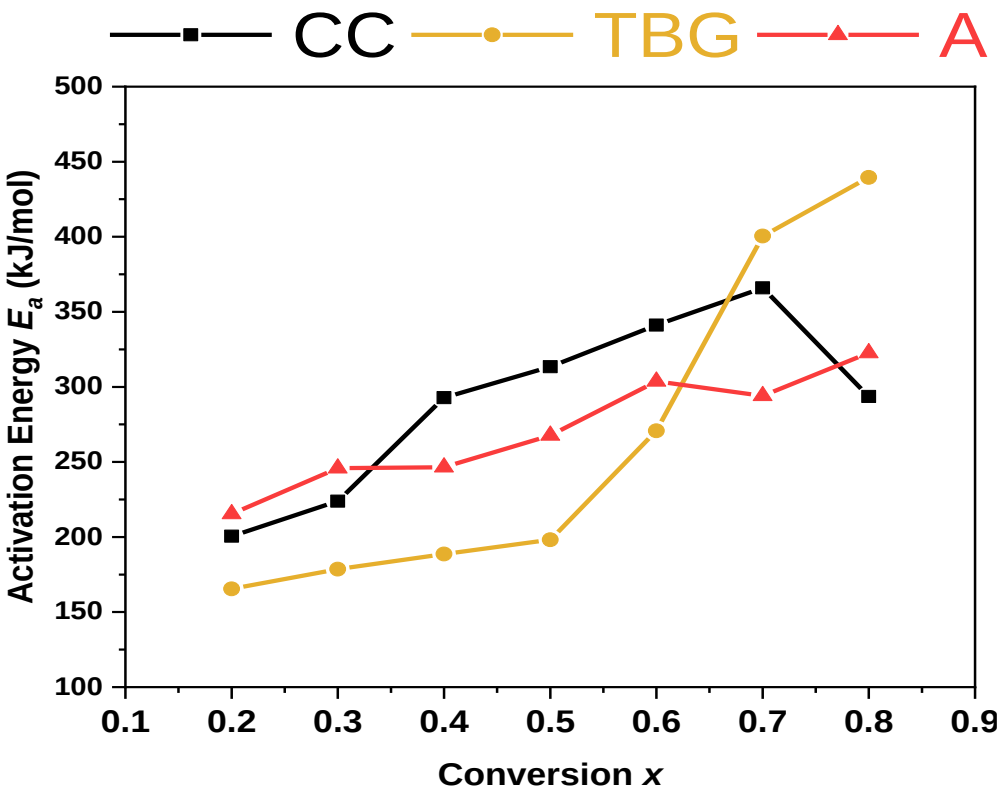

Figure 5.8: Activation energy E_a as a function of the conversion degree for charcoal (CC), torrefied Bana gas (TBG) and Coal A.

The increase in E_a for torrefied grass is notably larger. This is because at low conversion levels very large amounts of weakly bonded components evolved e.g., H_2O and CO_2 shown in Figure 5.4 (a), therefore less energy is required for them to be removed. Charcoal starts with lower E_a at conversion degrees of 0.2 and 0.3 compared to coal A, but coal A has lower E_a at conversion degree of 0.4 - 0.7. As can be seen in Figures 5.4 (b) and (c) charcoal produces larger amount of CO_2 at low temperature where coal A produces more of the other volatiles e.g., CH_4, C_2H_6 and H_2 at lower temperature which confirms the differences in the E_a values. Based on off-gas analysis and kinetic values charcoal with current properties is the more likely source of biomass which can replace thermal coal in HIsarna technology, however material handling and pre-treatment may need to be re-considered to optimise its use in the process.

5.6 Comparison of carbonaceous materials for HIsarna process

The results of this study indicate that different reactions take place during specific conversion degree for different carbon materials, therefore devolatilization is affected by the material properties which in turn is linked to volatile mater content. There have been similarities in devolatilization behaviour (such as devolatilization temperature),

which is essential for smelting reduction vessel in HIsarna process. Biomass samples produce significantly larger amount of H_2O and CO_2 at low temperatures, however, coal samples produce more CH_4, C_2H_6 and H_2.

Despite the pre-treatment of biomass charcoal samples, this study shows that there is still significant weight loss (release of H_2O) at low temperatures because H_2O is absorbed from atmosphere due to their porous structure of the charcoal. Torrefied grass releases a large amount of H_2O and CO_2 at the temperature between 300-400 °C due to its high oxygen potential. These gases and H_2O releasing at lower temperatures can cause temperature drop in the HIsarna furnace which needs heat compensation and due to high O_2 level much more carbon material may be needed. To avoid these problems and utilise torrefied grass efficiently, a pre-treatment at the temperature of up to 500 °C in inert atmosphere is necessary to reduce the oxygen content and produce bio-chars with similar chemical properties to thermal coal currently used in HIsarna. To complete this process heat sources from other parts of the steel plant can be utilized to keep the "green" credentials of biomass, the gasses and tars released in the pre-treatment process can be used to generate heat and power for HIsarna process.

Because of the porous structure of biomass carbon sources (e.g., charcoal), material handling needs to be different to avoid H_2O absorption from atmosphere which is evidence in the test results. It may need to consider pre-heating biomass to the temperature of ~200 °C before injection to remove all H_2O and other oxide impurities from biomass surface to maintain HIsarna process efficiency. Further studies may be required to investigate the effect of H_2O content in carbonaceous materials on HIsarna process such as materials handling and heat balance.

5.7 Conclusions

In order to enable the selection of suitable fuel mix in the novel HIsarna ironmaking process, four coals with notable differences in volatile matter content along with two biomass samples sourced from wood and grass origins were investigated in this study. The following conclusions can be obtained.

- The wt% of reducing gases e.g., H_2, CO, and hydrocarbons, and the temperature required for these gases to evolve was notably different for all the carbonaceous materials tested in this study, but the respective maximum peaks of evolution of these gases corresponded well to the maximum rate of mass loss.

- The off-gas analysis reveals torrefied grass contains large amount of water and carbon dioxide which will be released at very low temperature, therefore pre-treatment to the temperature of ~500 °C is necessary to produce chars with similar properties to coal injected in HIsarna.
- The change of reactivation energy E_a as a function of conversion degree is determined, which is linked to different reactions at different temperatures.
- Materials handling needs to be different for biomass (compared to thermal coal) to avoid H_2O absorption.

Chapter 6

Evaluation of devolatilization behaviour of different carbonaceous materials under rapid heating for the novel HIsarna ironmaking process

6.1 Hypothesis to be investigated

Hypothesis 2 – The devolatilization behaviour and solid char yield for carbonaceous materials can be measured using DTF-QMS techniques for injection and off-gas measuring under similar thermal condition (e.g., rapid heating and high temperature) to HIsarna SRV.

6.2 Introduction

Once the solid carbonaceous material is injected into the SRV, the particles rapidly go through a series of physical and chemical changes due to the extreme high temperatures (up to 1500 °C). Devolatilization is the first step, which results in the release of volatile matter (condensable and light gases), while the solid structure goes through dramatic transformation due to phenomena such as softening, swelling and fragmentation [32, 113, 68]. The volatile matter released, and the CO produced from carbon-slag reaction will increase a hot gas stream upward to enable partial reduction of ore and maintain the temperature in the CCF because of post-combustion. The remaining chars will dissolve into the hot metal and react with iron oxide in the slag in the SRV. The main gas species evolved during devolatilization step are H_2, CO, CO_2, H_2O and light hydrocarbons including CH_4 and C_2H_6, the balance of which will change the reducing environment and control the temperature throughout the full HIsarna technology [83]. Pre-reduction of iron ore in the cyclone is an essential step which needs to be studied to optimise HIsarna's operation and achieve high efficiency. Therefore, the reduction kinetics, melting and pre-reduction behaviour of hematite ore has been studied in reaction conditions of the smelting cyclone. To achieve these studies, thermal decomposition of hematite ore, and variation of temperature, particle size and gas concentration have been considered [26, 27,31, 114-116], while for gas composition variation effects on the reduction degree, the gas mixture with different post combustion ratios (PCR) was characterized at the temperature of 1377 °C [118]. It was found that thermal decomposition degree of hematite increases with the increase

of temperature [116], while reduction degree decreases with the increase of post combustion ratio (PCR) and particle size [114, 116]. The PCR is defined as equation (18) [117]:

$$\mathrm{PCR} = \frac{\%CO_2+\%H_2O}{\%CO_2+\%CO+\%H_2O+\%H_2} \text{ X } 100 \quad (18)$$

The devolatilization of carbonaceous materials injected into SRV provides gases for indirect reduction (e.g., reduction of iron ore by CO and H_2) and heat balance via post combustion in both SRV and CCF. Thus, this is integral to understanding the balance of productivity and heat during the pre-reduction of iron ore in CCF, which is considered as the first step of the process. In order to select the right mix of carbonaceous materials such as replacing thermal coal with biomass, it is essential to evaluate the devolatilization behaviour of different carbonaceous materials under HIsarna's thermal conditions (e.g., rapid heating and high temperature). Various factors may impact the devolatilization of the carbonaceous materials, such as structure, chemical composition and particle size of the carbonaceous materials, temperature, pressure, heating rate and reaction atmosphere [104]. A large number of studies have been performed to investigate gaseous product evolution at relatively low temperatures around 1000 °C and low heating rates of <1 °C/s using TGA-MS technique[97-99, 101-103]. However, when carbon particles are injected into SRV where the temperature is up to 1500 °C, it can experience an extremely high heating rate of 10^4-10^5 °C/s [32, 69].

Several techniques have been used to study the effect of rapid heating on carbonaceous materials devolatilization [65-69, 71, 80, 81, 113, 117-121]. Most of these experiments have been conducted at a relatively low final temperature up to 1000 °C, focusing on the characterization of char generated under high heating rates. For example, a wire mesh reactor (WMR) was used to study gas evolution from coal primary pyrolysis at heating rates of 500-1000 °C/s, and using gas chromatography and an FTIR spectrophotometer for gas analysis. It was found that the gaseous product yield increased with increasing pyrolysis temperature up to 1100 °C [81, 121]. The isothermal plug flow reactor (IPFR) was used to study the effect of rapid heating on biomass material with three torrefaction degrees, the reactivity of the chars was determined by calculating weight loss through the ash tracer method and it was found that the biomass with higher torrefaction has lower reactivity [121]. The filament

platinum pyrolyzer [120], custom made thermogravimetric analysis (TGA) furnace [122] and the drop tube furnace method [65-68, 71, 80, 120] have all been used to produce chars through rapid heating to different final temperatures. The solid char particles produced via these experimental techniques were used for further analysis to investigate the effect of different rapid heating conditions on char formation. By performing TGA, SEM and the ash tracer method on the remaining chars, the kinetic parameters, morphology, and the char reactivity were determined to help predict char gasification behaviour in the gasification plants. Through these investigations it was observed that higher pyrolysis temperatures produce more reactive chars, due to the formation of pores and roughness on the char surface. Yan et al [115] studeid the effects of coal properties, particle ultimate temperature and heating rate on coal devolatilization perfromances using a drop tube furance and a lab-scale plasma reactor. This study revealed that fast pyrolysis of coal would greatly increase the yield of light gases compared to a slow pyrolysis process. Zhang et al [71] investigated higher temperature (1000 −1300 °C) pyrolysis behaviour in a drop tube furnace with focus on the physiochemical characeristics and reation kinetics of the resultant char, it was found that higher temperature results in more CO but less CH_4. The study also reveals that temperature incease develops more pore structures and due to upgrade in the coal rank the activation energy increases for combution of resultant chars.

The devolatilization behaviour of thermal coal and biomass under HIsarna's thermal conditions (fast heating to high temperature up to 1500 °C) is an area which requires further investigation in order to understand the potential of the HIsarna process compared to the typical conditions covered in the literature. In order to select the right mixture of carbonaceous materials (e.g., substitution of coal with certain biomasses), and to ensure proper reduction (indirect reduction in SRV and pre-reduction in CCF) and heat balance (via post combustion), it is necessary to obtain accurate information of volatile matter yields, gaseous products, and their releasing rates under the thermal conditions similar to the HIsarna process. In this study, a drop tube furnace coupled with an online quadrupole mass spectrometer (DTF-QMS) was employed to evaluate the devolatilization behaviour of thermal coal and biomass materials under thermal conditions similar to HIsarna (rapid heating to high temperature up to 1500 °C), focusing on volatile matter yields, gaseous products and their evolving rates.

6.3 Experimental

6.3.1 Sample preparation

This chapter investigates three different carbon sources (one thermal coal and two biomass materials). The thermal coal (TC) is coal A, and a charcoal (CC) are listed in Table 4.1, while the Bana grass char (BGC) is pyrolysed torrefied Bana grass TBG under inert environment to temperature of 500 °C. The samples were prepared using the same procedures described in section 4.7.1. Table 6.1 shows the proximate and ultimate analysis data of the three samples.

Table 6.1: Proximate and ultimate values of the used thermal coal (TC), charcoal (CC) and Bana grass char (BGC).

	TC	**CC**	**BGC**
Proximate Analysis wt% (db)			
Moisture/ % (ad)	8.87	4.56	2.52
Volatile Matter	22.18	12.1	19
Ash	8.8	1.8	9.6
Fixed Carbon (by difference)	69.02	86.1	71.4
Ultimate Analysis wt% (db)			
Carbon	81.91	89.4	78.6
Hydrogen	4.27	3.11	3.28
Nitrogen	2.19	0.57	0.46
Sulphur	0.24	0.06	0.14
Oxygen by (difference)	2.59	5.06	7.92

db – dried basis; ad - air dried

6.3.2 Rapid devolatilization

The rapid devolatilization experiments were performed using a Carbolite-Gero high temperature vertical tube furnace described in section 4.2 shown in Figure 6.1. The furnace was coupled with Quadrupole Mass Spectrometer (QMS) to monitor gaseous products evolving from the samples during devolatilization. To protect the QMS from soot and condensable tar, disposable inline filter (Parker 1/4in G nylon) with maximum flow rate and working temperature of 152 L/min and 110 °C respectively was installed along the connection line. The combination of DTF-QMS allowed the

carbonaceous material samples to be rapidly heated to pre-set temperatures of 1000, 1250 and 1500 °C at the heating rate of approximately 10^4–10^5 °C/s [71], while the off-gas was continuously analysed. The carbon particles were injected into the pre-set temperature region through a particle feeder designed using a tee piece connected two ball valves and an argon line to create an inert atmosphere and carry the particles shown in Figure 6.1. The particle feeder was mounted to the top water-cooled flange and directly connected to an alumina lance (internal diameter 5 mm) which was inserted through the flange into the reactors hot zone. Before the experiment starts a sample of approximately 100 mg was placed on the seat of the bottom ball valve while in the "off" position, and an Ar (with a 99.999% purity) flush through the feeder was conducted to create an oxygen-free atmosphere before all valves were closed. While the furnace heated to the desired temperature at a heating rate of 10 °C/min, a carrier gas (Ar, 99.999% purity) at 1 L/min was purged through the furnace from the bottom to ensure an inert atmosphere.

When the furnace temperature reached the experimental temperature, the valve holding the sample was opened at the same time the valve controlling the Ar gas was switched to the feeder for ~10 seconds to maintain the atmosphere, while the samples were injected. The Ar gas also carried the sample particles to the crucible placed in the centre of the isothermal region in the furnace. The whole sample was fed at once to ensure it reach the desired place and temperature at the same time. The furnace was kept at the pre-set temperature for a total of 10 minutes while the furnace exhaust was connected to the QMS. The QMS was set to measure readings of the following gaseous products: N_2, O_2, CO, CO_2, Ar, H_2O, H_2, CH_4 and C_2H_6. After the reaction time was completed, the furnace was cooled down at the rate of 5 °C/minutes to room temperature in an Ar atmosphere and the char particles were collected in the alumina crucible for further analysis.

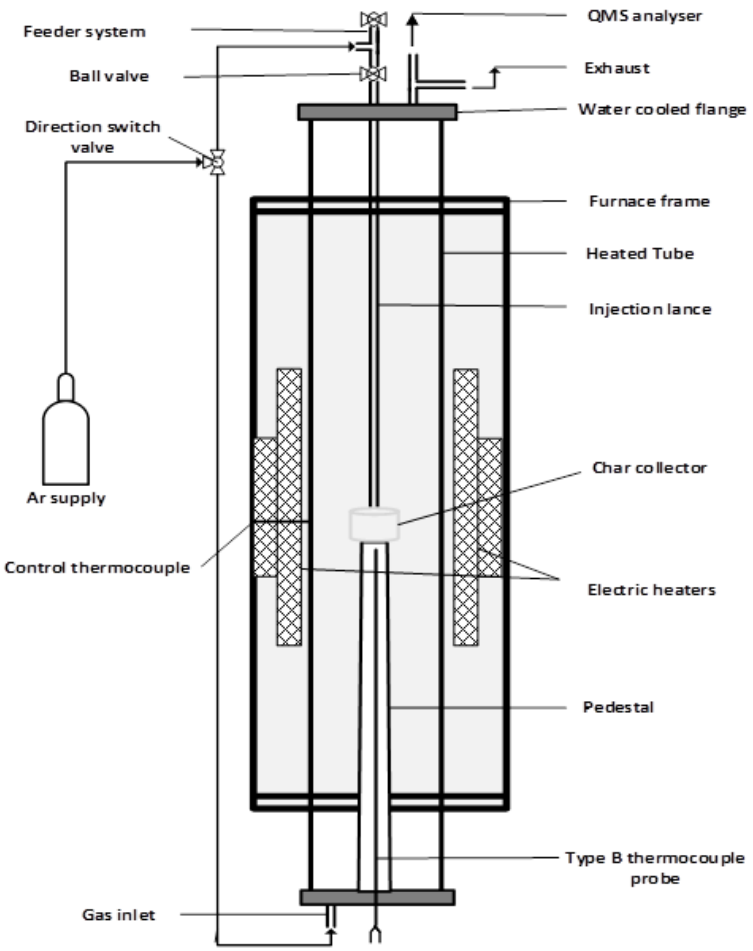

Figure 6.1: Drop tube furnace (DTF) setup with a mass spectrometry for rapid devolatilization study. The quadrupole mass spectrometer QMS is connected to the gas sampling port.

6.3.3 Char yield

The char yield was directly determined during devolatilization of the carbonaceous materials in the DTF at the temperatures of 1000, 1250 and 1500 °C. The material fed into the DTF was weighed before and after the heat treatment to calculate the weight loss. To validate the method and confirm good collection efficiency a series of experiments were perform in the DTF (as shown in Figure 6.1), at ambient temperature for each carbonaceous material. Three trials were performed using the same particle size used during the devolatilization experiments. Figure 6.2 shows the amount of materials collected in the alumina crucible placed in the centre of the hot-zone during validation trials. The weight of collected material was very close to the weight of fed material with an average of 99.1%, 96.13% and 98% of the fed materials collected for TC, CC and BGC respectively. CC was found to be less efficient with this

configuration which could be due to the physical properties of CC such as low density and less spherical particle shapes. Therefore, during the devolatilization experiments the sample weights were adjusted according to the expected mass balance shown in Figure 6.2 to ensure the correct calibrated mass of each sample was recorded after devolatilization tests. Devolatilization experiments were repeated three times at each temperature to produce concordant results.

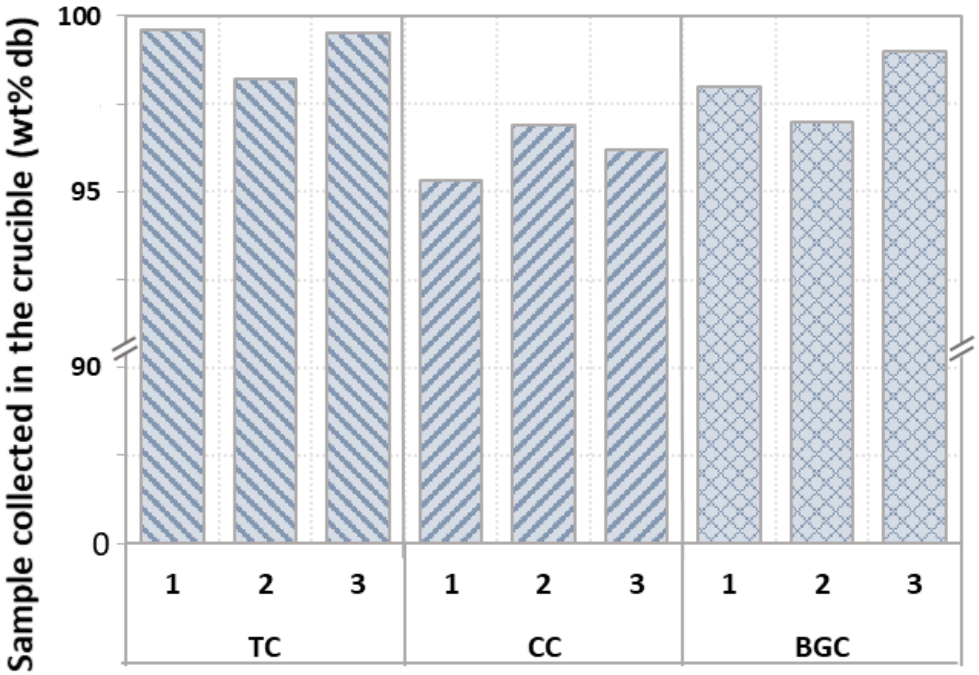

Figure 6.2: The amounts of carbon material particles collected in the crucible placed in the centre of DTF, after fed into the reactor at ambient temperature passing through the injection lance.

6.3.4 R-factor determination

The R-factor is an important parameter which is normally used to evaluate the feasibility of coal use for injection in the blast furnace process [68]. The R-factor stands for the volatile release ratio, which compares the weight loss that occurs under rapid heating conditions of carbon materials to the standardised volatile matter (VM) content. A high R-factor value means high carbon conversion to volatiles and less solid char residuals. The equation (19) below shows how the R-factor is calculated assuming the ash of the carbon material is inert:

$$\mathrm{R-factor} = \frac{\mathrm{V}}{\text{Prox VM content (dry ash free)}} \tag{19}$$

where V represents the total volatile yield, measured by difference in weight of the starting and collected material.

6.3.5 Raman Spectroscopy

The Raman spectra of the TC, CC and BGC chars produced during injection at 1500 °C were obtained with an excitation laser at 514.4 nm and grating of 1800 l/mm using Renishaw InVia Reflex Raman Spectrometer. Particles of each char samples were placed on a slide and were focused using a 20X objective lens. The Raman Spectra in the region 100 – 3500 cm^{-1} were collected, however the spectra range between 800 - 1900 cm^{-1} produces the most pertinent information on the degree of structural disorder of carbonaceous materials [54]. To determine the precise detailed differences of spectral features between TC, CC, and BGC chars, relevant spectra bands were fitted to pseudo-Voigt function using OriginPro 2019b to calculate area, bandwidth and relative intensities.

6.4 Results and discussion

6.4.1 Chemical structural characteristics of carbonaceous materials

Raman spectroscopy is one of the most common techniques used to study characteristics of carbonaceous materials [46, 122-124]. In order to study the degree of graphitic structure and evaluate its effect on the devolatilization behaviour of different carbon sources under HIsarna thermal conditions, the Raman spectra obtained in the range of 800 - 2000 cm^{-1} for TC, CC and BGC chars were analysed and presented in Figure 6.3.

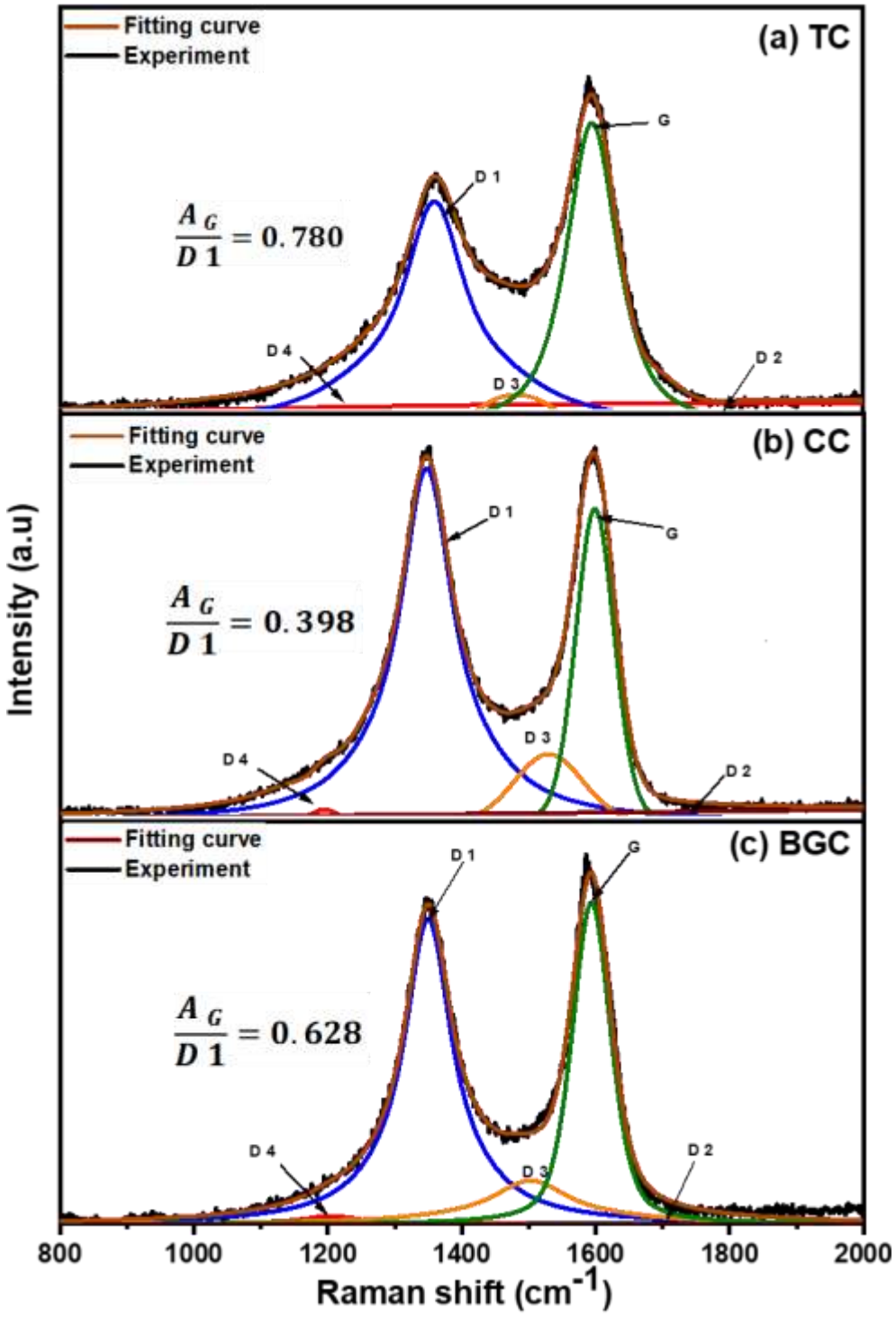

Figure 6.3: Raman spectra and peak fitting of (a) thermal coal char, (b) charcoal char and (c) Bana grass char produced during 1500 °C injection.

For this Raman spectra range carbonaceous materials can produce up to five characteristic spectra bands, which can be resolved into five peaks (D1, D2, D3, D4 and G) [127]. However, the spectra in Figure 6.3 show that only two significant peaks appeared at a shift of ~1350 cm^{-1} and ~1600 cm^{-1}, corresponding to the D and G bands.

It is well known that the spectra band positioned at 1360 cm^{-1} reveals weakness and disorder in the carbon structure while the spectra band at 1600 cm^{-1} represents the vibration of the ideal graphite lattice [54]. The ratio of the intensity of G/D1 is known to determine the order degree of carbon structure with greater ratio indicating more ordered graphite structure in the carbonaceous material. To obtain more accurate results, the area ratios ($\frac{A_G}{A_{D1}}$) for TC char, CC char and BGC char were calculated, and the ratios are approximately 0.780, 0.398 and 0.628 respectively. The area ratio for CC char was lowest followed by BGC char and then TC char, which confirms that charcoal has less ordered graphite structure and it is more amorphous carbon implying its being more reactive [128]. Therefore, it can be speculated that more disordered structure for carbonaceous materials will enhance its devolatilization rate.

6.4.2 Effect of temperature on devolatilization behaviour

In order to compare the effect of temperature on devolatilization behaviour, the DTF experiments for TC, CC and BGC were conducted at three different temperatures of 1000, 1250 and 1500 °C. Typical variations in the measured rate of volatile matter release with the change in temperature are given in Figure 6.4. An instant devolatilization reaction was observed from the gas formation curves at all three temperatures, however there was a few seconds delay in the detection of the gases by the online QMS due to the travelling distance in the DTF tube. This conversely led to the continued detection of devolatilization gases for a period of time after the process was completed as these gases passed through the remainder of the furnace.

The QMS was set to analyse CO, CO_2, H_2O, H_2, CH_4 and C_2H_6 gases, which are the main gas species produced during thermal treatment of carbon materials (determined through a calibration run where m/z (the mass-to-charge ratio) 0-50 was scanned throughout a devolatilization test to detect all species emitted). The formation of CO_2 and CO in the carbon materials is linked to decomposition of oxygen containing functional groups, but H_2 and hydrocarbons are formed from decomposition of heterocyclic and methyl groups. H_2O release is linked to the decomposition of different oxygen containing groups mainly OH groups [97, 99, 101].

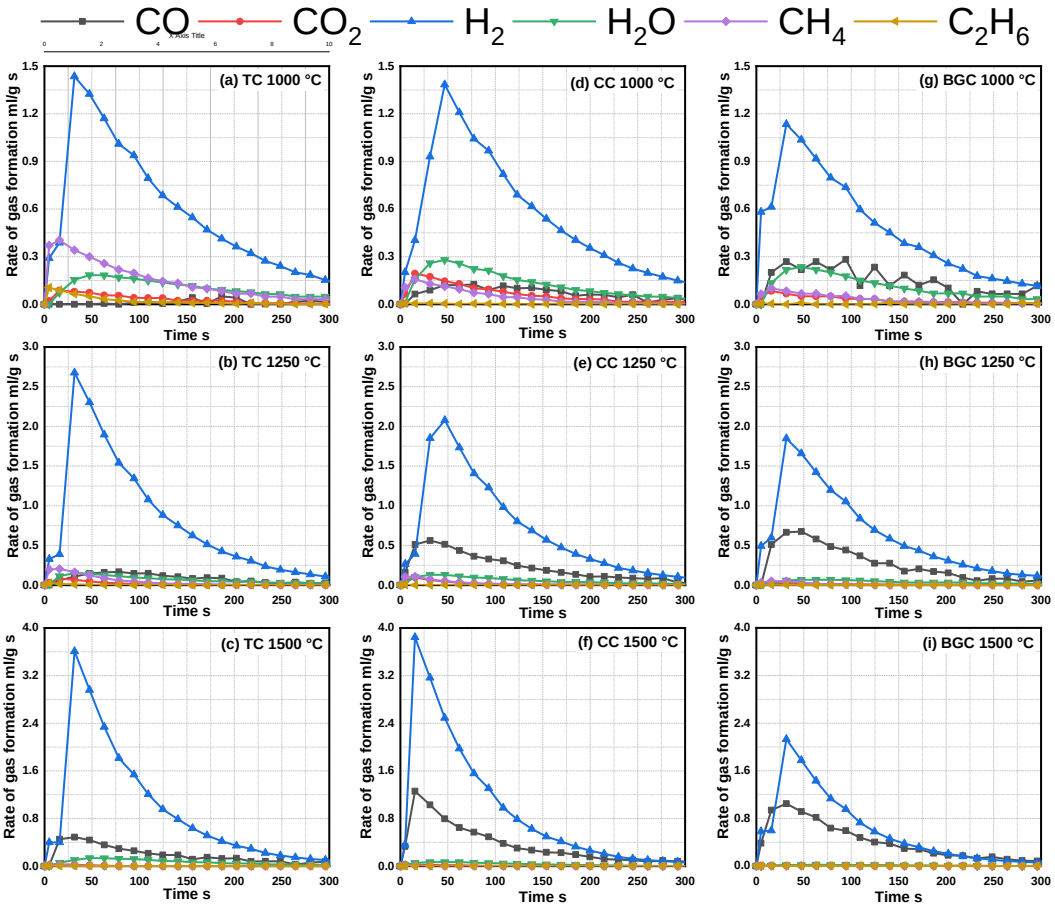

Figure 6.4: Rate of formation of gas species (CO, CO_2, H_2, H_2O, CH_4, and C_2H_6) for thermal coal (a, b and c), charcoal (d, e and f), and Bana grass char (g, h and i) at temperatures of 1000, 1250 and 1500 °C respectively in a high purity argon atmosphere.

Some common phenomena can be observed for all the samples as can be seen in Figure 6.4. The gas variation behaviour for all the samples were similar at three temperatures measured, and the evolution rate of H_2 is shown to be the highest out of all gas species. At 1000 °C, compared with CC and BGC, the rate of evolution of H_2 and hydrocarbon for TC was higher and the devolatilization time was slightly longer. A lower evolution rate and shorter devolatilization time for biomass samples could be related to the fact that CC and BGC have already been pre-treated to several hundred degrees during production and as such lower molecular weight/lower boiling point volatiles may have already undergone some devolatilization. However, higher O_2 content in CC and BGC caused the material to produce much more CO, CO_2 and H_2O in comparison to thermal coal. As shown in Figure 6.4, the rate of gas formation for CO_2, H_2O, CH_4 and C_2H_6 reached maximum values for all three samples at the temperature of 1000 °C. By

increasing temperature, the carbon conversion for all three materials increased significantly. It is also observed that the formation rate of both CO and H_2 increased, while CO_2, H_2O, CH_4 and C_2H_6 contents decreased sharply.

Figure 6.5 shows the yield variations for all major gaseous species produced under rapid devolatilization conditions for CC. As shown in Figure 6.5(b), the yield of CO_2 decreased with increasing temperature from 1000 to 1500 °C. At 1250 °C the yield of CO_2 decreases rapidly to the lowest value by the time of ~100 seconds. The yield of CO_2 reduced further with increasing the temperature to 1500 °C but a small amount of CO_2 was still detected, which may have evolved and escaped before any secondary reactions had taken place. Similar behaviour was observed for H_2O (Figure 6.5(d)), its yield decreased with increasing temperature from 1000 to 1500 °C and a small amount of H_2O was still detected at 1500 °C. The evolution of CH_4 (Figure 6.5(e)) followed the similar trend, its yield decreased with increasing temperatures, however, CH_4 was almost completely converted at 1500 °C by 50 seconds.

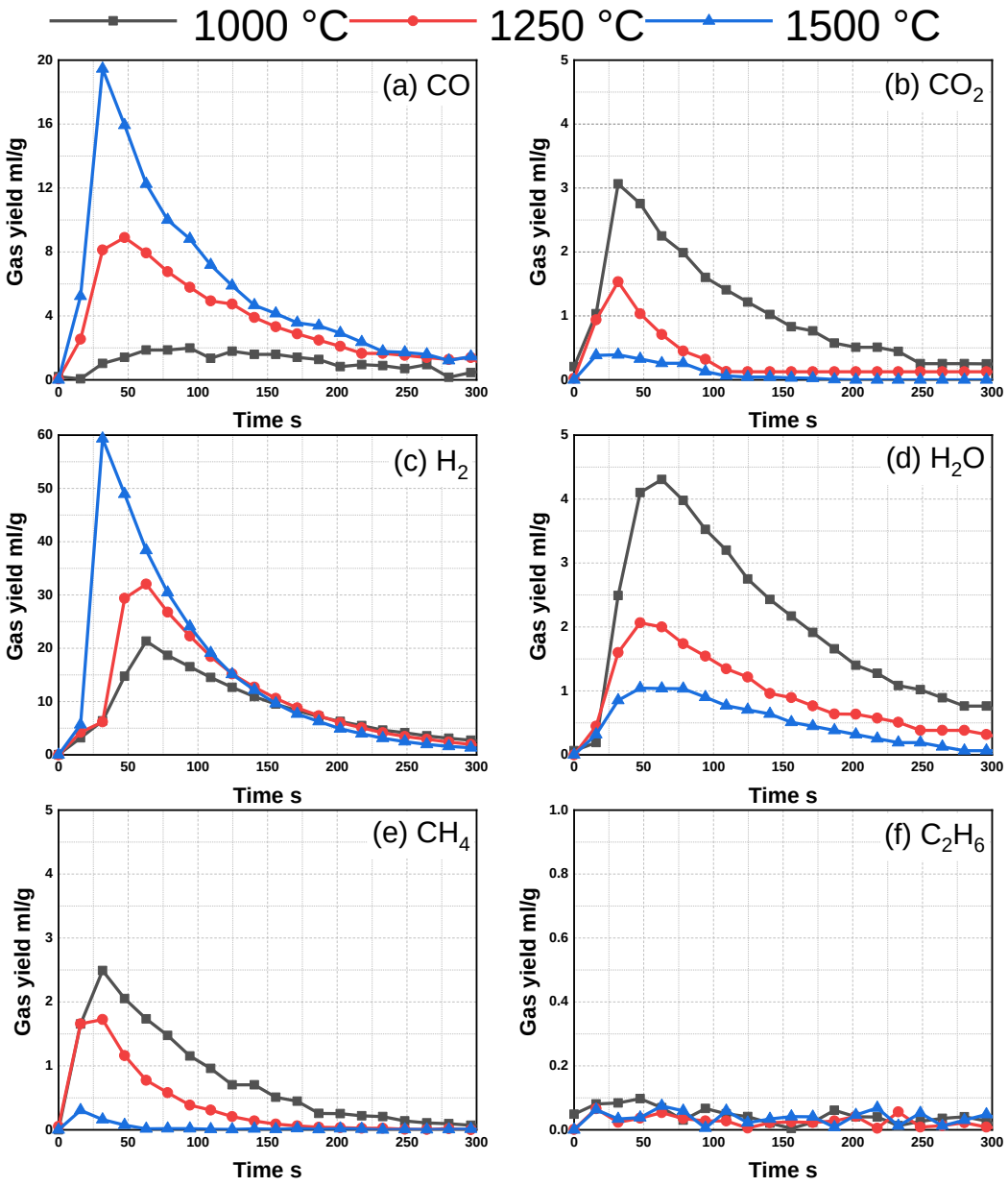

Figure 6.5: An off-gas analysis of (a) CO; (b) CO_2; (c) H_2; (d) H_2O; (e) CH_4; and (f) C_2H_6 produced during rapid devolatilization experiments for CC under argon atmosphere at three ultimate temperatures of 1000, 1250 and 1500 °C.

As shown in Figure 6.5 both H_2 and CO yield increase quite significantly with an increase in the temperature, and they are the main components of released volatiles at a temperature of 1500 °C. Although some of the CO and H_2 are generated at high temperature from decomposition of oxygen and hydrogen containing compounds, it is believed that carbon oxidation reactions through CO_2 and H_2O and other secondary reactions are taking place which results in an increase in these gas components [71]. In addition, the temperature increase results in the secondary tar cracking reactions which can partially convert tar into light hydrocarbons and contributes to an increase

in the yield of CO [115]. The light hydrocarbons evolved at higher temperatures will react with CO_2 and H_2O to form H_2 and CO [101, 110, 111]. The carbon oxidation and the secondary reactions are shown in equations (20) to (23):

$$C_{(S)} + CO_{2\,(g)} \rightarrow 2CO_{(g)} \quad (20)$$

$$C_{(s)} + H_2O_{(g)} \rightarrow CO_{(g)} + H_{2\,(g)} \quad (21)$$

$$CO_{2\,(g)} + CH_{4\,(g)} \rightarrow 2CO_{(g)} + 2H_{2\,(g)} \quad (22)$$

$$H_2O_{(g)} + CH_{4\,(g)} \rightarrow CO_{(g)} + 3H_{2\,(g)} \quad (23)$$

Furthermore, the thermal cracking of hydrocarbons is possible at temperature > 600 °C, cracking reactions can take place rapidly with an increase in temperature and decompose to H_2 and soot (solid carbon dust with few impurities) [129].

6.4.3 Mass balance of the devolatilization products

A mass balance of coal and biomass samples were conducted by determining the percentage of remaining char after heat treatment and quantifying the mass of light gases including H_2O from devolatilization. Figure 6.6 shows that there is a deficit beyond the measured char yield and light gases, which indicates that a certain amount of the material is lost in the form of condensable tar and soot during the process. As it can be seen in Figure 6.6, the variation in the yield of these gas species is greatly affected by changes in the experimental temperature and the carbonaceous materials as well. All parts of the DTF were visually inspected after each devolatilization experiment with no significant amount of heavy volatiles (condensable tars) found on the surfaces of the equipment after CC and BGC devolatilization, which could be attributed to the pre-treatment of the starting materials. In contrast, by using visual observation through the viewport on the top water-cooled flange it was noticed, that straight after the injection of CC during the experiments, a large amount of soot and fine particle flew out of the crucible with the carrier gas and some particles were found to be trapped in the gas line filter. This behaviour for CC samples could indicate that char fragmentation had occurred during devolatilization at high temperature and the low density for CC caused the deficit in char collection after the rapid heating. It has been reported by other researchers that high heating rate may result in a softening, melting, shrinking and fragmentation in some carbonaceous materials depending on their thermoplasticity [64, 80, 117]. Therefore, it has been speculated that CC has a low thermoplasticity, which resulted in comparatively more fragmentation behaviour in its particles. Previous studies have shown that the presence of low amounts of oily

tar gives further evidence of low thermoplasticity for CC as these two properties are strongly linked [130]. As shown in Figure 6.6, the deficit in the CC increased with increasing the temperature, which confirms that at higher temperature treatments particles are experiencing more extreme heating rate and results in more dust and fine particles formed due to an acceleration in fragmentation. the deficit for BGC was lowest for all the tested materials, this behaviour could be due to higher ash content and at these temperatures the ash components will melt and minimise char fragmentation at the same time vast majority of the condensable tar was removed during pyrolysis process.

The behaviour of the TC was observed in contrast where large amounts of tar was detected in the filter and on the surfaces of the equipment used. The increase in the heating rate and temperature was found to increase the tar formation, from the result of decrease in the tar condensation at high temperature. Tar condensation reactions are believed to be the dominant phenomena during slow heating/char making (specifically coal coking process), the recombination between solid particles and tar under slow heating leads to form more char and less tar, however during rapid heating the residence time is minimal, causing minimal condensation occurrence and an increase in tar yield [129, 84]. Although the temperature increases from 1000 to 1250 °C resulted in an increase in the deficit for thermal coal, at the temperature 1500 °C there was a decrease in the deficit. This behaviour indicates that tar cracking started to occur, which also resulted in an increase in light gases detected by QMS. Furthermore, it can be noted from reagent ultimate analysis results that thermal coal contains considerable amount of nitrogen, but this has not been detected during devolatilization experiments. Previous literature has shown the fate of N_2 during devolatilization to be largely the conversion to HCN and NH_3 [121, 130]. According to Di Nola et al. [119] the formation of N_2 partitioning is strongly temperature dependant, at the low temperature (≤600 °C) a large portion of N_2 is retained in the char and NH_3 is the main nitrogen gas product. However, at higher temperatures less N_2 is retained, which leads to the formation of large amounts of tar–N, with HCN being the main nitrogen containing gas component at temperature >1300 °C. The tar-N and HCN are not detected by the QMS, therefore it can be speculated that part of the deficit made in Figure 6.6 is contributed by these components.

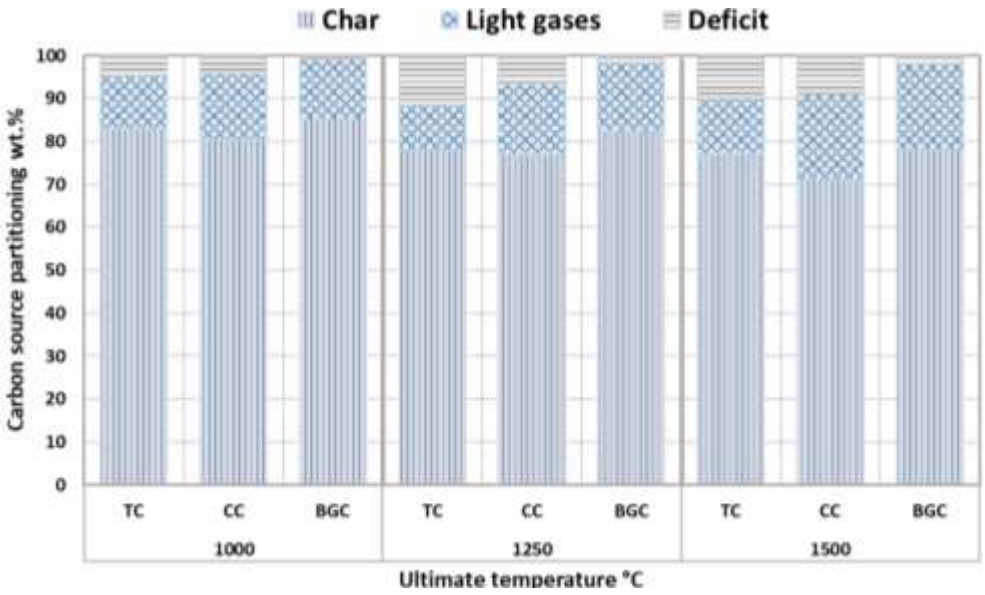

Figure 6.6: Mass balance of TC, CC and BGC during rapid devolatilization experiments at 1000, 1250, and 1500 °C in argon atmosphere.

The weight percentage of gas species formed during rapid devolatilization is presented in Table 6.2. The results show that gas variations are shifting toward H_2 and CO with an increase in the temperature formed from the thermally enabled secondary reactions. Despite high fixed carbon and low volatile matter content in CC the weight of the residual char collected was lowest at all temperatures. As mentioned above this could be due to higher particle loss and secondary reactions in CC under rapid heating. As shown in Table 6.2, both CO_2 and H_2O gas volumes decreased much more significantly for CC and BGC with increasing temperature than for TC, which indicates a greater extent of carbon oxidation reaction was completed for biomass materials than TC. This indicate that both CC and BGC are more reactive than TC to H_2O and CO_2 due to their amorphous carbon structure.

Table 6.2: Normalised gas species (wt.%) detected during devolatilization at 1000, 1250 and 1500 °C.

	CO	CO_2	H_2	H_2O	CH_4	C_2H_6
1000 °C						
TC	6.21	15.87	14.36	25.78	29.53	8.26
CC	23.60	31.50	11.21	25.34	7.27	1.09
BGC	44.44	14.25	10.47	24.10	5.51	1.22
1250 °C						
TC	35.30	9.23	22.15	20.33	10.79	2.21
CC	61.72	11.14	12.63	10.60	3.28	0.63
BGC	72.21	5.14	12.12	7.98	1.59	0.96
1500 °C						
TC	60.78	2.21	20.88	13.96	0.81	1.36
CC	79.11	1.94	13.55	4.29	0.33	0.79
BGC	87.36	1.65	8.67	1.22	0.17	0.93

The importance of devolatilization products for pre-reduction in the CCF of HIsarna has been discussed previously, however the iron ore reduction is completed in the SRV by char residuals formed from injected solid carbon through direct/indirect reduction reactions shown in equations (1) to (3). Thus, it is important to know the mount of solid char that will be delivered into the SRV bath after injection of different carbon sources.

By evaluating the R-factor, the ratio of total carbon conversion during rapid devolatilization of carbon materials can be measured to the standard volatile matter (VM) content of the starting materials [66, 120]. The R-factor parameter can give an indication of how efficiently the carbon material can yield solid char residuals under the HIsarna atmosphere. The values of R-factor obtained for the carbonaceous materials used in this investigation are shown in Figure 6.7 with error bars representing uncertainty in average either side of the mean.

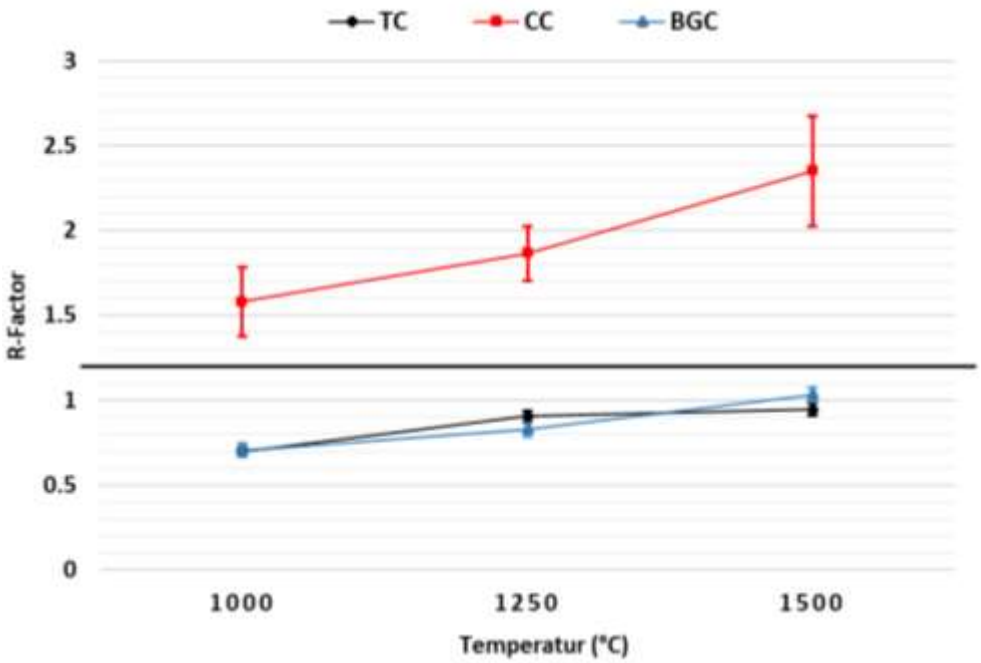

Figure 6.7: R-factor of TC, CC and BGC at reaction temperatures of 1000, 1250, and 1500 °C. Error bars represent uncertainty in average either side of the mean.

As described by equation 19, a higher R-factor indicates higher conversion of the carbon material during devolatilization. Figure 6.7 suggests that the value of R-factor increased with an increase in the experimental temperature, therefore the conversion of carbon also increases. The R-factor of TC and BGC are much smaller than the one of CC at all temperatures which means that TC and BGC either fails to completely liberate the volatiles or due to higher density of these materials the char yield is significantly higher. Despite the low volatile matter content for CC, the R-factor is significantly higher than the one for TC and BGC chars at all temperatures with a maximum value of 2.35 at the peak temperature of 1500 °C, accompanied with the biggest error bar between the test samples. This confirms that large amounts of fixed carbon will be converted into CO during CC injection into HIsarna, which may result in CC chars being less efficiently delivered to the SRV in comparison to TC and BGC chars. In addition, the extra CO formed during injection of CC may lead to a change in the behaviour of the reactors. Thus, it may be advised to enhance the productivity of the CCF to utilise this higher proportion of produced reductive gas to maintain overall efficiency of the process. From these results it should be emphasised that despite the lower VM content in CC, its R-factor is still significantly higher than that for TC and BGC. Therefore, the devolatilization extent is not determined by VM

content only, but it is also controlled by physical and chemical properties of the carbon source.

6.4.4 Comparison of rapid devolatilization behaviours for different carbonaceous materials

Several reactions take place simultaneously during rapid heating of the carbonaceous materials, including break-up of chemical bonds, vaporization, and condensation [96]. Previous studies have indicated that the post combustion ratio (PCR) value of reducing gas has an important influence on the pre-reduction degree in the HIsarna's cyclone, which is greatly influenced by carbonaceous materials devolatilization [30, 115]. The total yield of gas products evolved from the carbon sources (per 1 gram of sample) during rapid heating to the temperatures of 1500 °C is plotted in Figure 6.8. The volume was calculated from the concentration of the evolved gases detected by mass spectrometry. By knowing the carrier gas flow rate and the flow rate at which the MS was sampling, it was possible to obtain the concentration of each gas in the detected mixture.

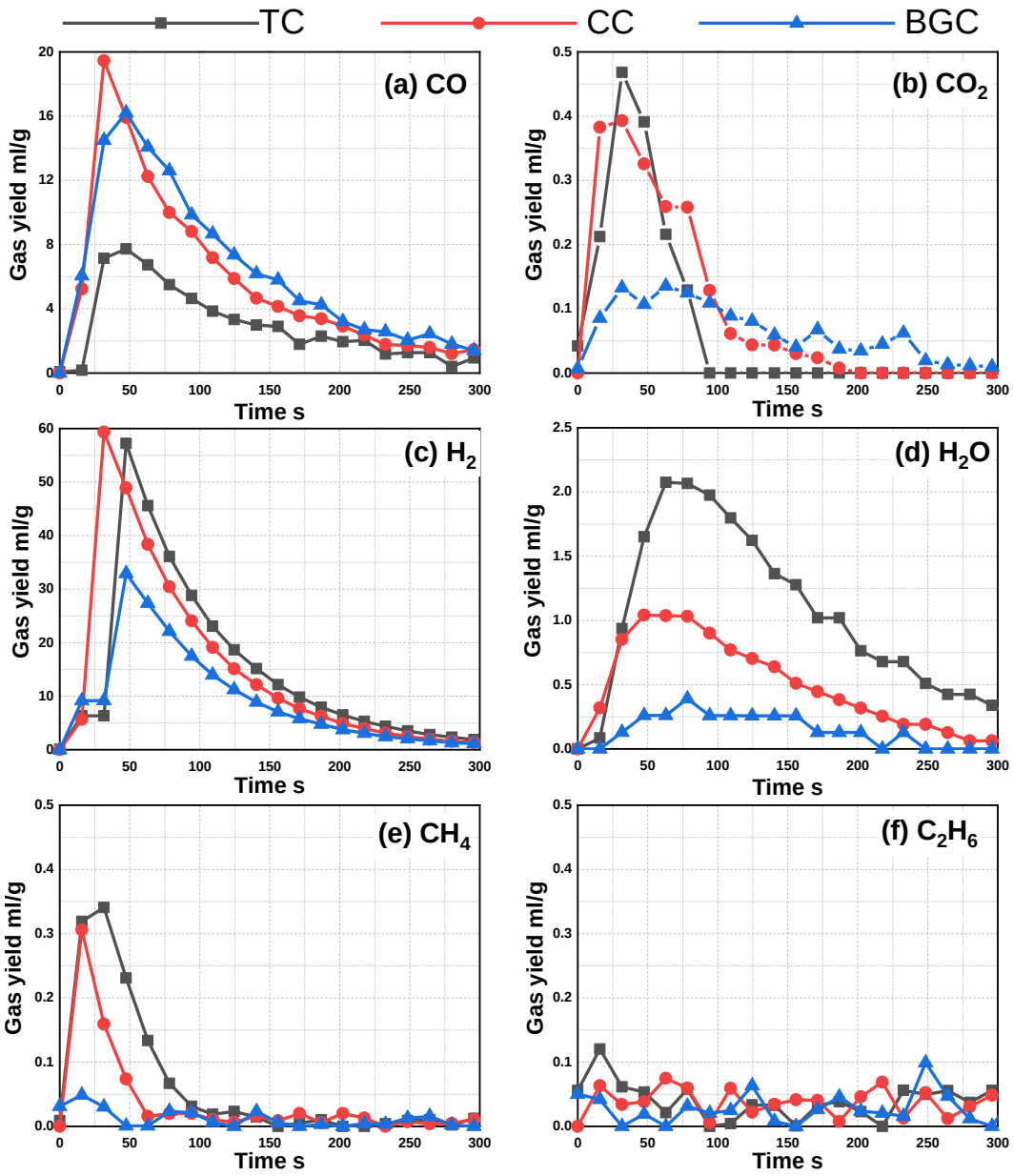

Figure 6.8: Comparison of gas species yield for (a) CO; (b) CO_2; (c) H_2; (d) H_2O; (e) CH_4; and (f) C_2H_6 produced during rapid devolatilization experiments for TC, CC, and BGC under argon atmosphere at 1500 °C.

The evolving of CO_2, H_2O and hydrocarbons are detected earlier than H_2 and CO for both materials. However, CC reaches its peak for both H_2 and CO a few seconds earlier than both TC and BGC which may be due to CC having higher reactivity with the surrounding gas atmosphere at temperature of 1500 °C.

There are a number of important differences between the materials which will affect the contribution of devolatilization product and the subsequent PCR, and ultimately will affect the pre-reduction within HIsarna. According to equation (18) PCR

decreases with an increase of either CO or H_2 or both, and the findings by Chen et al [117] show that decrease in the PCR value results in an increase in the pre-reduction degree in the CCF. As shown in Table 6.3, CC and BGC produced significantly larger volumes of CO than TC, while the difference in H_2 values was minimal for CC and TC but lower H_2 for BGC was observed.

Table 6.3: Volume (ml) of gas species detected per gram of sample during 1500 °C devolatilization.

Materials	CO	CO_2	H_2	H_2O	CH_4	C_2H_6
TC	63.58	1.46	303.67	21.47	1.47	1.41
CC	126.61	1.96	301.43	10.10	0.92	1.25
BGC	138.34	1.65	190.91	7.27	0.46	1.46

The values in Table 6.3 indicate that by substituting TC with biomass materials, much lower PCR will be achieved for CC and leads to higher pre-reduction, but similar PCR will be achieved for BGC. This is however at the expense of solid carbon chars required for SRV productivity/complete reduction in the case of CC. Since about 80% of the reduction takes place in the SRV via gas-slag-metal systems interacting, it is necessary to limit the conversion of carbon materials before they penetrate in the metal bath. Both CC and BGC contains larger amounts of O_2 which is likely to have controlled the variation of gas species and char yield. As mentioned above charcoal conversion is significantly higher than expected due to loss of particles and higher carbon oxidation, therefore an increase in the particle size and change in other parameters such as injection rate could help improve the overall efficiency of the low dense CC compared to the use under standard TC process parameters.

6.5 Conclusion

The characteristics and impact of the devolatilization of different carbon sources under high temperature conditions was investigated using DTF-QMS. The effect of change in reaction temperature and the nature of gas species produced during devolatilization process were determined. The following conclusions can be drawn from this study:

- There is a significant difference in carbon crystalline structure between TC, CC and BGC chars. The ratio of the intensity of G/D1 in Raman Spectra for the tested materials is as follows: CC char > BGC char > TC char, this indicates

that CC has more disordered graphite structure and it is more amorphous carbon, which can lead to higher conversion for CC.

- The devolatilization experiments demonstrated the strong impact of temperature on the rate of gas formation, which increases with increasing the temperature. In addition, an increase in the temperature results in an increased conversion for all carbonaceous materials tested in this study.
- The total yield of gaseous species increased with an increase in the devolatilization temperature, and the variation of these gases was greatly affected by an increase in the temperature. The yield of hydrocarbons, CO_2 and H_2O decreases significantly with an increase of temperature, however the yield of both H_2 and CO increase as a consequence. This behaviour indicates that temperature increase can enhance both carbon oxidation and secondary reactions which are taking place during devolatilization.
- Similar amount of H_2 was produced by charcoal and thermal coal at the temperature of 1500 ^oC, yet the amount of CO produced by charcoal was twice that of thermal coal. The weight contributed by CO to total gas yield for charcoal at 1000 °C was 23.60%, increased to 61.72% at 1250 °C and subsequently to 79.11% at 1500 °C, this suggests that large amount of carbon is oxidised by the O_2 functional groups/trapped oxygen within the material itself.
- Despite high fixed carbon and low VM content, charcoal has a high value of R-factor with a maximum value of 2.35 at the temperature of 1500 °C. Due to the fact that conversion degree was much higher than expected with weight loss of 29% at 1500 °C. In contrast the maximum R-factor values for thermal coal and Bana grass char are 0.94 and 1.03 at 1500 °C.
- Despite low conversion degree for thermal coal, higher deficits of cumulative material compared to starting mass is observed under all temperatures. It was evidenced that large amounts of heavy volatiles (condensable tar) are formed by thermal coal, and therefore it can be speculated that at the high temperature most of the N_2 components are removed from the char in the form of tar–N and HCN.

Chapter 7

Gasification and structural behaviour of different carbon sources and resultant chars from rapid devolatilization for HIsarna alternative ironmaking process

7.1 Hypothesis to be investigated

Hypothesis 3 – The gasification rate of carbonaceous materials is controlled by physical structure and chemical composition of the materials.

Hypothesis 4 – The thermal coal particles are expected to go through higher degree of structural transformation under rapid devolatilization compared to biomass materials.

7.2 Introduction

The carbonaceous materials injected into HIsarna SRV are subjected to a series of rapid physical and chemical changes including rapid heating (from ambient temperature to 1500 °C) and devolatilization. Depending on the ultimate temperature and the heating rate the devolatilization process can finish within several milliseconds under rapid heating or several hours under slow heating [115]. Devolatilization is the first step of all the thermochemical processes, and it comprises the release of volatile matter and change in the solid structure due to occurrence of different phenomena such as softening, swelling, fragmentation [58, 121]. Due to the extreme high temperature (up to 1500 °C) in SRV, a large amount of volatiles are released instantly after injection of carbonaceous materials which results in dramatic transformation in the solid particle structure. Previous studies confirm about 80% of the reduction reactions takes place in the SRV, through direct/indirect reactions between FeO in slag with solid char, dissolved carbon in the liquid metal and reducing gases respectively [32]. The overall reaction between FeO containing slag and solid carbon or carbon in molten iron at high temperatures can be described by equation (1).

Previous studies have shown that parameters including particle size, surface roughness, shape, porosity and chemical composition of the char as well as the reaction atmosphere affect the reduction of FeO in the slag and dissolution of carbon in the metal bath [24, 46, 48, 132-134]. It was found that the ultimate structure will have a significant effect on the wetting and the contact angle between materials, which

subsequently affects the reactivity of the char and will influence the reduction rate of FeO in the slag through direct/indirect reactions. It is well known that thermal treatment significantly affects the final char morphology of the carbon material, therefore an extreme high temperature in SRV will have a significant impact on the char structure e.g. shape, size, roughness and porosity [68, 69, 80, 117]. Therefore, to select the right mix of carbonaceous materials such as replacing thermal coal with biomass, it is essential to understand the changes in the char morphology and reactivity and the formation of char structure for each carbonaceous material caused by the rapid devolatilization under thermal conditions similar to the HIsarna SRV, that is, High-temperature and rapid heating.

Effects of experimental conditions such as temperature, heating rate, pressure, residence time and reaction atmosphere on physical and chemical properties of chars produced from coal and biomass materials have been extensively investigated [68, 71, 80]. These studies are carried out through evaluating the char morphology and size changes caused by the variation of these conditions, as well as the kinetics and char reactivity analysis under different oxidation conditions. Through examining the size and morphology of two biomass materials and chars produced under rapid heating to 1400 °C by Biagini et al. [120], it was revealed that the rapid heating caused significant structural variations in the chars produced in respect to the parent materials. The study also found that the char particle size reduced quite significantly by rapid heating for woody biomass, however the change in size was negligible for olive char. In another study by Biagini et al., it was found that the particle size for all the fuels decreases with severe heating and also the density of coal decreases, but the density of biomass fuels increases [137]. During the investigation of porous structure parameters for different grades of coal to compare with biomass char produced at high temperature by Smoliński and Howaniec [138], it was found that the micro pore surface, area and volume of carbonaceous materials depend on the chemical properties, therefore an increase in the fixed carbon content will result in decrease in the porous structure of the material. Biagini et al. [70] also studied the reactivity of char residues remaining from the rapid heating of two biomass materials to different final temperatures and concluded that the chars produced under higher temperatures are more reactive to air oxidation atmosphere than chars produced in milder conditions. The kinetic study carried out by Tanner and Bhattacharya [73] using different oxidation atmospheres

showed that the gasification atmosphere can affect the kinetic parameters but the particle size selected did not have big influence on the reaction kinetics. Karlström et al. [139] studied the apparent reaction order for different coals and a biomass, and concluded that depending on the operating conditions, the reaction order can vary for carbonaceous materials and the study showed higher reactivity for biomass char compared to coal. Moreover, other factors such as biomass torrefaction degree [121], particle size [123], and residence time [140], are shown to have an impact on the reactivity of the chars produced by high-temperature rapid devolatilization.

Although extensive research has been conducted on char characterization for different carbonaceous materials, the research reported was mostly carried out under low or medium temperature up to 1000 °C and focused on the properties of the chars and not much detailed explanation was given on how these properties may affect the utilization of char in ironmaking processes. To understand characteristics of the chars received in the SRV bath, the study of these materials needs to be undertaken under more extreme conditions similar to SRV e.g., higher heating rate and temperature, and investigate the implication of the char properties on the SRV behaviour. Therefore, the objective of this study is to investigate coal and biomass char particles produced under similar thermal conditions to the HIsarna's SRV. To simulate the sudden high heating rate and high temperature conditions that the carbonaceous materials experience, a drop tube furnace reactor (DTF) is used to produce char particles. The resultant chars are subsequently used for morphology, image analysis and reactivity test using SEM imaging, ImageJ software and thermogravimetric analyser (TGA) respectively. Also, the high temperature confocal scanning laser microscope (HT-CSLM) is used to monitor the real-time changes of carbonaceous particles during rapid heating. The HT-CSLM allows for continuous imaging of 2D plane within the small sample surface, to observe changes in size and shape of the particles under controlled high heating and cooling conditions applied.

7.3 Experimental

7.3.1 Sample preparation

This chapter investigates the same carbonaceous materials listed in the Table 6.1, prepared using the same procedures described in section 4.7.1.

7.3.2 High temperature char preparation

The high temperature chars are produced through rapid devolatilization of the carbonaceous materials in the drop tube furnace (DTF) which is schematically shown in Figure 7.1. Similar procedures to section 6.3.2 applied to produce the char particles at temperature of 1500 °C for this study. However, for this study the char particles collected at the bottom of the furnace to ensure the reaction time the char particles experience is similar to the instant reaction the carbonaceous materials experience when injected into the HIsarna SRV bath.

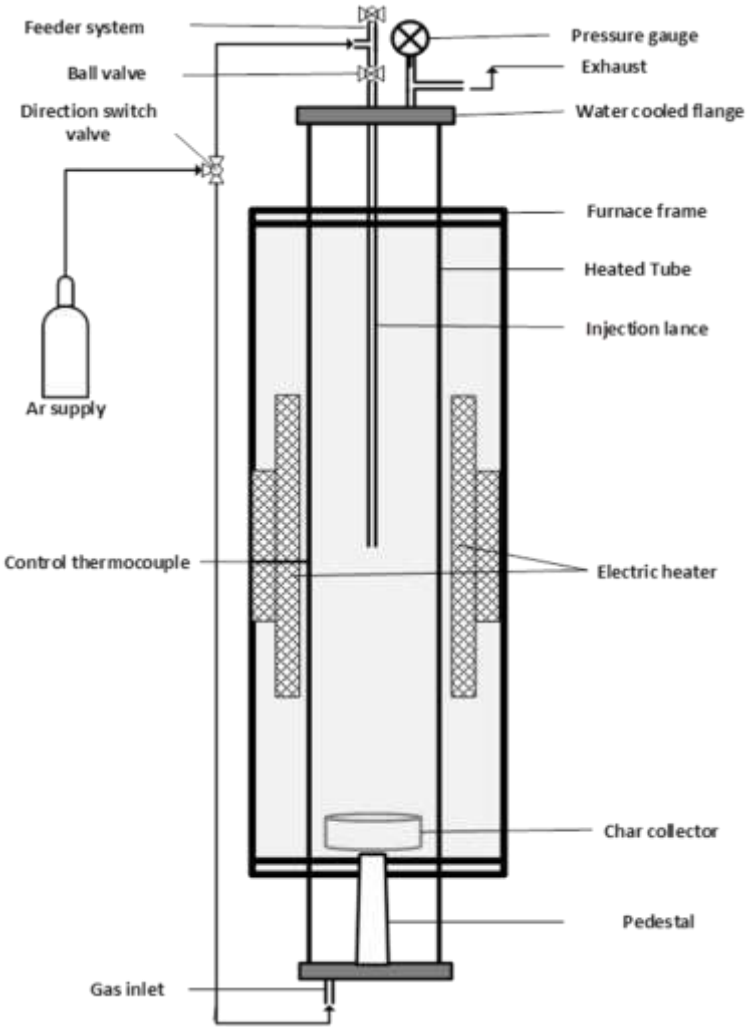

Figure 7.1: Drop tube furnace (DTF) for rapid devolatilization study to produce solid char particles.

The ash tracer method was applied to determine the char yield during the rapid heat treatment for each carbonaceous material, assuming the minimum mass remaining after combustion is the ash content of the samples. The ash tracer method assumes that ash is an inert material and maintained during combustion process [68]. One gram of dried materials for each raw carbon source and their devolatilized chars are added to

pre-weighted alumina boat and placed in the muffle furnaces under air atmosphere. The samples are heated at the heating rate of 10 °C/min, and then held at 800 °C for an hour to ensure that the combustion process is completed. The sample remaining and pre-weighted alumina boat are weighed again, then the initial alumina boat weight subtracted to obtain the weight of the ash, and using equation (24) below the char yield was calculated [67]: According to Liaw & Wu [67] the ash tracer method can overestimates char yield by 9−16% compared to direct measurement of char yield due to release of Na, K, Mg, Ca, Al, Fe, Ti, and P. However, the chars produced in this study already surpassed the temperature at which these elements expected to be release, therefore the elements retained as the ash for both raw material and chars is expected to be the same.

$$\text{Char yield } \% = \frac{\text{Ai}}{\text{Ac}} \text{ x}100 \quad (24)$$

Where Ai is the ash content in the raw carbonaceous material (on a dry basis) and Ac is the ash content in the char produced under HIsarna thermal condition (on a dry basis).

7.3.3 Analytical method for char characterization

Char particles produced during DTF injection in 7.3.2 and parent materials are analysed and compared. The reactivity test for the char particles was carried out using thermogravimetric analysis (TGA). A 20 mg ± 0.01 sample was placed in an alumina crucible (height 4 mm x diameter 6.8 mm). The alumina crucible with test sample was placed on a platinum stage, which has a thermocouple located directly underneath to provide real temperature for the sample tested. All the samples were heated from the ambient temperature to 1500 °C at the heating rate of 30 °C/min in a high purity (99.9999%) argon atmosphere with the flow rate of 50 ml/min. Once the desired temperature reached the sample was kept at that temperature for 10 minutes under Ar and then the gas atmosphere switched to (99.999%) CO_2 for 30 minutes with the flowrate of 50 ml/min to minimize the resistance around the particles resulting from the stagnant gaseous film. The mass loss of the sample was continuously recorded to analyse the effect of rapid heat treatment on each carbonaceous material in comparison to their parent materials. The test samples are subject to buoyancy effects, therefore, to eliminate the errors caused by these effects, the correction measurements were carried out by filling alumina crucibles with 20mg of inert Al_2O_3 powder and perform

similar test procedures to actual test samples, then the results of the inert tests were subtracted from the test results. To ensure the reliability and reproducibility of the method, the test for the same sample has been repeated three times to produce concordant results. The gasification test results are used to calculate parameter such as char conversion and reactivity index for each material. Carbon conversion due to gasification is defined by equation (13). While the gasification reactivity is evaluated by the reactivity index ($R_{0.5}$) which has units of %/min and expressed by equation (25) [141].

$$R_{0.5} = \frac{0.5}{t_{0.5}} \tag{25}$$

where $t_{0.5}$ is the time when char conversion is 50%.

7.3.4 Char structure analysis

Scanning electron microscopy (Sigma Zeiss SEM) images were obtained for each carbonaceous material sample before and after rapid heat treatment to investigate changes in shape and structure. Some random particles of each material were mounted to the carbon stub and placed in the SEM chamber. Magnification degree between 200 X to 400 X with the imaging conditions of 10 kV voltage applied for detailed study of SEM images for single particles e.g., surface roughness and porosity.

N_2 (77K) adsorption was applied to determine the carbonaceous material specific surface area, pore volume, and average pore diameter based on the multipoint Brunauer-Emmett-Teller (BET) method [138]. Approximately 1g of both raw and char samples for each carbonaceous material was degassed by heating at 200 °C under vacuum for 12 hours. Then using BET equipment (Micromeritics ASAP2020) the N_2 adsorption isotherms were obtained at liquid nitrogen temperature (77 K) and relative pressures between 0.011 and 0.996 for the degassed sample.

7.3.5 Direct observation under high temperature confocal scanning laser microscope (HT- CSLM)

The real-time changes in the char particles shape from different carbon sources under high temperature was observed using HT-CSLM microscope shown in Figure 4.3. A small quantity of dispersed particles from each material was added into the Pt crucible (height 4 mm x diameter 6.5 mm). The Pt crucible with the test sample was placed on alumina (Al_2O_3) spacer on the platinum stage within the reaction chamber, the alumina

spacer is used to prevent fusing between Pt crucible and the platinum stage at high temperatures.

Before starting experiments, the chamber was evacuated using rotary vacuum pump for a few seconds and being refilled with a high purity (99.9999%) argon gas. This procedure was repeated three times to ensure an inert gas atmosphere achieved. The experiments were then performed under continuous argon flow of 300 ml/min to remove volatiles released by the sample and maintain an inert atmosphere within the reaction chamber. The furnace was first heated from the atmospheric temperature to 200 °C, at the heating rate of 60 °C/min and held at that temperature for 60 seconds to dry the samples, to condition the bulb and evaporate isopropanol which was used for cleaning. Then the sample was heated to 1000 °C at the heating rate of 100 °C/min, to ensure the sample is devolatilized and clear images are captured to measure all the changes in the particle structure. Using an X5 objective lens the optical system positioned directly above the heating chamber was set to simultaneously record 2D plane images at a rate of 15 frames per second, which can be viewed as either a video or still images. Using ImageJ software, the change in the particle size was measured in terms of their 2D area at different temperatures. These measured areas were then used to calculate the swelling ratio of the particle at temperature (SR_t) which is defined by Equation (26) where A_0 is the area of the particle at the beginning of the test and A_t is the area of the particle at temperature t.

$$SR_t = \frac{A_t}{A_0} \tag{26}$$

To ensure representative results are produced, five particles in each sample were focused on and the changes in particle shape and size at different temperatures were measured to calculate mean particle change.

7.4 Results and discussion

7.4.1 Devolatilization results

To investigate the effect of rapid heating and high temperature devolatilization on carbonaceous materials and determine the difference in the behaviours of these three materials, DTF was used to produce chars. The produced char particles were considered to have similar physical and chemical properties to those encountered in the HIsarna process. During the rapid heating of carbonaceous materials several

reactions take place simultaneously, including break-up of chemical bonds, vaporization, and condensation. The moisture and volatile matter content decreased significantly because of the effect of high temperature, while the fixed carbon increased resulting from the vaporisation of the moisture and the release of the volatile matter. Using the ash tracer method, the char yield for TC, CC and BGC was calculated as 78.0 %, 69.9% and 80.2% respectively. This indicates that CC has gone through the highest conversion degree (30.1%), followed by TC (22.0%) and BGC (19.8%) which has lowest conversion degree during injection. According to the proximate analysis results CC has the lowest volatile matter content with the highest fixed carbon, yet the conversion degree was the highest, which indicates that oxidation of the carbon was most significant for CC during injection. These results agreed with char yield calculation determined by weighing the carbonaceous material before and after the rapid heat treatment (described in section 6.3.3) at temperature of 1500 °C.

On the other hand, the conversion of both TC and BGC was much lower than CC and the conversion due to rapid devolatilization agrees with the volatile matter content in their raw materials. This behaviour for CC confirms that injection of CC can lead to lower char yield in HIsarna's SRV bath compared to TC and BGC, but higher combustible gas yield which could affect the HIsarna reactors behaviour. For example, it may be necessary to increase the HIsarna's CCF efficiency (i.e., the efficiency of iron ore pre-reduction in CCF by CO off-gas evolved from the SRV) to utilise the extra reductive gas proportion produced during CC injection to maintain the overall efficiency for combination of CCF and SRV. Furthermore, the results reveal that despite the lower VM content in CC, its conversion is significantly higher, therefore the char yield is not determined by VM content only, but also the physical and chemical properties of carbonaceous materials directly influence the solid char yield during rapid devolatilization.

7.4.2 Gasification analysis using Thermogravimetric analyser (TGA)

To compare the gasification behaviour of the carbonaceous materials selected and study the effect of rapid devolatilization, the reactivity with CO_2 is analysed using TGA for the char particles produced during DTF injection and their parent materials. The relative reactivity of the three carbonaceous materials and their chars prepared under rapid devolatilization are compared using their weight-loss profile in TGA, as shown in Figure 7.2.

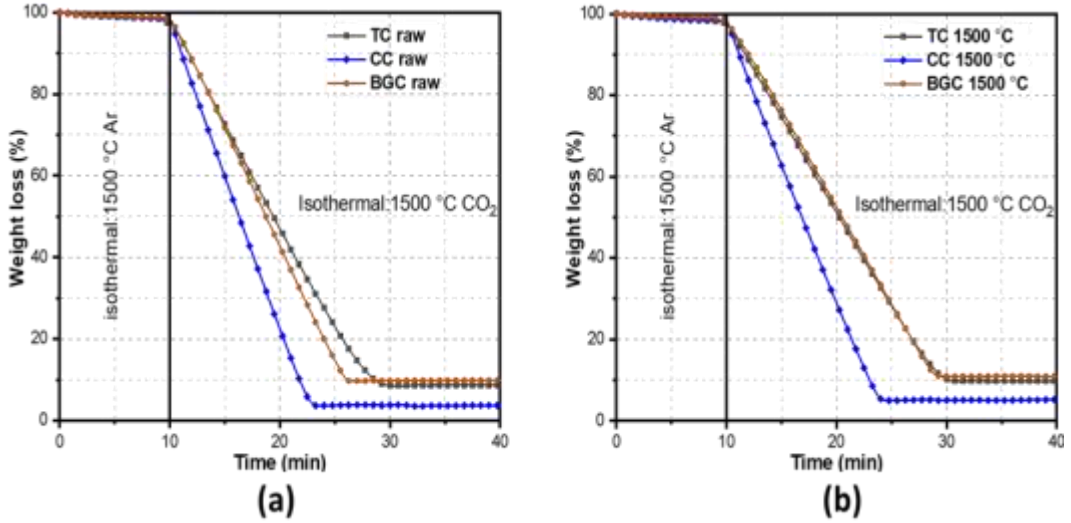

Figure 7.2: The isothermal weight loss profile under carbon dioxide at 1500 °C for (a) raw carbonaceous materials and (b) chars produced during rapid devolatilization in the DTF.

Clearly, the raw CC has the fastest gasification reaction with CO_2, followed by the BGC raw and TC raw (Figure 7.2a). The CC char produced from rapid devolatilization has the fastest gasification reaction with CO_2, but the BGC and TC chars produced from rapid devolatilization showed very similar behaviour as can be seen in Figure 7.2b. Based on this weight loss profile, the reactivity index values with the error bars representing average uncertainty in either side of the mean are calculated and shown in Figure 7.3. As shown in Figure 7.3, rapid devolatilization causes the carbonaceous materials to be less reactive with CO_2, and this effect has been more significant for BGC. Previous studies have reported that rapid devolatilization could promote the char gasification characteristics due to the accelerated release of the volatile matter, which can increase the internal pressure of pores and destroy their structures to increase the specific surface area [139, 140]. However, the rapid devolatilization at high temperatures (e.g.,1500 °C) reduces the chemical functional groups and increase the ash content, while the carbonaceous materials ranking is upgraded (e.g., fixed caron and energy content increased). This results in more compact stable structures hindering the char gasification [71]. The reactivity index for all three chars produced by rapid devolatilization process at 1500 °C was lower than that for the raw carbonaceous materials with the index ratio for BGC 1500 °C, TC 1500 °C and CC 1500 °C being 84.21%, 92.11% and 94.23% of their raw materials respectively.

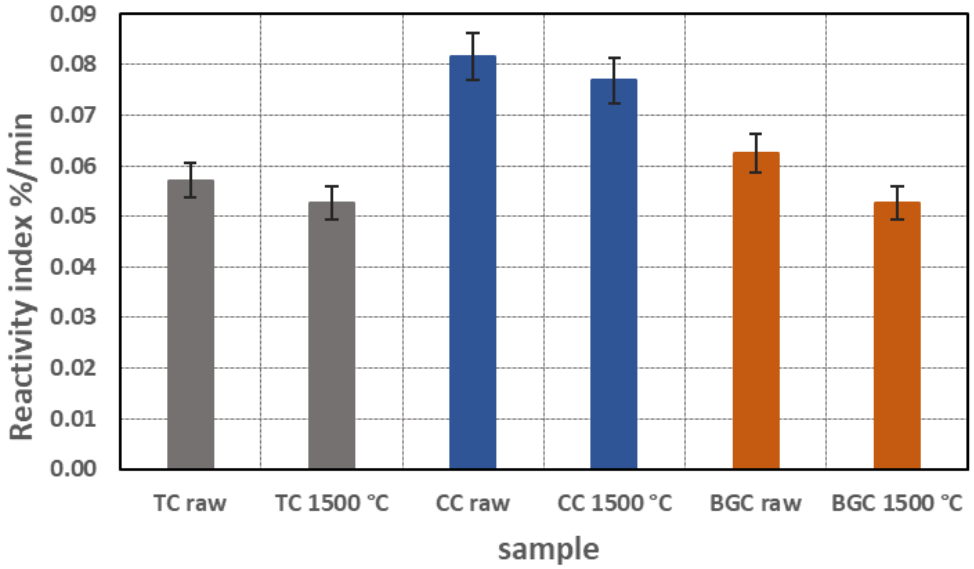

Figure 7.3: Reactivity index for raw materials and devolatilized chars produced under rapid heating at 1500 °C. Error bars represent uncertainty in average either side of the mean.

The results in Figure 7.3 further confirm that CC will be the most reactive carbonaceous material in HIsarna SRV, while TC and BGC have very similar gasification behaviour. The higher reactivity for CC may cause instability in the SRV due to behaviours such as foaming from faster CO formation and changes in furnace temperature, and may lead to lower efficiency in SRV, therefore it is necessary to enhance the productivity of the CCF during CC injection to utilize the extra CO generated from the CC devolatilization.

7.4.3 Qualitative SEM analysis

SEM images of all three raw materials and their chars produced from rapid devolatilization at 1500 °C are shown in Figure 7.4. These images represent a bulk behaviour for each carbonaceous material. furthermore, an individual particle from each material before and after rapid devolatilization is magnified for an in-depth study and represented in Figures 7.5 and 7.6 respectively.

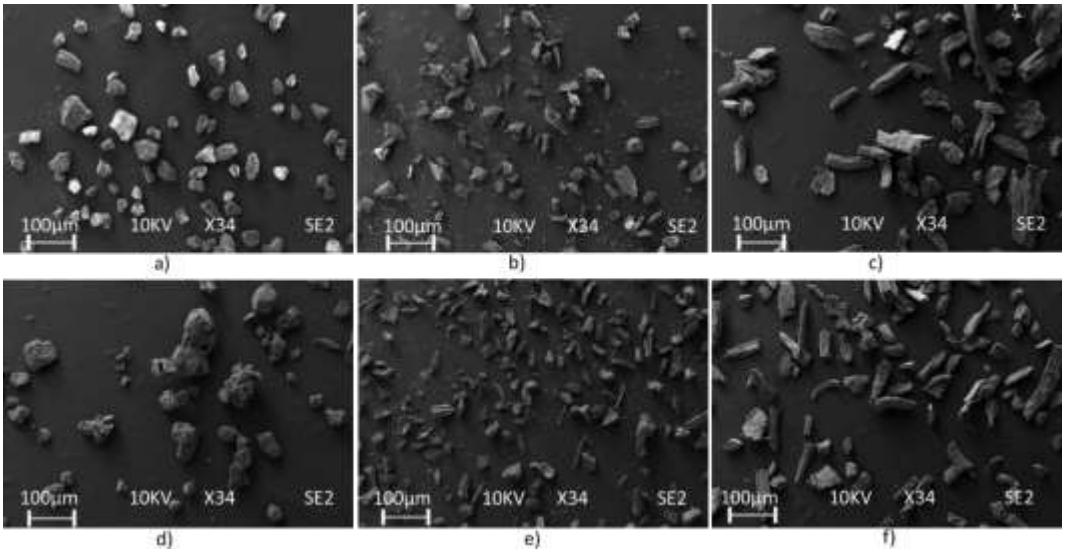

Figure 7.4: SEM images of bulk materials (a) TC raw; (b) CC raw; (c) BGC raw; (d) TC 1500°C; (e) CC 1500 °C; and (f) BGC 1500 °C.

Comparison of these chars from rapid devolatilization and their corresponding parent materials shows significant morphological changes caused by the rapid devolatilization process. These images are taken after a preliminary analysis of a large sample to ensure that typical morphologies observed for each sample. The difference in size, shape and surface roughness can be noticed for parent materials and their chars produced from rapid devolatilization. The TC particles are observed very compact with irregular shape and smooth and non-porous surface as can be seen in Figure 7.5a. However, both biomass samples (CC and BGC) have maintained their fibrous structure, and the cross-section view of CC shows that the capillaries from the wood are still present with a large number of micropore and mesopores of non-uniform size on the plane surface which will contribute to the relatively larger specific surface for CC as shown in Figure 7.5b. Less capillaries of small diameter and coarser particle surface can be observed through the BGC particle (Figure 7.5c).

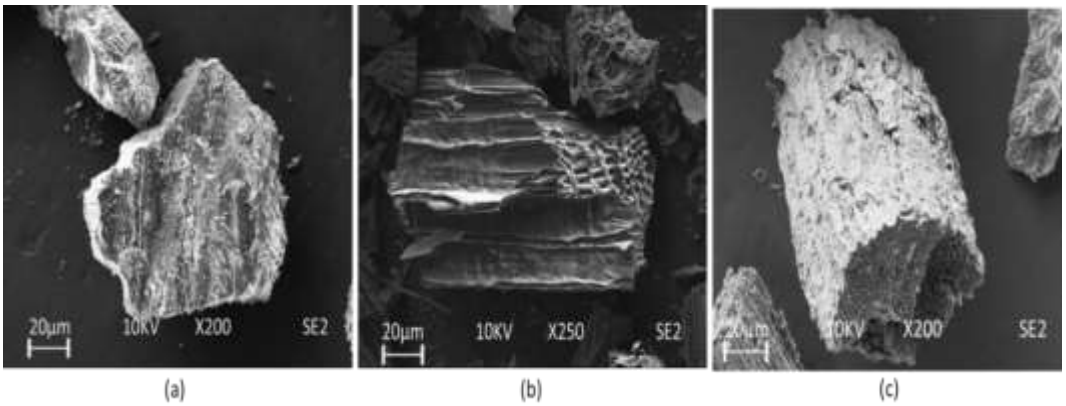

Figure 7.5: SEM images of raw materials (a) Thermal coal TC (b) Charcoal CC (c) Bana grass char BGC.

The oblong particles observed for BGC with the length of the particle is larger than the sieve range (90-300 μm) used. During sieving process only the width of the particle is considered, since oblong particles may pass through the mesh with its minor size, as a result the representative size is much higher than it is counted for, which has also been reported by other researchers [143]. In contrast, CC is the mixture of more irregular shape with some spherical and oblong particles.

As it can be noted in Figure 7.6 all the char particles produced from rapid heating at 1500 °C maintained similar shapes to their parent materials, however the size of the char particles is reduced compared to the parent materials, although some of the particles are sintered for TC. This change can be linked to mechanisms such as particle shrinking or fragmentation depending on the thermal treatment. Both biomass samples were able to maintain the morphology similar to their parent materials, because the natural porosity within the materials allows the release of the volatile products without severe change in the particle structure. In contrast, TC sample has gone through much more severe transformation, as it can be seen in Figure 7.6a, large openings on the char surface are observed, which are caused by the release of volatile products through a melting surface of the char during the rapid devolatilization at 1500 °C.

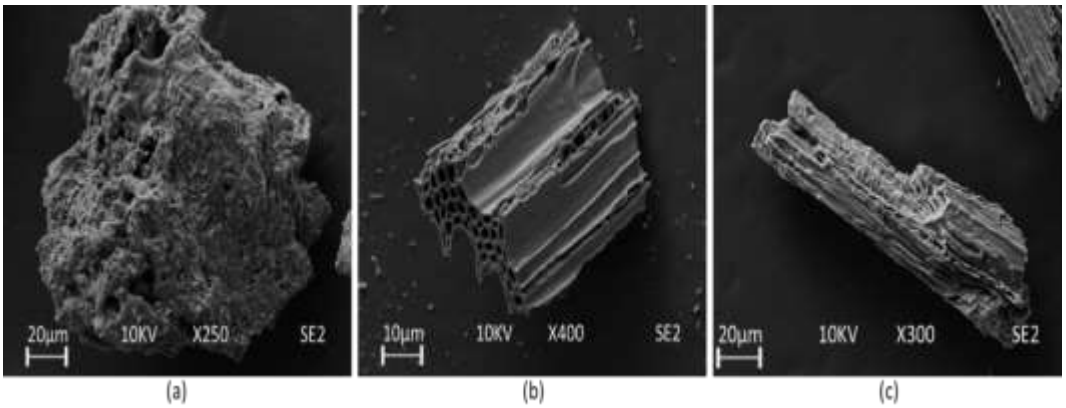

Figure 7.6: SEM images of chars produced from rapid devolatilization at 1500 °C for (a) Thermal coal TC, (b) Charcoal CC, and (c) Bana grass char BGC.

During the rapid heating, the solid matrixes of carbonaceous materials are softened, resulting in some of the pores to be clogged. Then the volatile matters generated inside the particle creates an overpressure, which leads to bubbles formation and

subsequently burst to the openings on the char surface [70]. This phenomena is more evident in the TC particle due to more compact structure and thermal coal also known to have higher thermoplasticity [130], as a result swelled surfaces and large cavities under the surface can be seen in Figure 7.6a. It can be speculated that this behaviour in TC particle can create smoother surface, which can cause the material to be less reactive for the subsequent steps of oxidation. Although the chars of CC and BGC after rapid devolatilization retained their parental shapes, this rapid heating is likely to have caused collapsing phenomena due to melting of ash and softening in the solid matrix, as a result more compact structure has been produced than their parental materials. This explains the slowdown in the gasification behaviour during the reactivity tests for all carbonaceous materials, BGC with the highest ash content is expected to suffer the most, followed by TC and CC as shown in Figure 7.2 and Figure 7.3.

7.4.4 Quantitative BET analysis

The porosities of the raw carbonaceous materials and their chars produced by the rapid devolatilization at 1500 °C are measured by the N_2 adsorption–desorption isotherms and shown in Figure 7.7. According to the International Union of Pure and Applied Chemistry (IUPAC) classifications the isotherms for both TC raw and TC 1500 °C belong to type III isotherm as can be seen in Figures. 7.7a &7.7d respectively. The flat region corresponds to the monolayer formation, which indicates weak interaction between the adsorbent-adsorbate, and this could be due to non-porous or existent of macroporous only on the TC structure [144]. The rapid devolatilization caused the adsorption isotherm to increase slightly for TC, and it has resulted in an increase in the average pore diameter and BET surface area as shown in Table 7.1. The adsorption isotherms for both CC raw and BGC raw shown in Figures. 7.7b & 7.7c belong to type I isotherm, which indicate more microporous in these materials [143-145]. Also for both materials steep uptake is visible at very low p/p_0, which is due to high interactions between adsorbent-adsorbate in narrow micropores as a result micropores are filled at very low p/p_0 [144].

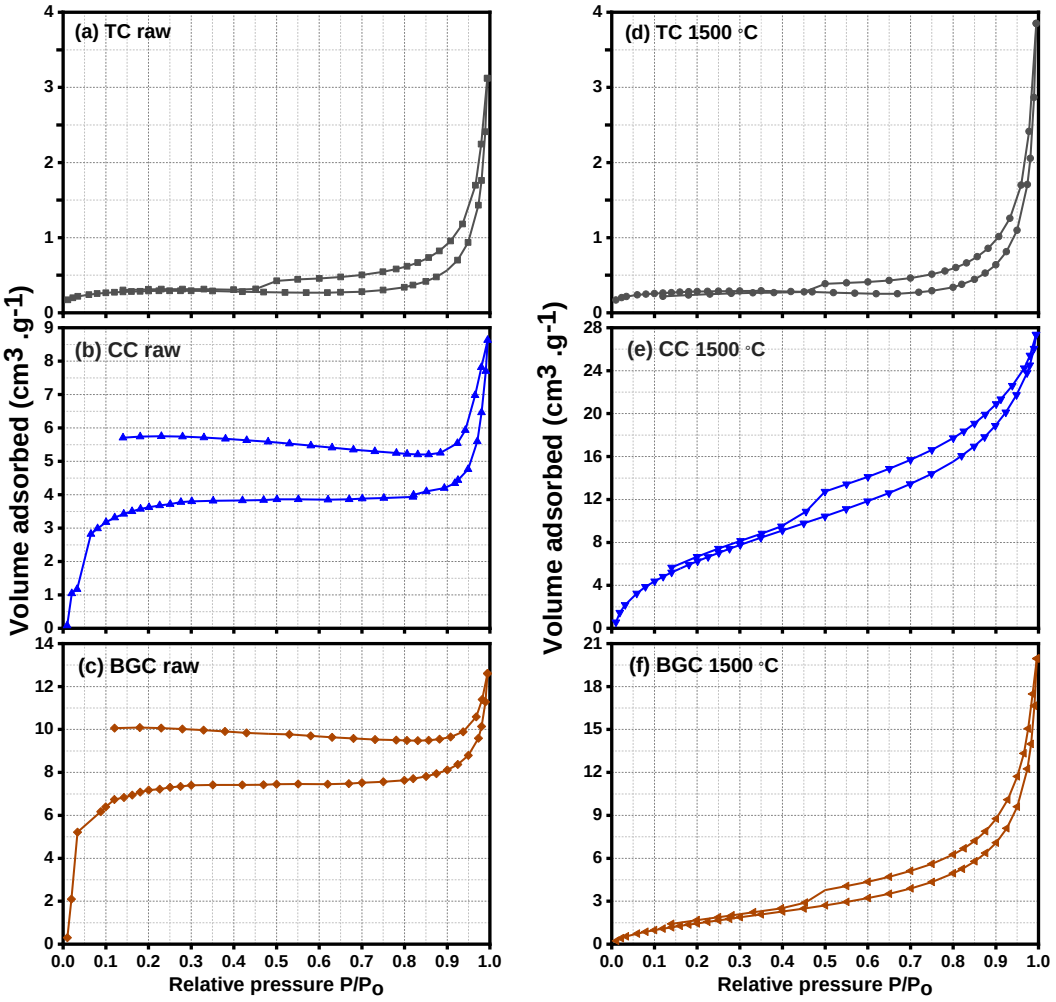

Figure 7.7: Nitrogen adsorption–desorption isotherms of (a) TC raw; (b) CC raw; (c) BGC raw; (d) TC 1500°C; (e) CC 1500 °C; and (f) BGC 1500 °C.

As shown in Figures 7.7e and 7.7f, both CC 1500 °C and BGC 1500 °C belong to type II isotherm, which confirms changes in the pore structure for both materials under the rapid heating [144]. Although steeper uptake is visible for the BGC raw compared to the CC raw at low p/p_0, the isotherm for CC 1500 °C (Figure. 7.7e) is significantly steeper than the isotherm for BGC 1500 °C (Figure. 7.7f) at low p/p_0. This could be due to higher collapsing of micropores in BGC compared to CC from the results of higher ash content in the BGC which can melt and soften the solid matrix during the rapid heating at 1500 °C. As it can be seen in Figures 7.7b & 7.7c, both CC and BGC raw isotherms present a non-reversible desorption branch, and this is due to presence of constricted micropores which limits the adsorption of the N_2 at 77K. In contrast, all the other materials including CC 1500 °C and BGC 1500 °C produced a hysteresis loop at the relative pressure between 0.45 and 0.99. Similar findings has been reported

by Wang et al. [148] which has been linked to the difference in the evaporation behaviour compared to condensation within the pores due to capillary condensation in mesopores.

The BET surface area, pore volume and average pore diameter determined are shown in Table 7.1 for all three raw materials and their chars after the rapid heating at 1500 °C. Despite the slight increase in the BET surface area and average pore diameter after rapid devolatilization, both TC raw and TC 1500 °C appear to have significantly smaller surface area compared to the biomass materials, which results in the lower reaction rate for the TC samples. As expected, CC raw has very large surface area that was further increased by the rapid devolatilization at 1500 °C, while the average pore diameter decreased significantly. This could be due to particle fragmentation during the rapid heating resulting in the smaller particles and high surface area, subsequently larger amount of N_2 adsorbed while the average pore diameter decreased which could be due to blockage or collapse of some of the original pores [147].

Table 7.1: BET surface area and pore characteristic parameters for both raw carbonaceous materials and chars produced during rapid devolatilization at 1500 °C (Data obtained by Dr Volkan Degirmenci School of Engineering- University of Warwick).

Samples	BET Surface area[a] /m^2 g^{-1}	Pore volume[b] /cm^3g^{-1}	Average Pore diameter[c] /Å
TC raw	1.1	0.004	216.7
TC 1500 °C	1.5	0.005	249.0
CC raw	36.0	0.025	459.8
CC 1500 °C	61.7	0.060	52.7
BGC raw	48.6	0.032	553.5
BGC 1500 °C	13.4	0.030	111.4

[a]BET equation was applied between p/p_0=0.05-0.3 at adsorption branch of the isotherm. [b]Total pore volume at p/p_0=0.99. [c]Desorption average pore width by BJH method.

BGC raw appears to have higher BET surface area compared to other raw materials, but the BET surface area and average pore diameter decreased quite significantly by the rapid heating. This behaviour in BGC again could be due to the high ash content,

ash composition and morphology in the BGC raw and the ash in BGC raw material will melt during the rapid heating and create more compact structure with smaller surface, hence this is also evident in the gasification tests. The BET results show that the gasification behaviour influenced by several parameters such as particle shape, porosity, ash content and chemistry rather than the surface area only for the materials selected for this study.

7.4.5 Temperature effect on char size and shape variation

It is apparent from Figures 7.5 & 7.6 that rapid devolatilization results in changes in size and shape of the carbonaceous materials caused by the release of the large amount of volatile products in a short period of time. The size and shape of the solid carbonaceous materials may play an important role in the HIsarna reactor due to their effects on the fluid dynamics and the diffusion mechanisms. To better understand the variation in size and shape under thermal treatment, the high temperature confocal laser scanning microscope (HT-CSLM) has been applied. The main advantage of using this technique is that HT-CSLM allows continuous imaging of 2D plane of particles at the temperature under controlled high heating rate (up to 100 °C/min) while the changes in the size and shape are taking place. Figure 7.8 shows the comparison of the average change in the particle size and shape for all the parent carbonaceous materials studied. The results show that the final swelling ratio for all materials is smaller than 1, which confirms that devolatilization results in decrease in the particle size for all the materials.

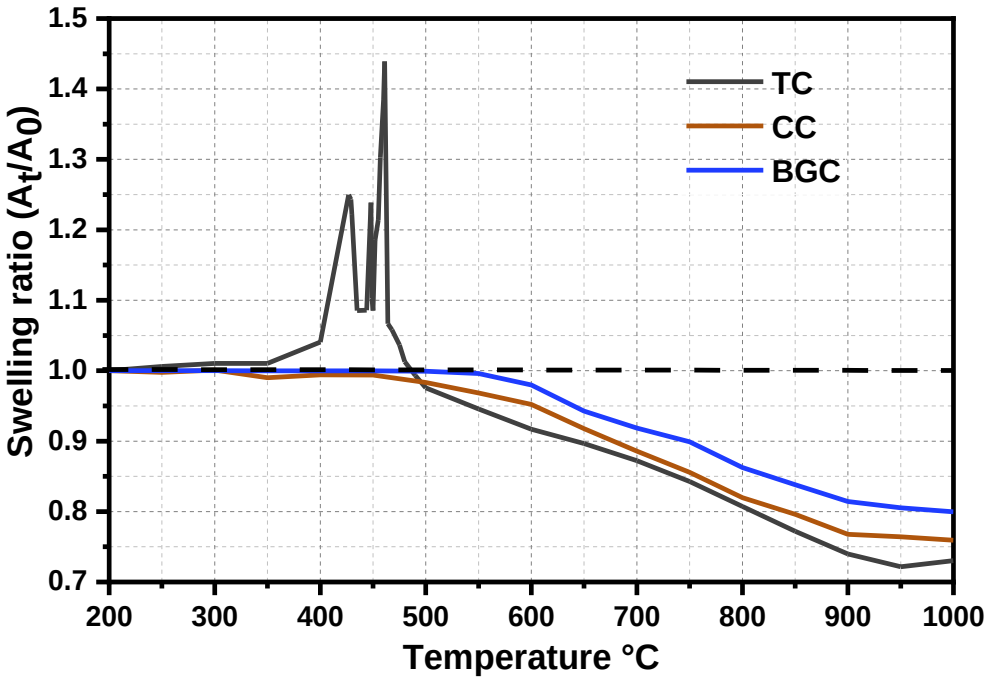

Figure 7.8: A comparison of an average swelling profile for five particles of each raw carbonaceous material under argon at heating rate of 100 °C/min in the HT-CSLM.

The swelling ratio profile for TC shows that at the temperature between 380 °C and 470 °C the swelling ratio increases in a series of oscillation. This behaviour in TC can be linked to the formation and rupture of bubbles due to the release of volatile products and reformation of bubbles within that temperature range as shown in Figures. 7.9b to 7.9d. This phenomenon is most obvious in particle one and particle five which are highlighted. It is believed that this variation in the swelling profile in that temperature range is attributed to the release of different volatile products due to decomposition of different components at a specific temperature. This behaviour agrees with the authors' previous findings for the same thermal coal material, which shows that each volatile products such as CO, CO_2, H_2 and light hydrocarbons is released at specific temperatures within the temperature range between 400 °C and 500 °C during thermal decomposition [125]. After reaching the maximum swelling ratio at 460 °C the reformation of bubbles no longer takes place, and the particle size decreases rapidly due to severe bubble ruptures and particle shrinking. As a result, the average particle size is reduced to around 72% of the particles' starting surface area, which proves that higher degree of transformation (i.e., structural change) takes places in TC than biomass samples.

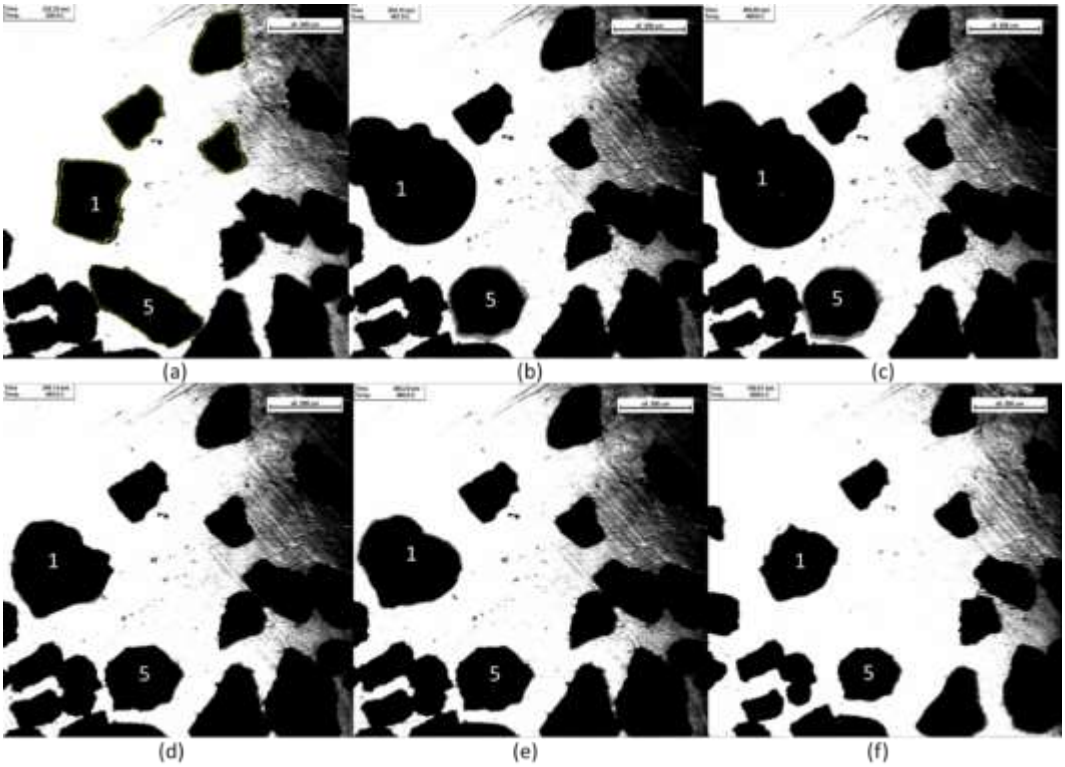

Figure 7.9: Illustration of swelling behaviour of TC at (a) 200 °C; (b) 457 °C; (c) 460 °C; (d) 464 °C; (e) 468 °C; and (f) 996 °C during heating in the HT-CSLM at 100 °C/min.

The behaviour of biomass samples (CC and BGC) differs from that observed for TC. No swelling was observed for either biomass sample, but the particle size for both materials was observed to decrease. The decrease in the swelling profile starts at different temperatures for each biomass sample. The decrease in the average particle size for CC starts at temperature around 350 °C, at a very slow ratio but it accelerates at the temperature > 450 °C with the final particle size being around 76% of starting particle. Again this result agrees with previous finding by Khasraw et al. [125] on devolatilization behaviour for the same material, and this confirms that the size decrease is due to release of volatiles and reactions at the particle surface. As shown in Figures. 7.10d to 7.10f the decrease in the swelling ratio for BGC was observed to start at the temperature >550 °C, this could be related to the fact that BGC has already been pre-treated to 500 °C during production and as such lower molecular weight/lower boiling point volatiles may have already undergone some devolatilization.

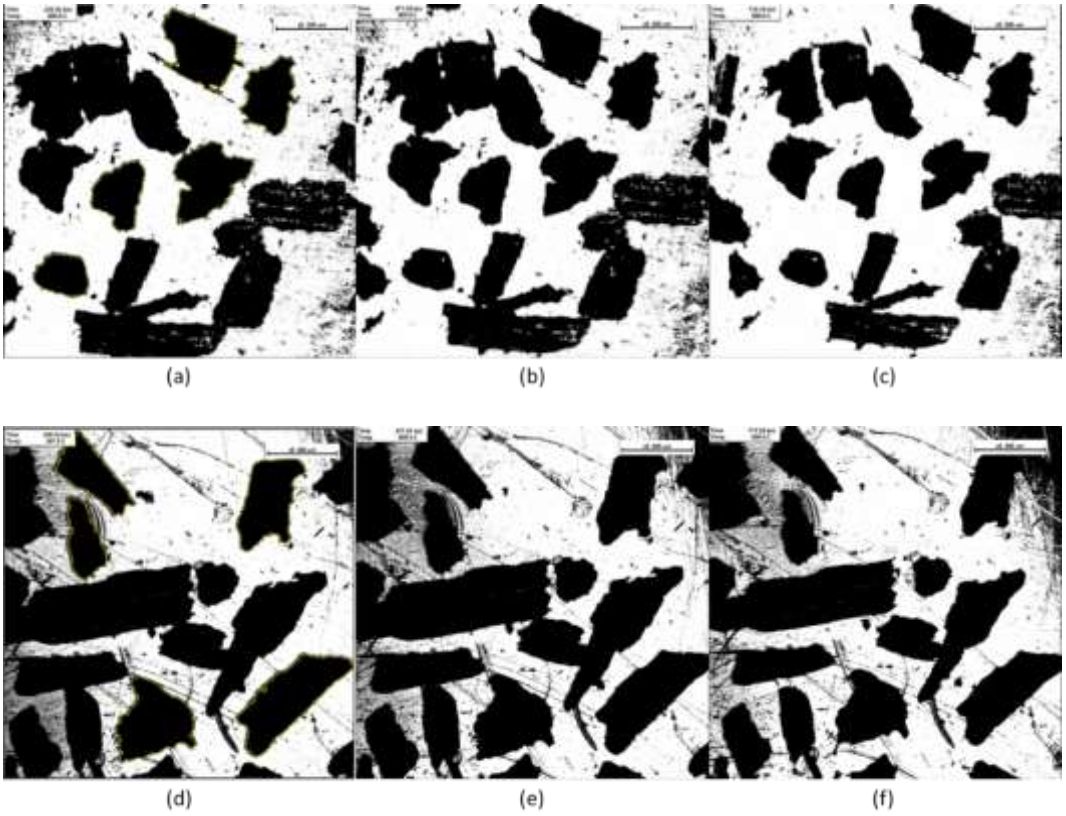

Figure 7.10: Illustration of changes in particle size and shape of CC at (a) 200 °C; (b) 600 °C; (c) 996 °C; and BGC at (d) 200 °C; (e) 600 °C; and (f) 998 °C.

The final average particle area for BGC was reduced to 80% of the starting particle area. Furthermore, there is no change in shape of biomass samples, and both CC and BGC retained the shapes of their parental materials, but TC particles suffered much more severe physical changes and the particle roundness increased.

7.5 Conclusion

To understand the behaviour of carbonaceous materials during injection in the novel HIsarna ironmaking process, chars of three different carbon sources are produced by rapid devolatilization at 1500 °C which is similar to the thermal conditions the injected carbonaceous materials undergo in the HIsarna process. The behaviours (reactivity, morphology change, surface area and swelling) of three different carbon sources and their chars produced from rapid devolatilization at 1500 °C were investigated using analytical and morphological methods. The following conclusions can be drawn from this study:

- CC has gone through the highest carbon conversion degree (X) during rapid devolatilization, followed by TC and BGC, 30.1%, 22.0% and 19.8%

respectively. This confirms that the devolatilization conversion is not determined by the volatile matter (VM) content only, but the physical and chemical properties of the carbonaceous materials also directly influence the conversion degree during rapid devolatilization.

- CC has shown the fastest gasification reaction before and after rapid devolatilization, followed by BGC raw and TC raw. Rapid devolatilization caused the chars produced from all materials to be less reactive with CO_2, but this behaviour was more significant for BGC. As a result, both TC 1500 °C and BGC 1500 °C have shown very similar gasification reaction.
- Rapid devolatilization resulted in the decreased particle size for all carbonaceous materials due to the release of volatiles and fragmentation. SEM images showed that chars produced from TC have gone through severe degree of structural transformation while chars from biomass samples (CC and BGC) maintained their parent structural shapes. This is confirmed by the direct observation of the structural change for all three carbonaceous materials using HT-CSLM.
- The BET results indicate that TC is non-porous or contains macroporous only, while both raw biomass samples (CC and BGC) contain a large number of constricted micropores and mesopores which resulted in significantly larger surface area for biomass samples. However, the average pore diameter decreased significantly for both CC and BGC because of rapid heating leading to blockage or collapse of some of the original pores. Furthermore, the gasification reaction is controlled more by parameters such as particle shape, porosity, ash content and chemistry rather than the surface area.

Chapter 8

Reduction of FeO in molten slag by solid carbonaceous materials for HIsarna alternative ironmaking process

8.1 Hypothesis to be investigated

Hypothesis 5 – Biomass chars will react differently with FeO-containing molten slag in comparison to thermal coal chars.

8.2 Introduction

It is known the in the literature that there are five possible rate-limiting steps which will control the reduction mechanism for FeO reduction in the molten slag by solid carbon. Most of the research conducted in this field has been reviewed in section "2.4 Reaction mechanism of FeO reduction in smelting slag by solid carbon". Among the research reviewed here, there are some discrepancies in the rate controlling step and mechanisms for the reaction between iron oxide contenting slag and carbon from different sources. Limited information is available in the literature about the reaction kinetics for smelting reduction of FeO in the slag by solid carbon injection concerning HIsarna technology. Therefore, the purpose of this work is to investigate the reduction of FeO in synthetic HIsarna slag by injecting solid chars produced from different carbonaceous materials, i.e., thermal coal which is used in HIsarna trials and biomass which has potential to be trialled. To conduct this study a novel technique using drop tube furnace coupled with an online quadrupole mass spectrometer (DTF-QMS) was employed to study the reactions under thermal conditions similar to HIsarna SRV. The amount of CO and CO_2 evolved from the reactions are measured using the online QMS to calculate FeO concentration in the slag and determine the overall reaction kinetics in the temperature range from 1450 to 1525 °C. The extent of FeO reduction in the reacted slag samples is also quantitatively measured by Wavelength Dispersive X-Ray Fluorescence (WDXRF). Based on the experimental results, the kinetic parameters, the reaction mechanisms, and the rate limiting steps for the reduction of FeO in the synthetic HIsarna slag are found for different carbonaceous materials.

8.3 Experimental

8.3.1 Slag and carbon preparation

The synthetic slag with the weight composition of 41.7% CaO, 33.3% SiO_2, 13% Al_2O_3, 6% MgO and 6% FeO was prepared using reagent grade oxide powders (supplied by Sigma-Aldrich). The FeO powder used has purity ≥ 99.7%. The chemicals were mixed carefully to homogenize, and then stored in well-sealed dry containers. Thermodynamic calculation by FactSage indicates that the first liquid slag forms at 1240 °C and the slag is fully molten at 1398 °C.

The solid chars used were prepared from three different carbon sources one coal and two biomass materials (thermal coal (TC), charcoal (CC) and Bana grass char (BGC)). All the samples were crushed into small particles with the size range from 90 to 300 μm, and then chars were prepared by heating each material to 1300 °C in high purity (99.999%) argon atmosphere at the heating rate of 10 °C/min and held for 3 hours to ensure all the volatiles are removed. The proximate and ultimate analysis data of the carbonaceous materials used in the preparation of chars are given in Table 6.1.

8.3.2 High temperature slag-carbon reaction

Experiments to study the reduction reaction of FeO in the slag by solid char were performed in the DTF described in section 4.2 which is schematically shown in figure 6.1. The injection method reported in section (6.3.2 Rapid devolatilization) applied to deliver the char particles into a molten slag and Quadrupole Mass Spectrometer (QMS) used to measure the reaction off-gas. DTF-QMS combination allowed the slag samples containing FeO to be heated to pre-set reaction temperatures of 1450, 1475, 1500 and 1525 °C and then injected chars particles into the molten slag. The reduction reactions in chapter needed to conduct at temperatures higher than the melting point of the slag to simulate the smelting reactions taking place in the HIsarna SRV. The furnace used for this study have limitations to go much higher than the temperatures selected for this study, as a result wider temperature range could not possibly be selected for these experiments and 25 °C increments chosen as suitable range for the study.

Approximately 20 g of slag samples were placed in an alumina crucible (height 65 mm x diameter 42 mm) on the alumina pedestal and lifted to the hot zone of the DTF. The char particles were injected into the molten slag in the pre-set temperature zone through the lance connected to the particle feeder on one side and positioned on the top of the crucible containing the slag on the other side. Considering the ash content

of each material is different and assuming the volatile matters are completely liberated, the carbon element with FeO is calculated to be 1:1 within the char weight to fully reduce iron oxide to metallic iron and if the reaction products are Fe and CO only. Before the experiment starts, a char sample of approximately 225.5, 204.2 and 226.9 mg produced from TC, CC and BGC respectively was placed on the seat of the bottom ball valve on the "off" position, and Ar (with a 99.999% purity) flush through the feeder to create an oxygen-free atmosphere and then closed all the valves. While the furnace was heated to the desired temperature at the heating rate of 10 °C/min, a carrier gas (Ar, 99.999% purity) at the flow rate of 1 L/min was purged from the furnace bottom to ensure an inert atmosphere.

When the furnace temperature reached the pre-determined high temperature, the alumina lance was lowered into the crucible directly above the slag. The valve holding the char sample was then opened, and at the same time the valve controlling the Ar gas was switched to the feeder for ~10 seconds to maintain the Ar atmosphere while the char particles were injected into the molten slag in the furnace. The experiment was continued for 1 hr, and during that time the QMS was set to measure readings of the following gaseous products: N_2, O_2, CO, CO_2, Ar, H_2O, H_2, CH_4 and C_2H_6. Then the furnace was cooled down at the rate of 5 °C/minutes to room temperature in an Ar atmosphere, and the samples were collected for further analysis.

8.3.3 Wavelength dispersive X-ray fluorescence (WDXRF)

The wavelength dispersive X-ray fluorescence (Rigaku Primus IV WDXRF with a Fluxana RAW package) was used for chemical analysis of the reduced slags to determine the total iron content to measure the extents of reduction. Prior to commencing the sample tests, the machine was calibrated against standards fused beads to produce accurate results. The samples were prepared into 40 mm fused beads using fully calibrated Fluxana Vitriox Electric fuser. The powders were fully dried prior to weighing (1 g sample to 8 g flux). These prepared sample beads were placed in the XRF machine, and then the XRF chamber was evacuated, and the sample was ionized with X-rays, which allows the iron content to be measured accurately in a cross section.

8.3.4 Analytical Techniques for reacted samples

The metallic iron produced from the slag-carbon reaction was separated from slag using magnets, which was found to be very effective to recover metallic iron [149]. Then the carbon and sulphur contents in the metal droplets were determined using an ELTRA CS-2000 carbon sulphur determination PC controlled model. The machine was calibrated by performing three tests using calibration standard for carbon/sulphur under the same condition used for sample tests. Approximately 350 mg of iron was placed in the crucible and 250 mg of tungsten accelerator was added, and then the crucible was placed on the pedestal for the analysis to start in the software.

Scanning electron microscopy (TM3030Plus) images were obtained for the slag-carbon (char) reaction samples. The technique was used in the research for clarification of the Fe-C alloy and reveal information about the samples before and after reaction including external morphology (texture), chemical composition, and crystalline structure by mapping the samples. Different magnification degree between 40 X to 1000 X with the imaging conditions of 10 kV voltage applied for detailed study of iron droplets e.g., carbon content and carbon dissolution in the Fe-C alloy.

8.4 Results and discussion

8.4.1 Effect of temperature

To understand the effect of temperature on the reduction rate of FeO in molten slag and gas evolution, the DTF experiments for TC, CC and BGC char injections were conducted at four temperatures of 1450, 1475, 1500 and 1525 °C, respectively. It was observed that the rate of FeO reduction increases with increasing the reaction temperature and the ratio of gas composition measured changes. As an example, figure 8.1 shows the rate of CO and CO_2 gas evolution with the time during the reduction of molten FeO in the slag by injection of solid chars produced from CC at various temperatures. Note that the rates are in ml/s with no surface area included. This is because there is no fixed contact area, and the particle size are expected to change (swell or shrink) during the reaction therefore the contact surface was unknown. There was a short incubation period (15 to 20 seconds) at the beginning of each reaction due to slow reaction at that time and the time required for gases to travel from the reaction zone to the detection point at the online QMS, which is similar to the findings reported by Bafghi et al. [53] and Sun and Easman [150]. The travelling distance and gas mixing within the furnace may cause consistent slight delay in the gas detection as a

result there is a small amount of gas measured for a period after the process is completed.

The char particles injected were devolatilised and to confirm the gas species generated are from slag-carbon only, the QMS was set to analyse CO, CO_2, H_2O, H_2, CH_4 and C_2H_6 gases. These gases are the main gas species produced during thermal treatment of carbon materials (determined through a calibration run where m/z (the mass-to-charge ratio) 0-50 scanned). The main gas species detected were CO and CO_2 in the Ar balance, while the content of the other gas species was insignificant.

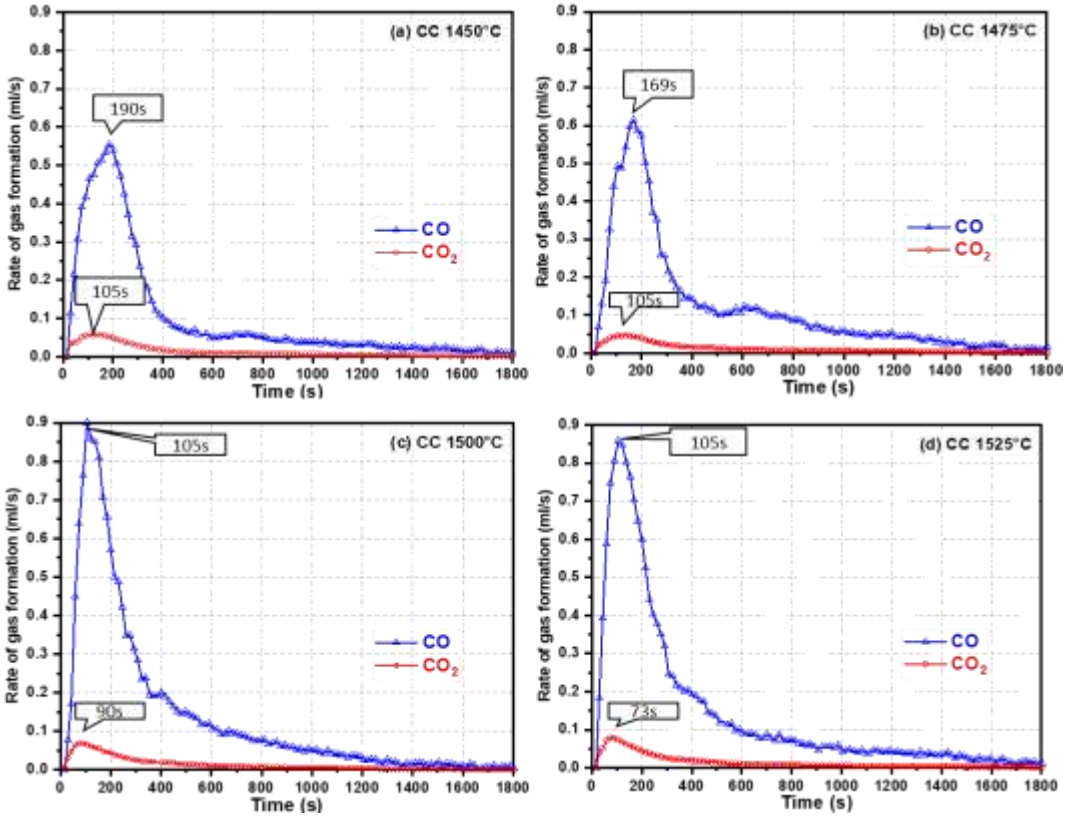

Figure 8.1: Rate of CO and CO_2 formation for char particle injection produced from CC into 20g of molten slag containing 6% FeO at 1450, 1475, 1500 and 1525 °C respectively in a high purity argon atmosphere.

Some common phenomena can be observed for the reaction at all the temperatures, as shown in Figure 8.1 The gaseous product from all the tests consists of both CO and CO_2 and there are two peaks for CO with one sharp peak which requires different time length to reach its maximum value depending on the reaction temperature. The second peak is partially superimposed on the late phase of the first peak, and it could be from the bubble explosion. This behaviour is more obvious at lower reaction temperature

due to slower reaction rate, and it suggests that the mechanism for reduction reaction change during the test. When the char particles are first injected the FeO concentration in slag is high, therefore the reduction rate is controlled by Boudouard reaction. After a short period of reaction, FeO concentration is decreased and Boudouard reaction is weakened. Therefore, the reaction controlling mechanism shifts from the chemical reaction to liquid phase mass transfer or mixed controlling mechanism which agrees with the other researchers' findings on similar reactions [41, 42, 45]. As shown in figure 8.1. the rate curve for CO_2 appears to be approaching zero after ~500 s for all temperatures, this means the reaction slows down beyond that point and the gas-slag reaction (Equation (2)) is slower than gas-carbon reaction (Equation (3)) which again confirms the shift in the controlling step. Moreover, the time required for the first CO peak to reach the maximum value decreases with an increase in the reaction temperature, approximately 190 s for 1450 °C , 170 s for 1475 °C, and ~100 s for both 1500 °C and 1525 °C.

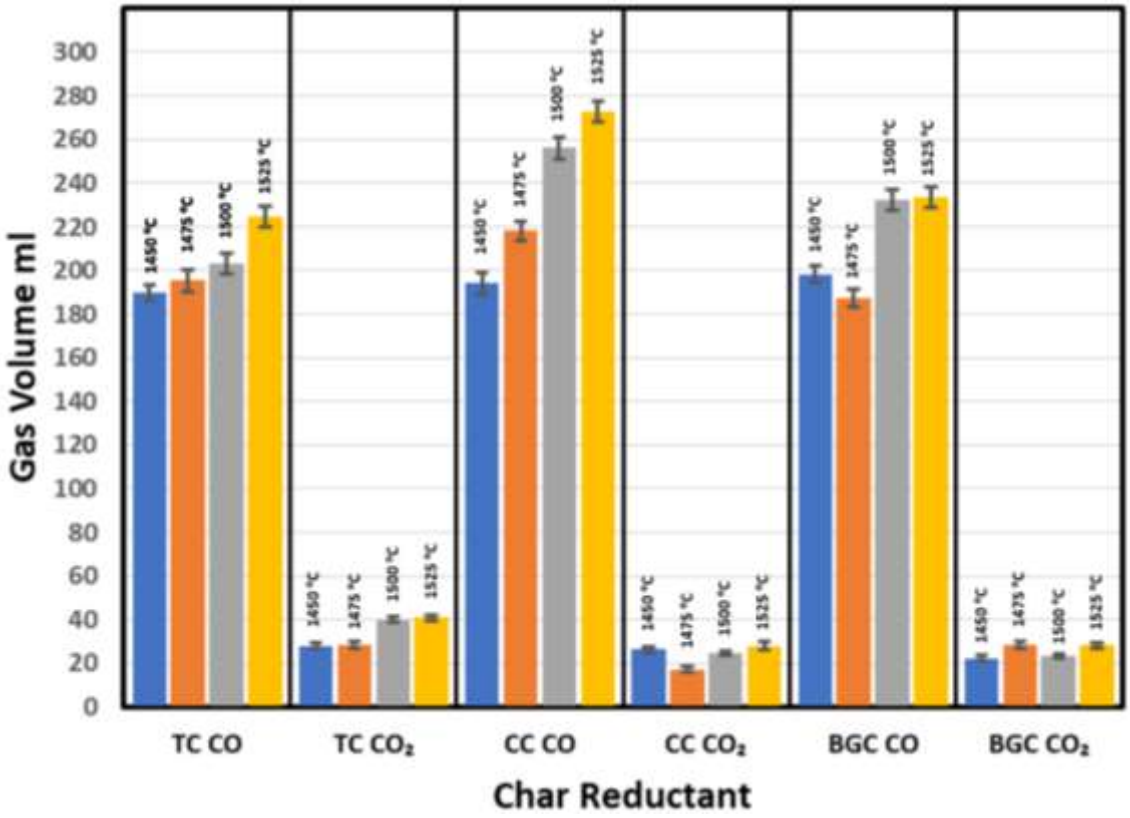

Figure 8.2. The amount of CO and CO_2 detected during reaction of TC, CC and BGC chars with 20g slag containing 6% FeO for 1 hour at 1450, 1475, 1500 and 1525 °C in an argon atmosphere. Error bars represent uncertainty in average either side of the mean.

Figure 8.2 shows the volume of gas species generated from the slag–char reactions at different temperatures. The results in Figure 8.2 show similarity in the behaviour of all three carbonaceous materials, i.e., in general, the gas volume increases with an increase in the reaction temperature. TC produced a larger amount of CO_2 at all temperatures compared to the two biomass materials (BGC and CC). This behaviour indicates that the reduction rate is controlled by the Boudouard reaction, since carbon gasification is responsible for gas variation. Gas diffusion in the halo can also be considered to have an influence on the rate controlling step at the first stage of the reaction. In the previous findings by Khasraw et al, [151], TC was shown to be less reactive with CO_2 while CC was the most reactive material. From this it can be assumed that the chemical reaction at the gas-carbon interface (Equation (3)) is the rate limiting step for the first stage of the reaction. Also, these results confirm that the gas variation and reaction paths are critically dependent on carbon type used as a reductant.

8.4.2 Extent of FeO reduction in the molten slag by different chars

The degree of FeO reduction in the molten slag by char particles produced from the three carbonaceous materials was determined at the temperatures ranging from 1450 to 1525 °C. The extent of the reduction and the rate were determined from CO and CO_2 gas measurements recorded by QMS during the reactions. The amount of oxygen removed, which equates to the moles of FeO reduced, is calculated from CO and CO_2 gas measurement. By knowing the initial weight of the FeO in the slag, the amount of FeO remaining in the bulk slag can be obtained with time by the QMS measurement. To confirm the results obtained via QMS, the reduced slag sample at 1500 °C was examined using WDXRF for quantitative analysis. The reactions observed for different chars at temperatures ranging from 1450 to 1525 °C are presented in Figure 8.3, where decrease in the FeO content of the slag with reaction time is shown. The extent and rate of FeO reduction in slag vary with the chars made of different carbonaceous materials, suggesting that the reaction kinetics are influenced by chemical and physical properties of solid chars. The reduction process proceeds through two steps, i.e., an initial fast reduction period and a slow secondary stage when the FeO concentration in slag is low. Clearly, the initial reduction rate of FeO by CC chars is the fastest, followed by TC chars almost for all temperatures.

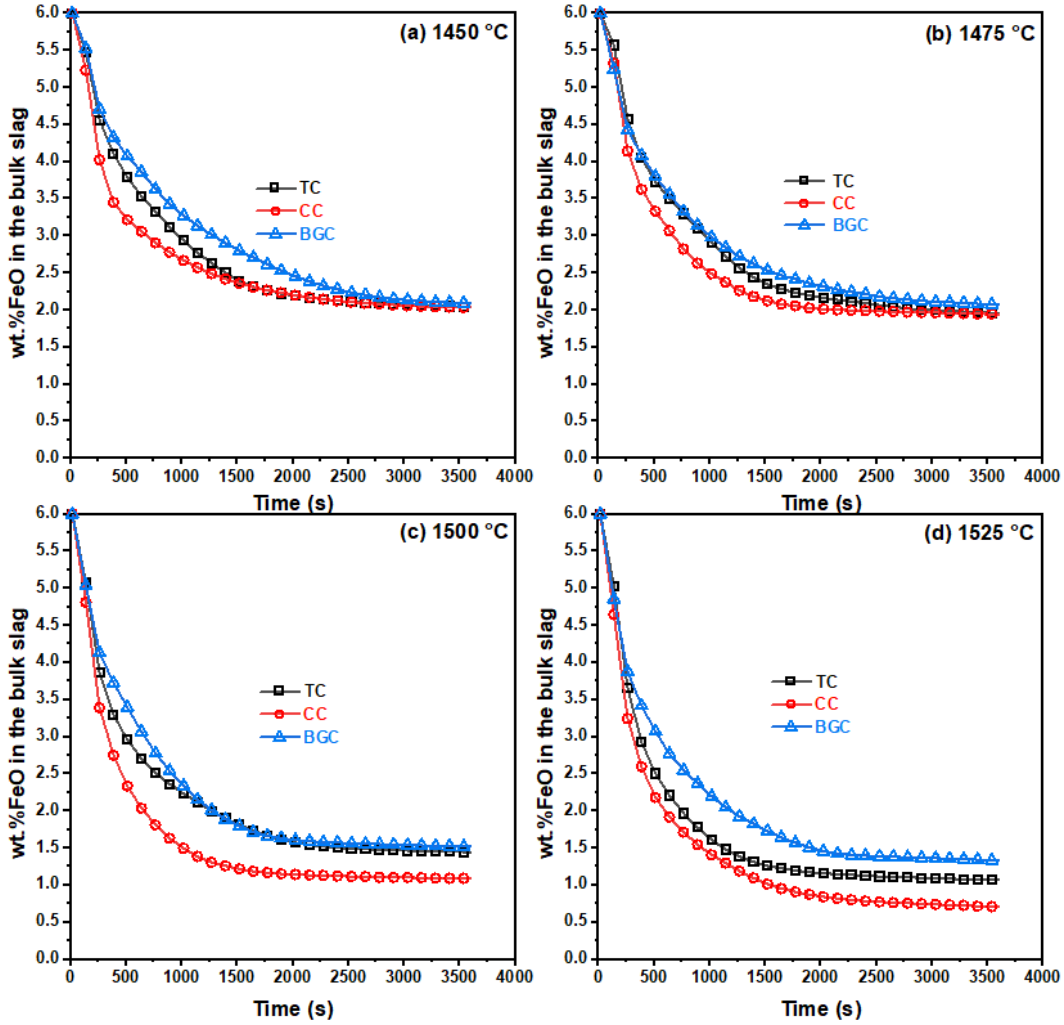

Figure 8.3: Reduction curves of FeO in a molten slag with different char particles at (a) 1450, (b) 1475, (c) 1500, and (d) 1525 °C.

However, the final concentration of FeO in the slag was similar for all three materials at 1450 °C and 1475 °C. The TC char particles appear to have higher reaction rate at initial stage compared to BGC chars but the final concentration of FeO in the slag was similar after 1 hour. The extent of FeO reduction achieved in the first 500 s under same conditions is over 60% for CC char, ~50% for TC char and just over 40% for BGC char. The extent of FeO reduction with char particles under different temperatures are presented in Table 8.1.

Table 8.1: The degree of FeO reduction by chars from different carbon sources at the temperature range of 1450 -1525 °C.

Temperature °C	TC wt%	CC wt%	BGC wt%
QMS gas analysis			

1450	66.01	66.10	65.10
1475	67.29	69.71	65.38
1500	75.76	81.88	74.70
1525	82.19	88.20	77.75
WDXRF slag chemical analysis			
1500	73.48	76.77	73.59

The QMS results in Table 8.1 show that the slag reduction degree with CC char was the highest at all temperatures and it has become more significant at 1500 and 1525 °C. TC and BGC chars are shown to have similar reducibility with TC char performing slightly better, however at 1525 °C the gap was widened, and TC char performed much better (82.19% reduction degree) compared to BGC char (77.75 % reduction degree). On the other hand, WDXRF analysis on the reacted slags (Table 8.1) confirmed that the extent of reduction was the highest for reaction with CC char at 1500 °C, while TC and BGC chars achieved similar reduction degree. The extent of reduction determined by QMS gas analysis was slightly greater than those measured by WDXRF for all reactions at 1500 °C. Overall, the reduction degree by different char particles calculated by QMS gas analysis is in good agreement with that calculated by WDXRF slag analysis.

With regards to the obvious difference in the reduction degree by different char particles in the initial stage (the first 500 s in Figure 8.3), this may be attributed to the difference in their physical and chemical properties of different char particles such as crystalline structure, particle surface roughness and ash content, which ultimately control the slag interaction with solid carbon particle and governing carbon reactivity [151], Biomass samples (CC and BGC) have non-compact, low dense fibrous structure, and capillaries from the parent materials are still present, while TC char particle are very compact with more spherical shape and smooth and non-porous surface [151]. The structure and capillaries on biomass char surface contribute to the relatively larger specific surface for interaction. The Raman spectroscopy results in section 6.4.1 confirms that CC contains disordered graphite structure and is more amorphous carbon compared to TC which will enhance the reactivity of CC. The study by Huang et al. [54] proposes that the FeO reduction by solid carbon is controlled by wetting characteristics of the carbonaceous materials and the carbon crystalline structure governs the interaction with the slag. While the same study suggests that

carbonaceous material ash content does not influence the slag–carbon interaction. In contrast many other researchers [14, 44, 149, 150] suggested that the ash content has strong influence on the reaction rate between slag and carbon. Assuming the chemical reactions (at char-gas and slag-gas interfaces) control the reduction process, then direct contact is not required, but gas diffusion between carbon and slag is necessary. The minerals (oxides) in carbonaceous materials can be partially or fully fused to form a physical layer on the carbon surface which can act as a physical barrier to inhibit or even prevent CO and CO_2 penetration in the halo. The ash content of the carbonaceous materials selected are 8.8 %, 1.8 % and 9.6 % for TC, CC and BGC, which shows that there is a correlation between ash content and FeO reduction rate for different char particles. Hence, it can be concluded that an increase in the ash content has a negative effect on the carbonaceous materials reducibility.

8.4.3 Quantitative and qualitative analysis of reduced slag and resultant iron droplets

The slag-carbon reaction produced metallic iron droplets which can clearly be seen and easily separated, as shown in Figure 8.4. Chemical composition of the reduced slag and the metallic iron droplets produced as well as the morphology of the droplets were then analysed using WDXRF**,** carbon/sulphur, and SEM images, respectively. Since there was no metallic iron in the initial slag sample, these iron droplets seen on the slag surface are the product of the slag-carbon reduction reactions.

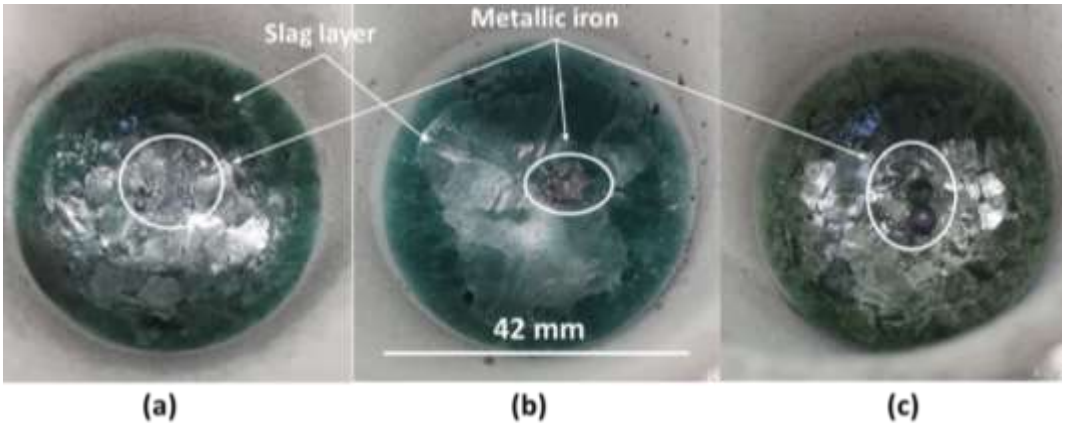

Figure 8.4: Iron droplets in the slag produced by slag-char reaction by (a) TC; (b) CC; and (c) BGC chars at 1520 °C contained in the crucible with 42 mm diameter.

According to equation ((7) and Figure 2.7) when the solid carbon injected contacts the molten slag, solid iron and gas are generated, and the gas then forms a film (gas halo)

around the carbon particle. The iron droplets formed can exist in liquid and solid phases at the slag-carbon interface [25]. However, under the experimental temperatures in this study, the droplets are expected to be in the solid phase unless they are carburised. Solid iron nuclei initially formed in the liquid slag close to the carbon surface. The nuclei then grow to form larger droplets, and the growth of these nuclei as well as their composition and morphology depend on the droplets contact with the slag, gas, and solid carbon. The iron droplets can be carburised by solid carbon and CO gas diffusion. Carburisation can lower the melting temperature of iron droplets (i.e., Fe-C alloy) and the Fe-C alloy formed can re-react with the slag to reduce iron oxide. Several studies concluded that the rate of FeO reduction by Fe-C alloy is much faster than by solid carbon, thus carbon dissolution rate can play an important role in the overall rate of reduction process [40, 45, 150].

The carbon and sulphur contents in the reduced iron droplets are presented in Table 8.2. During the reduction process carburisation and decarburisation of the Fe-C alloy occurs, through reactions with the slag, solid carbon, and existing gases, and this will determine the iron alloy states. If the rate at which carbon removed from the iron droplet is faster than the rate of carbon supply then the carbon content decreases as a result the iron droplet formed will remain completely solid [25]. The result in this study demonstrates that the carburisation was highest for the reaction with TC char particles, while carburisation by CC and BGC chars were significantly lower which shows the carburisation and carbon dissolution strongly dependant on the carbon type. The reaction temperature is shown to have influenced the carburisation level for droplets for all three carbons, and at both temperatures of 1475 and 1500 °C, CC char resulted in lowest carburisation. There was no significant difference for sulphur content for these reactions, this could be linked to the reaction between CaO and sulphur which results in CaS compound formation.

Table 8.2: Carburization of the iron droplets formed from FeO reduction by chars from different carbonaceous materials.

Materials	Carbon %	Sulphur %
Slow cooling at °C/min		
TC 1500 °C	3.97	0.0084
TC 1475 °C	4.99	0.0044

CC 1500 °C	0.87	0.0075
CC 1475 °C	1.39	0.0057
BGC 1500 °C	1.48	0.0117
BGC 1475 °C	3.04	0.0095

The mophology observation from cross section of the reacted slag samples containg Fe-C alloy formed during slow cooling are shown in figure 8.5. The microstructure of the droplet produced during slag reaction with TC char is shown to have higher carbon content and during slow cooling different phases formmed predominantly flaky graphite. The Fe-C droplet formed by BGC char is very simlar to TC char but slighly less carbon saturated as for CC droplet less dissolved carbon is evedenced and the existing phases are mainly pearlite.

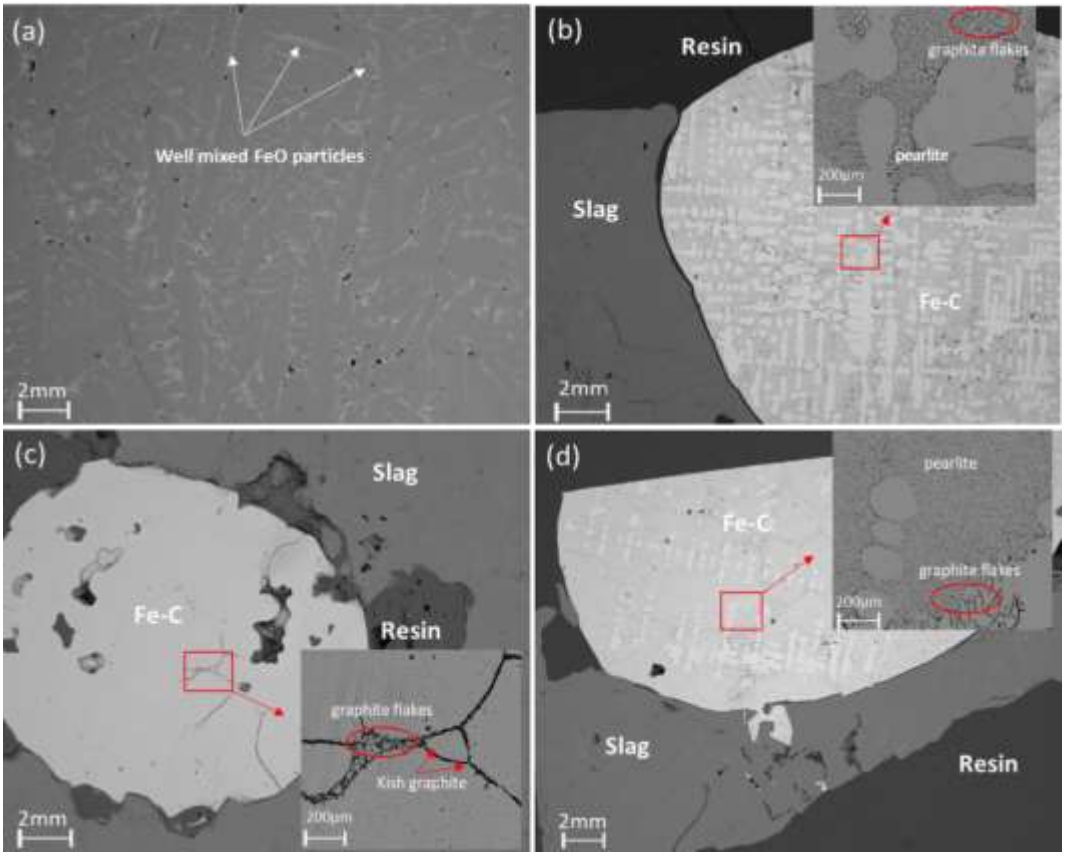

Figure 8.5: Morphology of sample cross section of (a) unreacted slag and reduced slag samples by (b) TC char; (c) CC char; and (d) BGC char formed at 1475 °C.

Furthermore, Figure 8.5 shows that there is significant change in the slag texture from the unreacted slag (Fig. 7(a)) to the reduced samples to the reduction of FeO in slag. The existence of FeO particles (brighter gray phase) in the slag matrix is visible and

this confirms FeO is evenly distributed within the slag. The visibility change of these particles after reaction confirms nearly all FeO reduced to metallic iron.

8.5 Isothermal kinetics analysis

8.5.1 kinetic models of FeO containing slag reduction

The reduction degree (α) of iron oxides in the slag is defined as the ratio of the oxygen removed by solid carbon at a given time t to the initial oxygen (i.e. the total oxygen of FeO in the starting salg), which can be expressed by equation (27) [154]. Please note the removed oxygen by reaction with solid carbons is determined through off-gas measurements for (CO and CO2) recorded by QMS. These results are subsequently used to calculate the real-time conversion of FeO in the slag system to allow the model-fitting method to be used for kinetic analysis.

$$\alpha = 1 - \frac{mt}{mi} \tag{27}$$

where mi is the initial weight of the total oxygen in FeO, mt is the instant weight of the the total oxygen in FeO at time t, which is calculated from the amount of oxygen removed at the time, forming CO and CO_2 gases measured by QMS during the reactions.

The reaction rate for FeO reduction being function of (α) can be described by equation (28).

$$\frac{d\alpha}{dt} = k(T)f(\alpha) \tag{28}$$

where α, $\frac{d\alpha}{dt}$, k(T) and f(α) denote the reduction degree, reduction rate, temperature-dependent rate constant and reaction function, respectively.

The reaction rate constant k (T) can be expressed by the Arrhenius equation (29):

$$k(T) = A\, e^{\left(-\frac{Ea}{RT}\right)} \tag{29}$$

By combining equations (28) and (29) the overall reaction conversion rate can be expressed by Equation (30):

$$\frac{d\alpha}{dt} = A\, e^{\left(-\frac{Ea}{RT}\right)} f(\alpha) \tag{30}$$

An integral form of equation (30) is written as equation (31) [149, 152].

$$G(\alpha) = \int_0^{\alpha} \frac{d\alpha}{f(\alpha)} = A\int_0^{t} e^{\left(-\frac{E_a}{RT}\right)}dt = k(T)t \quad (31)$$

where $G(\alpha)$ is the integral form of reaction models shown in table 8.3, while T, R, t, A and E_a are the absolute temperature (K), ideal gas constant (J mol $^{-1}$ K $^{-1}$), the time (s), pre-exponential factor (s $^{-1}$), and activation energy (kJ mol $^{-1}$) respectively.

Table 8.3: Some common rate and integral kinetic models for isothermal reactions [150, 153, 154].

Code	Models	G(α)=kt	n
Diffusion models			
D1 (α)	One dimension (parabolic)	α^2	0.62
D2 (α)	Two-dimensional (Valensi–Barrer)	(1-α) ln(1-α) +α	0.57
D3 (α)	Three-dimensional (Jander)	$[1-(1-a)^{1/3}]^2$	0.54
D4 (α)	Ginstling–Brounshtein	$(1-2/3\alpha) -(1-\alpha)^{2/3}$	0.57
Avrami−Erofeev models			
A2 (α)	Random nucleation and 2D growth	$[-\ln(1-\alpha)]^{1/2}$	2.00
A3 (α)	Random nucleation and 3D growth	$[-\ln(1-\alpha)]^{1/3}$	3.00
Geometrical contraction models			
R2 (α)	Contracting area	$1-(1-\alpha)^{1/2}$	1.11
R3 (α)	Contracting volume	$1-(1-\alpha)^{1/3}$	1.07
Chemical reaction-order models			
F0 (α)	Zero order	A	1.24
F1 (α)	First order	- ln(1-α)	1.00
F2 (α)	Second order	$(1-\alpha)^{-1}$ -1	0.83

8.5.2 Conversion degree (α)

The isothermal reduction of FeO in the slag by chars from the three carbonaceous materials was conducted at the temperature range of 1450 – 1525 °C. The reduction degree of FeO is obtained for each reductant through measurement of evolved gas from their reactions with the slag using equation (27). As an example, Figure 8.6b shows the FeO reduction degree by CC chars as a function of time and temperature. It can be seen from Figure 8.6 and Table 8.1 that the reduction rate and conversion degree of FeO increased sharply with increasing temperature. There is a linear increase in the conversion degree at the initial stage of reduction for all temperatures, which

then plateaued after a certain reaction time. The temperature increase resulted in the earlier completion of the initial stage and earlier occurrence of the plateau. When the temperature increased from 1450 to 1525 °C, the completion time for the initial stage reduced from ~300 s to 270 s for the reaction with CC char, also the conversion degree at the initial stage increased from ~35% to over 50% (Figure 8.6b).

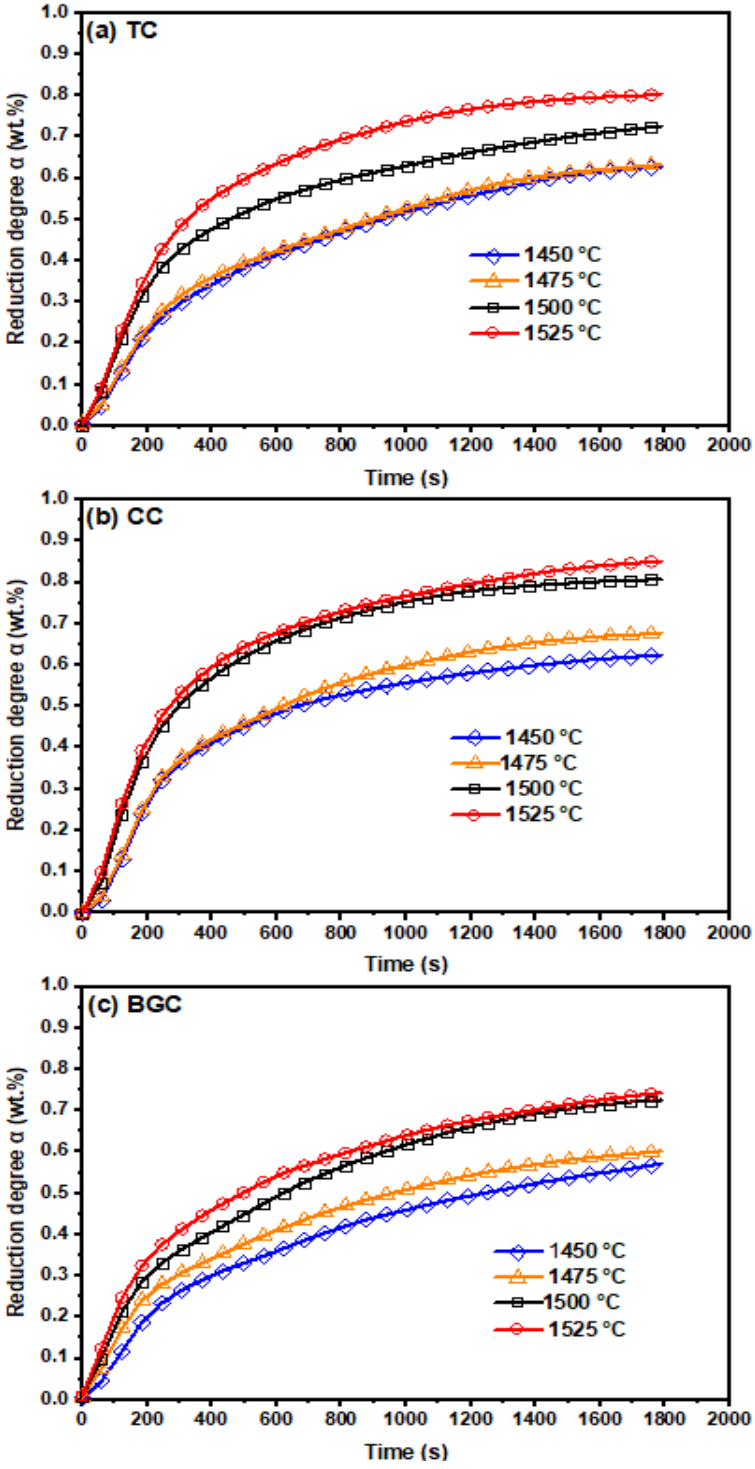

Figure 8.6: FeO reduction degree (α) as a function of time by (a) TC, (b) CC, and (c) BGC chars at different temperatures.

8.5.3 Reaction mechanism

As previously stated, the reduction of FeO in slag by solid carbon may be controlled by chemical reactions at carbon-gas or slag-gas interface, mass transfer in the slag to interface, and or diffusion through liquid or gas halo formed around solid carbon particle. The kinetic models which can describe these reaction mechanisms to determine the reaction rate are categorized into, Random nucleation and subsequent growth (A), diffusion (D), geometric contraction (R), and chemical reaction-order models (F) [153, 155, 156]. Dickinson and Heal [153] reported 27 kinetic models in total and those well-established models are listed in Table 8.3.

8.5.3.1 ln−ln Analysis Method

The Avrami–Erofeev equation is widely used to analyse isothermal kinetics [159], [160] therefore the model is employed to describe the reduction kinetics of slag containing FeO in this study. The Avrami–Erofeev equation can be written as below [160]:

$$1 - a = e^{(-kt)^n} \tag{32}$$

By taking the logarithm of both sides of equation (32), equation (33) is derived:

$$\ln[-\ln(1 - a)] = n \ln t + n \ln k \tag{33}$$

Where a is the conversion degree, k is the reaction rate constant, t is the time, and n is Avrami exponent, which provides information about the conversion mechanism involved during the reduction process [160]. The n values for all the selected models are presented in table 8.3.

To evaluate experimental data and select the suitable model, ln [−ln (1−a)] is plotted against lnt using equation (33). The slope and intercept of the fitting lines are n and nlnk, respectively. Figure 8.7 shows the experimental data fitted into equation (33) for CC char reaction, the slop n and intercept nlnk for reactions with different reductants are presented in Table 8.4. Regardless of the reductant used the first stage values of the slope n were between 0.79 - 0.90 for the temperature range studied. These values are closely matching with n value for F2 model 0.83 in Table 8.3. Therefore, it can be speculated that the rate limiting step is chemical reaction for the first stage of the reaction, then the second order model F2 is proposed and represented by the kinetic equation: $(1-\alpha)^{-1} - 1 = kt$.

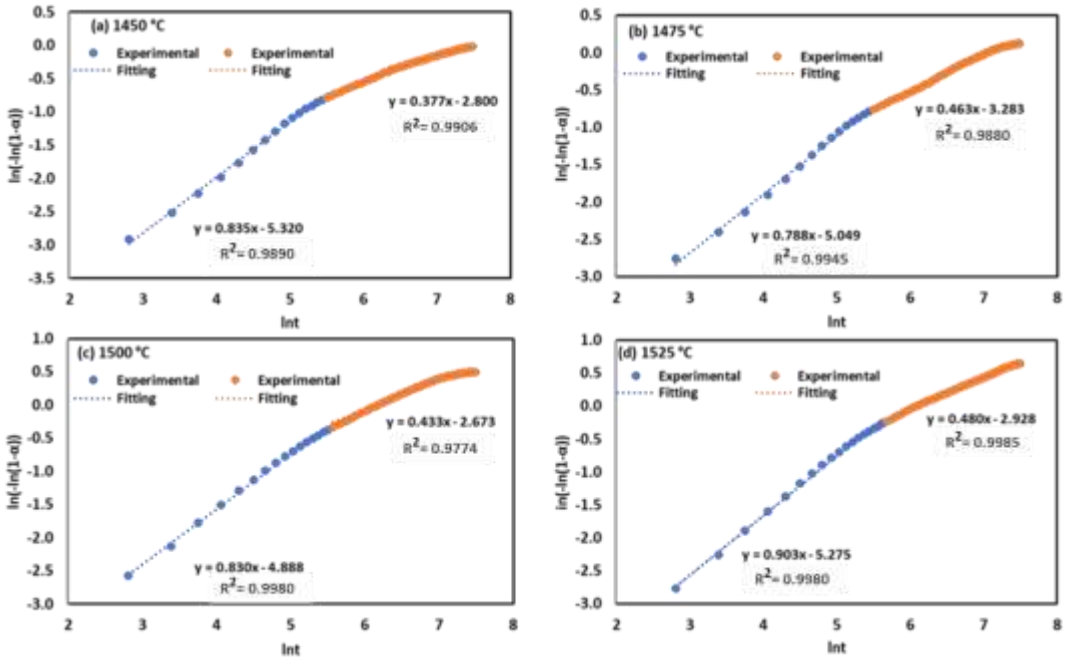

Figure 8.7: Avrami plots of ln[−ln(1 – α)] vs lnt for CC char reductant at different temperatures (a) 1450, (b) 1475, (c) 1500, and (d) 1525 °C.

On the other hand, the slope n vales for second stage are between 0.38 -0.57, and considering most of the values are less than or closely matching with 0.54, then three-dimensional diffusion is the proposed model, and represented by the kinetic equation: $[1-(1-a)^{1/3}]^2 = kt$. From these results it can be stated that gas diffusion or mass transfer of FeO in the liquid phase to slag-carbon interface is the rate limiting step when FeO concentration decreased in the second stage of the reaction.

Table 8.4: Data - fitting values determined by ln–ln analysis method at different temperatures for slag reaction with chars produced from TC, CC, and CC.

	First stage					Second stage			
Reductant	Temperature °C	conversion (α)	slope (n)	Intercept (lnk)	R^2	conversion (α)	slope (n)	Intercept (lnk)	R^2
TC	1450	0 - 0.30	0.90	-6.02	1.00	0.30 - 0.62	0.57	-4.23	1.00
	1475	0 - 0.32	0.88	-5.86	1.00	0.32 - 0.63	0.55	-4.06	1.00
	1500	0 - 0.42	0.85	-5.30	1.00	0.42 - 0.73	0.44	-3.04	1.00
	1525	0 - 0.46	0.88	-5.28	1.00	0.46 - 0.80	0.48	-3.03	0.99
CC	1450	0 - 0.35	0.84	-5.32	1.00	0.35 - 0.63	0.38	-2.80	0.99
	1475	0 - 0.36	0.79	-5.05	1.00	0.36 - 0.68	0.46	-3.28	0.99

	1500	0 - 0.49	0.83	-4.32	1.00	0.49 - 0.81	0.43	-2.67	0.98
	1525	0 - 0.52	0.90	-5.28	1.00	0.52 - 0.85	0.48	-2.93	1.00
BGC	1450	0 - 0.29	0.83	-5.82	0.99	0.29 - 0.57	0.56	-4.36	1.00
	1475	0 - 0.32	0.82	-5.67	0.99	0.32 - 0.60	0.53	-4.00	1.00
	1500	0 - 0.35	0.81	-5.29	0.99	0.35 - 0.73	0.53	-4.32	1.00
	1525	0 - 0.37	0.80	-5.04	1.00	0.37 - 0.74	0.52	-3.59	1.00

Moreover, the reaction with CC char resulted in much higher conversion in the first stage of the reaction followed by TC and BGC chars. This phenomenon is due to the higher reactivity of CC chars compared to the other selected carbons [151]. This indicates that the carbon type can have a great influence on the rate of reaction, and chemical reaction is the controlling mechanism for the first stage. Regardless of the carbon type used, the conversion degree is more similar at a given temperature for reactions at the second stage. This shows the influence of the carbon type on the rate is weakened and the controlling mechanism shifts at the second stage.

8.5.3.2 Model-Fitting Method

Figure 8.8 shows the linear fitting of G(α) against time (t) for selected model functions for the two reduction stages using equation (31). The slope is representing the reaction rates k(T) at given temperature for reaction with chars from different carbon sources. The values of k(T) obtained at different reduction stages and the details of the mechanism which is likely to control the reaction steps are represented in Table 8.5.

Based on the data fitting for ln−ln analysis method for the first stage, the best fitting function was confirmed as $(1-\alpha)^{-1}$ -1 for all tests, which represents a second order model. As shown in table 8.5, the correlation coefficients (R^2) values for the first stage of the reactions are between 0.98 and 1.00, which confirms that the regression model fits very well with the observed data. Regardless of the materials used as a reductant, the value of k(T) increased with the temperature increase. CC char as a reductant has the highest k(T) values which is related to the material's higher reactivity in the first stage while the values for TC and BGC chars were much closer.

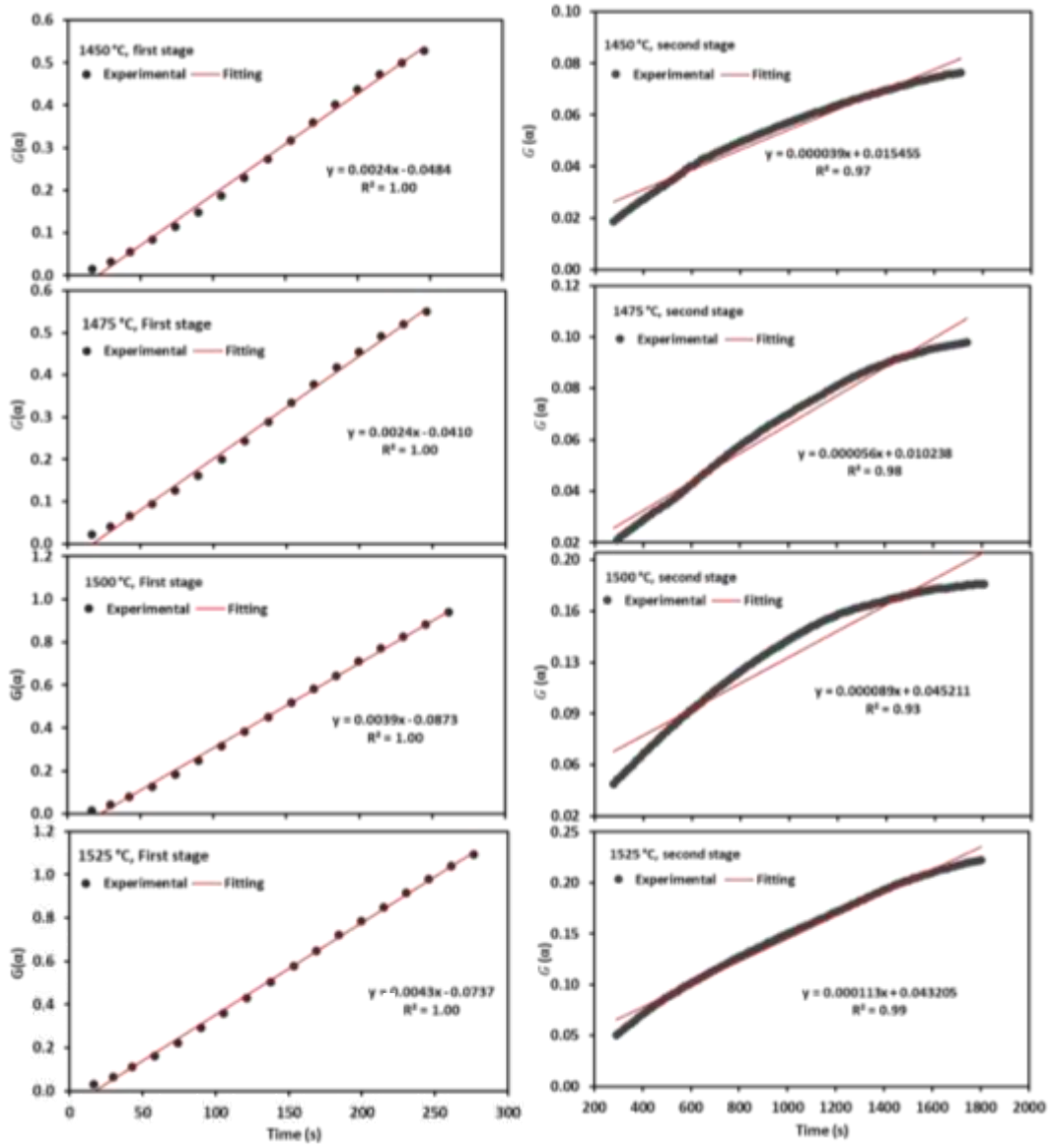

Figure 8.8: Integral function of conversion G(a) versus time (t) at different temperatures for CC char reaction with the slag at two reduction stages.

As for the second stage, the best fitting function is $[1-(1-a)^{1/3}]^2$, which describes three-dimensional diffusion model. The correlation coefficients (R^2) values for the second stage of the reactions are between 0.93 and 1.00, the correlation is good for most of the linear graph in table 8.5. Again, the reaction rate k(T) with CC chars is the highest followed by TC and the BGC chars, this shows higher reactivity of CC char also influences the second stage of the reaction.

Table 8.5: Reaction rate k (T) values for slag reaction with chars from three carbon sources at different temperatures determined by model fitting method at two reduction stages.

Reductant	Temperature °C	First stage		Probable rate controlling step	Second stage		Probable rate controlling step
		K(t) 10^{-3}	R^2		K(t) 10^{-5}	R^2	
TC	1450.00	1.55	1.00	2nd order Chemical reaction ($kt=(1-\alpha)^{-1}-1$)	4.72	1.00	Three-dimensional diffusion ($kt=[1-(1-\alpha)^{1/3}]^2$)
	1475.00	1.68	1.00		5.12	1.00	
	1500.00	2.76	1.00		6.19	0.99	
	1525.00	3.36	1.00		10.50	0.97	
CC	1450.00	2.38	0.99		3.88	0.97	
	1475.00	2.44	0.99		5.57	0.97	
	1500.00	3.95	1.00		8.90	0.94	
	1525.00	4.26	1.00		11.25	0.99	
BGC	1450.00	1.22	0.99		3.55	1.00	
	1475.00	1.47	0.98		4.27	1.00	
	1500.00	2.04	0.99		7.52	0.99	
	1525.00	2.60	1.00		7.33	1.00	

8.5.4 Reaction activation energy

The activation energy Eα values for two reaction stages can be obtained based on the Arrhenius equation. By taking logarithm of equation (29), the Arrhenius equation is written in the below form [159]:

$$\ln k(T) = \ln A - \frac{Ea}{RT} \tag{34}$$

Figure 8.9 shows the linear fitting of lnk(T) versus 1/T for different char reaction at different reduction stages using equation (34) to calculate Eα. The CC char has the lowest Eα of 229 kJ/mol for the first stage of the reaction, while TC and BGC chars have higher Eα with 290 kJ/mol and 267 kJ/mol respectively. These Eα values correlate reasonably well with others findings in the literature that the range of 41 to 97 kcal/mol (171.5 - 405.8 kJ/mol) has been reported for reaction between slag with similar properties and solid carbon from coal char or graphite [42, 51]. Min et al. [44] has predicted the chemical reaction at the carbon surface likely to be the rate limiting step measured Eα of 60 kcal/mol (251 kJ/mol) for reaction of the slag containing 10% FeO with graphite at similar temperature range. The values obtained in this present study are in the good agreement with the results obtained by Min et al. [44], therefore chemical reaction at carbon interface is likely to be rate controlling for the first stage of the reduction reaction.

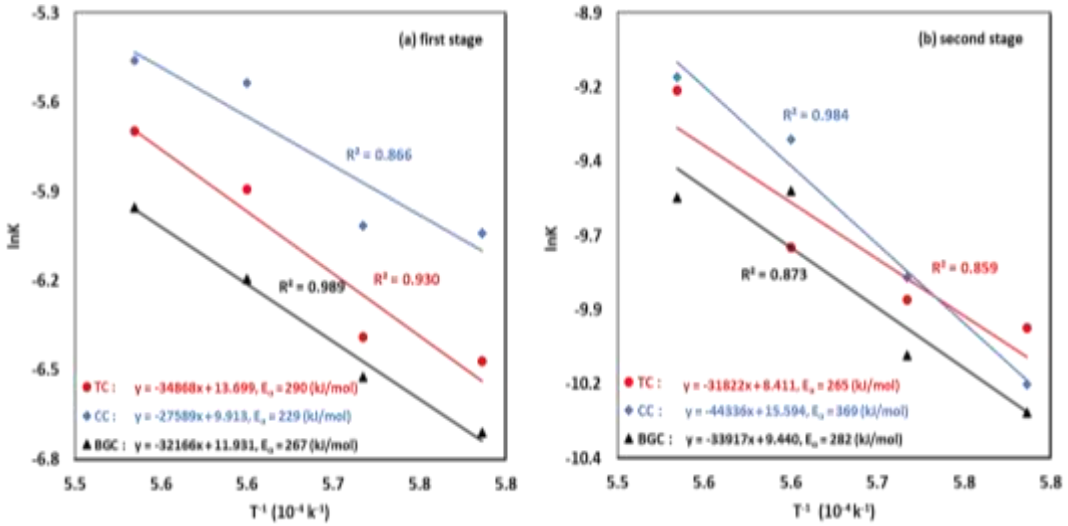

Figure 8.9: fitting curve of lnk vs T^{-1} at different temperatures for slag reaction with TC, CC, and BGC chars at different reduction stages: (a) first stage and (b) second stage.

In contrast, reaction with CC char resulted in the highest Eα (369 kJ/mol) for the second stage which is much higher than the first stage for the same material. The Eα values for both TC and BGC char reactions were (265 and 282 kJ/mol respectively) for the second stage which are much closer to their first stages and smaller than the Eα obtained for CC char. As shown in table 8.4, the conversion degree for first stage reaction with CC char was the highest for all temperatures, while TC char was the second highest. This higher conversion leads to much lower FeO concentration when the second stage begins for CC reductant compared to the second stage for TC and BGC chars. It appears that the lower FeO concentration resulted in higher Eα value for the second stage for CC, due to lower gas formation which results in lower agitation of the slag layer. As for second stage reaction with TC char, the Eα value was lower than the first stage despite achieving the second-best conversion for the first stage. This indicates that the liquid phase mass transfer influences the reaction mechanism for second stage of the reaction. On the other hand, despite achieving the lowest conversion (α) in the first stage as shown in Table 8.5, the second stage of the reaction with BGC was slower which indicates that the chemical reactions at char interface is still likely to influence the controlling mechanism. Therefore, it can be speculated that this slower reaction behaviour for BGC in the second stage is due to higher ash content. As the carbon particle shrinks due to conversion on the surface the ash content increases, and it covers the surface of the carbon particle to act as a

physical barrier to inhibit or even prevent CO and CO_2 penetration in the halo. Considering these concerning elements, the second stage reaction is likely to be controlled by more than one mechanism, and the mechanism controlling the reaction is expected to be the mixed limiting step.

As shown in Table 8.2 and Figure 8.5, TC reaction resulted in significantly higher carburisation of the iron droplets and it has been reported in the literature that the chemical reaction rate of carbon from an Fe-C alloy is much faster than solid carbon with FeO in the slag [48, 158]. Therefore, it can be speculated that this higher dissolution of carbon into the iron droplets during the first stage of reaction for TC char has subsequently improved the overall reaction kinetics and resulted in lower $E\alpha$. This behaviour again confirms the second stage reaction controlled by more than one mechanism; therefore, the overall reaction will be governed by a mixed control mechanism.

8.6 Conclusion:

The focus of this study has been on the reduction of HIsarna synthetic slag (CaO-SiO_2-Al_2O_3-MgO-FeO) using chars from three carbon sources. The reduction rate of FeO in the slag was measured using the mass spectrometer confirmed with slag analysis, and the kinetic parameters are evaluated from these results. The following conclusions can be drawn from this study:

- A strong impact of temperature on the reduction rate of FeO in slag by chars is found that the reduction rate increases with the increase in temperature. This is also demonstrated by the significant effect of temperature on the variation of gas products CO and CO_2.
- The FeO reduction process can be divided into two steps: the first stage with a sharp increase in the conversion degree with time and a slow second step. In the first 500s , the reduction degree achieved at 1500 °C was over 60 % by CC char, ~50 % by TC char and just over 40 % for BGC char. Furthermore, the slag reaction with CC char resulted in the highest final degree of reduction under all temperatures, but the difference between TC and BGC char was smaller with TC performed slightly better at higher temperatures.
- The metallic iron droplets produced from TC char reaction have undergone the highest degree of carburisation under all conditions. The carbon content of the

Fe-C alloys formed were 3.97, 0.87 and 1.48% for reaction with TC, CC and BGC chars, respectively. These results suggest that the carbon structure controls the rate of carbon dissolution into liquid iron. Therefore, a more ordered graphite structure and complex bonding for TC means a longer time required for its particles to be fully dissolved in the hot metal, therefore decarburisation is slower.

- The first stage of the reaction is represented by the second order model (F2), and the activation energy values obtained for the reactions with TC, CC and BGC chars were 290, 229 and 267 kJ/mol, respectively. The initial stage of reaction rate is controlled by chemical reaction at the solid carbon interface, while the second stage described by three-dimensional diffusion model (D3) and mixed influence from gas diffusion, liquid phase mass transfer, chemical reaction and carbon diffusion are likely to control the reduction rate.

Chapter 9

Conclusions and Suggested Further Work

9.1 Conclusions

9.1.1 Development of novel techniques

A novel technique, drop tube furnace coupled with a quadrupole mass spectrometer (DTF-QMS), has been applied for real time measurement of the reduction rate of FeO in the molten slag. This technique allows HIsarna synthetic slag to be melted and solid char particles from different carbon sources injected into the melt under heating environment similar to HIsarna SRV. The mount of CO and CO_2 evolved due to injected char reaction with the slag measured continuously using the online QMS to calculate FeO concentration in the slag.

The closely controlled atmosphere within the furnace and the ability to flush through the feeder to create an oxygen-free and to carry the particles into the melt allows to simulate the reactions that are taking place during carbon injection into SRV. These experiments provide information required to understand the reaction controlling mechanism and kinetic parameter under similar temperature conditions to HIsarna process.

9.1.2 Devolatilization characteristics of coal and biomass materials

The non-isothermal devolatilization experiments were performed to compare the thermal behaviour of four coals with notable differences in volatile matter content (with low to high volatile matter content) and two biomass samples sourced from wood and grass origins. The results show that similar types of volatiles components were produced for all the carbonaceous materials. However, the wt% of reducing gases e.g., H_2, CO, and hydrocarbons, and the temperature required for these gases to evolve were notably different, but the respective maximum peaks of evolution of these gases corresponded well to the maximum rate of mass loss recorded by TGA. It can be concluded from the outcome of this study that the devolatilization is affected by the material properties which in turn is linked to volatile mater and oxygen content.

Despite pre-treatment of both biomass materials (torrefied grass and charcoal), the weight loss at low temperature from 100 to 200 °C which is mainly associated to removal of H_2O was significantly larger than that for thermal coals. This could be due

absorption of H_2O from atmosphere due to their porous structure, therefore materials handling may need to be different for biomass (compared to thermal coal) to avoid H_2O absorption. Overall, the biomass samples produced significantly larger amount of H_2O and CO_2, but coal samples produced more CH_4, C_2H_6 and H_2.

Furthermore, the off-gas analysis reveals that torrefied grass contains a large amount of H_2O and CO_2 which are released at low temperatures up to 600 °C. These gases can cause temperature drop in the HIsarna furnace which needs heat compensation and may result in increased carbon consumption. Therefore, pre-treatment to the temperature of ~ 500 °C is necessary to produce chars with similar properties to coal injected in HIsarna process and for Bana grass material to be utilised effectively.

9.1.3 Evaluation of rapid devolatilization and behavior of resultant chars

The thermal coal (coal A) and charcoal used in HIsarna trials and Bana grass chars produced at pyrolysis temperature up to 500 °C were analysed under thermal conditions similar to HIsarna SRV using drop-tube furnace with quadrupole mass spectrometer (DTF-QMS). Through this combination the devolatilization behaviour of the carbonaceous materials under rapid heating and at high temperatures were studied. The experiments demonstrated strong impact of temperature on the rate of volatile formation, which was increased with a temperature increase. The variation of gas species released was also affected by temperature change, that is, the yield of hydrocarbons, CO_2 and H_2O decreases with temperature increase while both H_2 and CO increase consequently. This behaviour indicates that temperature increase can enhance both carbon oxidation and secondary reactions which are taking place during devolatilization. The gas species detected were found to be similar for coal and biomass samples but char oxidation for charcoal (CC) was significantly faster. Therefore, despite high fixed carbon and low VM content, the weight loss (under rapid devolatilization) for charcoal (29%) was higher than that for thermal coal (23%) and Bana grass char (22%) at 1500 °C, which could lead to low solid char yield during CC injection.

Furthermore, the reactivity test conducted at 1500 °C has shown that CC chars produced under rapid heating has the fastest CO_2 gasification reaction with reactivity index of (0.077) while the value was (0.053) for both TC and BGC chars produced under same temperature conditions. This behaviour is likely to be governed by a

combination of low ash content, ash composition, crystalline structure, and char morphology. CC produced at 1500 °C has the largest BET Surface area (61.7 m^2/g) compared to TC produced at 1500 °C (1.5 m^2/g) and BGC produced at 1500 °C (13.4 m^2/g), but lowest ash content. The crystalline structure suggests that charcoal has less ordered graphite structure, but it is more amorphous carbon compared to TC and BGC implying its being more reactive. These results confirm that gasification reaction is controlled by more than one parameter, e.g., high surface area and less ordered graphite structure can enhance gasification reaction while higher ash content can have a negative effect.

9.1.4 Reaction mechanism for FeO reduction in the molten slag

The reactions between carbonaceous materials and molten slag under simulated HIsarna thermal conditions were carried out by injecting chars produced from different carbonaceous materials (CC, TC and BGC) into a molten synthetic HIsarna slag in laboratory. The gas analysis from these reactions indicates strong temperature impact, and the reduction rate is found to increase with the temperature increase which is demonstrated by temperature effect on the variation of gas products (CO and CO_2). The results show that the FeO reduction proceeds through two stages, starting with an initial rapid reduction and followed by gradual levelling off until the end of the process. The reduction rate of FeO in the molten slag was highest with CC chars, achieving over 60 % reduction at 1500 °C in the first 500s, compared to only ~50 % and just over 40 % with TC and BGC chars respectively for the same reaction time. Furthermore, the slag reaction with CC char resulted in the highest final degree of reduction under all temperatures, but the performance between TC and BGC chars was similar with TC performing slightly better at higher temperatures.

The kinetic analysis suggests that the first stage reaction is controlled by chemical reactions at the carbon-slag interface and represented by second order model (F2). The apparent activation energy values for the first stage were 290, 229 and 267 kJ/mol for reactions with TC, CC and BGC chars respectively. On the other hand, the second stage can be described by three-dimensional diffusion model (D3) and the following activation energy values 265, 369, and 282 kJ/mol were obtained for reactions with TC, CC and BGC chars respectively. The rate controlling mechanisms for the process were determined by analysing the experimental data and activation energy values. It appears that the first stage is controlled by chemical reactions on the carbon surface,

and the mixed influence from gas diffusion, liquid phase mass transfer, chemical reaction and carbon diffusion are likely to control the reduction rate for second stage.

9.2 Potential industial impacts

The findings in this study suggest that different reactions take place during decomposition of carbon materials, which link to the chemical properties of the materials. Therefore, these results have a direct implication on the biomass material slection for HIsarna process and the pre-treatment conditions required to produce the chars with similar properties to the injected coal.

The rapid devolatilization experiments indicate that despite low volatile matter content charcoal conversion due to devolatilization is extremely high compared to thermal coal. Therefore, coal substitution with charcoal will result in significantly lower solid char yield in HIsarna's SRV but higher reducing gas atmosphere for CCF will be produced. On the other hand, charcoal has much faster gasification reaction with CO_2, and this can result in chars to burn prematurely before they penetrate into the metal bath during injection. The extra CO produced from gasification and the reducing volatiles from devolatilization can combust in the post combustion zone and may result in the change of the furnace temperature, pre-reduction degree of iron ore in CCF and may lead to underperforming for SRV.

Finally, the reaction rate for chars produced from charcoal with FeO in the slag was much faster than with coal chars. This higher rate could potentially have a greatly effect on the behaviour of SRV bath due to increase in the rate of CO formation and could possibly change the slag composition.

9.3 Further Work

To build on the current findings and for efficient use of biomass or other alternative fuels, the following points for further research are suggested:

1. This study indicates that charcoal injection results in low solid char yield due to high devolatilization conversion and gasification reaction. The biomass (e.g., charcoal) / coal blending can help to increase solid char yield in the SRV bath to maintain process efficiently. This can be done by blending charcoal and coal with specific physical and chemical properties (e.g., low reactivity coal, and specific ash and volatile matter content) to create a balance between solid char and reducing gases atmosphere.

2. In the literature it is known that the increase in the particle size of carbon sources (biomass and thermal coals) will influence the performance of the carbonaceous materials. The effect of particle size could be further investigated with the potential that it may help to increase the solid char yield and slow down gasification reaction.

3. The continuation of slag - carbon reaction by quenching reacted samples into cold water from reaction temperature after certain reaction time. By rapid cooling the reacted samples real-time composition and microstructure present at the reaction temperature is preserved unchanged. Using quantitative and qualitative analysis methods, the morphology and composition of the reacted slag and the iron droplets produced can be analysed.

4. Slag chemical composition (e.g., different FeO content) plays an important role in the bath smelting, heavily influencing the reduction of FeO in slag/carbon reaction. The influence of slag composition could be studied for reduction of FeO in the slag with biomass and thermal coal chars in Ar atmosphere and under HIsarna's thermal conditions to find optimal composition.

5. Various impurities from raw materials could affect the reduction rate of FeO-containing slag by solid carbon. The impurities including TiO_2 coming from Ti-containing iron ore will affect fluidity and foaming of the slag and residuals from scrap addition will compete for free oxygen, and sulphur from carbon sources will act as an interface inhibitor blocking reaction sites. The influence of impurities could be studied for both biomass and thermal coal.

6. The results of this study suggest that ash content and ash chemistry may influence the reactivity of carbonaceous materials. The effect of ash content and chemistry could be further investigated to determine the extent of these influences on the char gasification behaviour and on the slag chemistry.

7. The Fe-C droplets created in the SRV by coal injection into the iron melt play an important role in FeO reduction in the slag during the smelting process. Fe-C formation rate can differ for reaction with carbonaceous materials with different chemical properties. The carburisation of metal bath is expected to happen from the injected carbon sources, therefore the rate at which carbon dissolves in molten iron is a key aspect to be investigated. This study can be conducted by injecting

solid chars into molten metal. When the carburization completed and if the samples are rapidly cooled by quenching, the amount and the depth of carbon diffusion in the metal can be analysed.

References

[1] Word Steel Association, “World Crude Steel Production - Summary The Largest Steel-Producing Countries,” no. January, p. 27, 2020, [Online]. Available: https://www.worldsteel.org/media-centre/press-releases/2020/Global-crude-steel-output-increases-by-3.4--in-2019.htm

[2] World Steel Association, “Major steel-producing countries 2018 and 2019 million,” 2020 World steel Fig., no. 30 April, pp. 1–10, 2020, [Online]. Available: http://www.worldsteel.org/wsif.php

[3] H. Suopajärvi et al., “Use of biomass in integrated steelmaking – Status quo, future needs and comparison to other low-CO2steel production technologies,” Appl. Energy, vol. 213, no. January, pp. 384–407, 2018, doi: 10.1016/j.apenergy.2018.01.060.

[4] K. V. N. Pardo, J.A. Moya, Prospective Scenarios on Energy Efficiency and CO. 2013. doi: 10.2790/64264.

[5] A. Orth, N. Anastasijevic, and H. Eichberger, “Low CO2 emission technologies for iron and steelmaking as well as titania slag production,” Miner. Eng., vol. 20, no. 9 SPEC. ISS., pp. 854–861, 2007, doi: 10.1016/j.mineng.2007.02.007.

[6] J. Diczfalusy, Bo Wisniewski, “Energy Consumption and CO2 Emissions in Ironmaking and Development of a Novel Flash Technology,” Metals (Basel)., p. 59, 1012.

[7] H. Suopajärvi, Bioreducer Use in Blast Furnace Ironmaking in Finland. Techno-economic Assessment and CO2 Emission Reduction Potential, no. July. 2014. [Online]. Available: http://cc.oulu.fi/~kamahei/z/tkt/Suopajarvi_vk.pdf

[8] A. Hasanbeigi, M. Arens, and L. Price, “Alternative emerging ironmaking technologies for energy-ef fi ciency and carbon dioxide emissions reduction : A technical review,” Renew. Sustain. Energy Rev., vol. 33, pp. 645–658, 2014, doi: 10.1016/j.rser.2014.02.031.

[9] International Energy Agency., “Iron and Steel Technology roadmap : Towards more sustainable steelmaking,” Treatise Process Metall., vol. 3, p. 190, 2020, [Online]. Available: www.iea.org

[10] OECD/OCDE, “Future Investment Projects in the Global Steel Industry and Implications for the Balance of Steelmaking Processes,” Organ. Econ. Co-operation Dev., no. 2014, 2015.

[11] M. Abdul Quader, S. Ahmed, S. Z. Dawal, and Y. Nukman, “Present needs, recent progress and future trends of energy-efficient Ultra-Low Carbon Dioxide (CO2) Steelmaking (ULCOS) program,” Renew. Sustain. Energy Rev., vol. 55, pp. 537–549, 2016, doi: 10.1016/j.rser.2015.10.101.

[12] J.-P. Birat, “Steel and CO 2 – the ULCOS Program , CCS and Mineral Carbonation using Steelmaking Slag,” no. August, 2009.

[13] E. Bellevrat and P. Menanteau, “Introducing carbon constraint in the steel sector: ULCOS scenarios and economic modeling,” Rev. Métallurgie, vol. 106, no. 9, pp. 318–324, 2009, doi: 10.1051/metal/2009059.

[14] J. W. K. Van Boggelen, H. K. A. Meijer, C. Zeilstra, H. Hage, and P. Broersen, “HIsarna - Demonstrating low CO 2 ironmaking at pilot scale,” no. September 2018, pp. 25–27, 2018.

[15] C. Zeilstra, H. Hage, J. Van Boggelen, and P. Broersen, “THE USE OF LD-SLAG AS A FLUXING AGENT IN THE HISARNA PROCESS Using LD-slag in HIsarna,” pp. 325–328, 2019.

[16] Peter Tom Jones, Daneel Geyson, Muxing Guo, and Bart Blanpin, Slag Valorisation Symposium, vol. 45, no. 1. 2009. doi: 10.7202/1016404ar.

[17] LumenCandela, “Ch. 25 The Industrial Revolution, Steel Production.” https://courses.lumenlearning.com/suny-hccc-worldhistory2/chapter/steel-production/

[18] posco, “The Evolution of the Steel Production Process,” 2016, [Online]. Available: https://newsroom.posco.com/en/the-evolution-of-the-steel-production-process/

[19] W. Alasdair, G., Katya, “Net-Zero Steel Initiative,” Mission possible Partnership, pp. 1–4, 2021.

[20] M. A. Díez, R. Alvarez, and C. Barriocanal, “Coal for metallurgical coke production: Predictions of coke quality and future requirements for cokemaking,” Int. J. Coal Geol., vol. 50, no. 1–4, pp. 389–412, 2002, doi:

10.1016/S0166-5162(02)00123-4.

[21] steeluniversity.org, “MAN01032 – Blast Furnace Steelmaking,” 2019. https://steeluniversity.org/courses/man01032-blast-furnace-steelmaking/ (accessed Jun. 10, 2021).

[22] G. Jha and S. Soren, “Study on applicability of biomass in iron ore sintering process,” Renew. Sustain. Energy Rev., vol. 80, no. January, pp. 399–407, 2017, doi: 10.1016/j.rser.2017.05.246.

[23] M. Geerdes, H. Toxopeus, and C. Van Der Vliet, Modern Blast Furnace lronmaking. 2004. doi: 10.3233/978-1-61499-499-2-i.

[24] A. Agarwal and S. Saha., “Determining the Flow Characteristics of Synthetic Slag and Optimizing the Slag Characteristics Determining the Flow Characteristics of Synthetic Slag and Optimizing the Slag Characteristics,” Dep. Metall. Mater. Eng. Natl. Inst. Technol. Rourkela, 2012.

[25] S. L. Teasdale and P. C. Hayes, “Kinetics of Reduction of FeO from Slag by Graphite and Coal Chars,” ISIJ Int., vol. 45, no. 5, pp. 634–641, 2005, doi: 10.2355/isijinternational.45.642.

[26] K. Meijer, C. Zeilstra, C. Teerhuis, M. Ouwehand, and J. Van Der Stel, “Developments in alternative ironmaking,” Trans. Indian Inst. Met., 2013, doi: 10.1007/s12666-013-0309-z.

[27] Y. Qu, Y. Yang, Z. Zou, C. Zeilstra, K. Meijer, and R. Boom, “Kinetic study on gas molten particle reduction of iron ore fines at high temperature,” Ironmak. Steelmak., vol. 42, no. 10, pp. 763–773, 2015, doi: 10.1179/1743281215Y.0000000021.

[28] Y. Qu, Y. Yang, Z. Zou, C. Zeilstra, K. Meijer, and R. Boom, “Reduction kinetics of fine hematite ore particles with a high temperature drop tube furnace,” ISIJ Int., vol. 55, no. 5, pp. 952–960, 2015, doi: 10.2355/isijinternational.55.952.

[29] M. Abdul Quader, S. Ahmed, S. Z. Dawal, and Y. Nukman, “Present needs, recent progress and future trends of energy-efficient Ultra-Low Carbon Dioxide (CO2) Steelmaking (ULCOS) program,” Renew. Sustain. Energy Rev., vol. 55, pp. 537–549, 2016, doi: 10.1016/j.rser.2015.10.101.

[30] European Commission, “Development of a Low CO2 Iron and Steelmaking Integrated Process Route for a Sustainable European Steel Industry,” 2018. https://cordis.europa.eu/project/id/654013 (accessed Jun. 20, 2021).

[31] Z. Chen, C. Zeilstra, J. van der Stel, J. Sietsma, and Y. Yang, “Review and data evaluation for high-temperature reduction of iron oxide particles in suspension,” Ironmak. Steelmak., vol. 0, no. 0, pp. 1–7, 2019, doi: 10.1080/03019233.2019.1589755.

[32] Y. Qu, Y. Yang, Z. Zou, C. Zeilstra, K. Meijer, and R. Boom, “Thermal decomposition behaviour of fine iron ore particles,” ISIJ Int., vol. 54, no. 10, pp. 2196–2205, 2014, doi: 10.2355/isijinternational.54.2196.

[33] K. Meijer, C. Guenther, and R. J. Dry, “HIsarna Pilot Plant Project,” InSteelCon, no. July, pp. 1–5, 2011.

[34] I. J. Van Der Stel and K. Meijer, “Update to the Developments of Hisarna An Ulcos alternative ironmaking process,” no. November, 2013.

[35] P. Prachethan Kumar, L. M. Garg, and S. S. Gupta, “Modelling of Corex process for optimisation of operational parameters,” Ironmak. Steelmak., vol. 33, no. 1, pp. 29–33, 2006, doi: 10.1179/174328106X80037.

[36] U. Jain, “COREX & FINEX - New Developments in Utilization of Low Grade Raw Materials,” Dep. Mater. Sci. Metall. Eng. MANIT Bhopal, 2013.

[37] P. P. Kumar, S. C. Barman, B. M. Reddy, and V. R. Sekhar, “Raw materials for Corex and their influence on furnace performance,” Ironmak. Steelmak., vol. 36, no. 2, pp. 87–90, 2009, doi: 10.1179/174328108X378152.

[38] E. Mousa, C. Wang, J. Riesbeck, and M. Larsson, “Biomass applications in iron and steel industry: An overview of challenges and opportunities,” Renew. Sustain. Energy Rev., vol. 65, pp. 1247–1266, 2016, doi: 10.1016/j.rser.2016.07.061.

[39] H. Vakkilainen, K. Kuparinen, and J. Heinimö, “Large Industerial Users of Energy Biomass,” Lappeenranta University of Technology, IEA Bioenergy, Task 40: sustainable international bioenergy trade.

[40] H. Suopajärvi, E. Pongrácz, and T. Fabritius, “The potential of using biomass-based reducing agents in the blast furnace: A review of thermochemical

conversion technologies and assessments related to sustainability," Renew. Sustain. Energy Rev., vol. 25, pp. 511–528, 2013, doi: 10.1016/j.rser.2013.05.005.

[41] R. Wei, L. Zhang, D. Cang, J. Li, X. Li, and C. C. Xu, "Current status and potential of biomass utilization in ferrous metallurgical industry," Renew. Sustain. Energy Rev., vol. 68, no. February 2016, pp. 511–524, 2017, doi: 10.1016/j.rser.2016.10.013.

[42] B. Sarma, A. W. Cramb, and R. J. Fruehan, "Reduction of FeO in Smelting Slags by Solid Carbon: Experimental Results," Metall. Mater. Trans. B Process Metall. Mater. Process. Sci., vol. 27, no. 5, pp. 717–730, 1996, doi: 10.1007/BF02915600.

[43] S. Kwangyong and R. J. Fruehan, "Reduction of FeO in slag with coal char," ISIJ Int., vol. 40, no. 1, pp. 7–15, 2000, doi: 10.2355/isijinternational.40.7.

[44] D. J. Min, J. W. Han, and W. S. Chung, "Study of the reduction rate of FeO in slag by solid carbon," Metall. Mater. Trans. B Process Metall. Mater. Process. Sci., vol. 30, no. 2, pp. 215–221, 1999, doi: 10.1007/s11663-999-0050-5.

[45] S. R. Story, B. Sarma, R. J. Fruehan, A. W. Cramb, and G. R. Belton, "Reduction of FeO in smelting slags by solid carbon: Re-examination of the influence of the gas-carbon reaction," Metall. Mater. Trans. B Process Metall. Mater. Process. Sci., vol. 29, no. 4, pp. 929–932, 1998, doi: 10.1007/s11663-998-0152-5.

[46] F. Fun, "Rates and mechanisms of FeO reduction from slags," Metall. Trans., vol. 1, no. 9, pp. 2537–2541, 1970, doi: 10.1007/BF03038380.

[47] S. L. Teasdale and P. C. Hayes, "Kinetics of reduction of FeO from slag by graphite and coal chars," ISIJ Int., vol. 45, no. 5, pp. 642–650, 2005, doi: 10.2355/isijinternational.45.642.

[48] M. Ozawa, S. Kitagawa, S. Nakayama, and Y. Takesono, "Reduction of FeO in Molten Slags by Solid Carbon in the Electric Arc Furnace Operation," Trans. Iron Steel Inst. Japan, vol. 26, no. 7, pp. 621–628, 1986, doi: 10.2355/isijinternational1966.26.621.

[49] R. J. Fruehan, "The rate of reduction of iron oxides by carbon," Metall. Trans.

B, vol. 8, no. 1, pp. 279–286, 1977, doi: 10.1007/BF02657657.

[50] A. Sato, G. Aragane, K. Kamihira, and S. Yoshimatsu, “Reducing Rates of Molten Iron Oxide By Solid Carbon or Carbon in Molten Iron.,” Trans. Iron Steel Inst. Japan, vol. 27, no. 10, pp. 789–796, 1987, doi: 10.2355/isijinternational1966.27.789.

[51] F.-Z. Ji, M. Barati, K. Coley, and G. A. Irons, “Kinetics of Coal Injection Into Iron Oxide Containing Slags,” Can. Metall. Q., vol. 44, no. 1, pp. 85–94, 2012, doi: 10.1179/000844305794409751.

[52] M. S. Bafghi, H. Kurimoto, and M. San0, “Effect of Slag Foaming on the Reduction of Iron Oxide in Molten Slag by Graphite,” ISIJ Int., vol. 32, no. 10, pp. 1084–1090, 1992, doi: 10.2355/isijinternational.32.1084.

[53] M. S. Bafghi, H. Kurimoto, and M. San0, “Composition on the Kinetics of the Reduction of lron Molten Slag by Graphite e A V [iO AA,” vol. 32, no. 1 992, pp. 280–286, 1992.

[54] X. A. Huang, K. W. Ng, L. Giroux, and M. Duchesne, “Carbonaceous Material Properties and Their Interactions with Slag During Electric Arc Furnace Steelmaking,” Metall. Mater. Trans. B Process Metall. Mater. Process. Sci., vol. 50, no. 3, pp. 1387–1398, 2019, doi: 10.1007/s11663-019-01569-1.

[55] F. Ji, M. Barati, K. Coley, and G. A. Irons, “A kinetic study of carbon injection into electric arc furnace slags,” 7th Int. Conf. Molten Slags, Fluxes Salts, vol. Jonhannesb, no. January 2004, p. 1, 2004, [Online]. Available: http://www.saimm.co.za/Conferences/Slags2004/056_Ji.pdf

[56] F. Ji, M. Barati, K. S. Coley, and G. A. Irons, “Some experimental studies of coal injection into slags Experimental Set up,” no. January, pp. 511–524, 2002.

[57] P. Wei, M. Sano, M. Hirasawa, and K. Mori, “Kinetics of reactions between high carbon molten iron and FeO containing slag,” Trans. Iron Steel Inst. Japan, vol. 28, no. 8, pp. 637–644, 1988, doi: 10.2355/isijinternational1966.28.637.

[58] R. H. Smith and R. J. Fruehan, “Effect of carbon content on the rate of reduction of FeO in slag relevant to iron smelting,” Steel Research, vol. 70, no. 8. pp. 283–295, 1999. doi: 10.1002/srin.199905643.

[59] D. J. Min and R. J. Fruehan, “Rate of reduction of FeO in slag by Fe-C drops,”

Metall. Trans. B, vol. 23, no. 1, pp. 29–37, 1992, doi: 10.1007/BF02654033.

[60] J. Biswas, K. Gu, and K. S. Coley, “A Decarburization Model for a Fe–C Droplet Reacting in Oxidizing Slag,” Metall. Mater. Trans. B Process Metall. Mater. Process. Sci., no. August, 2021, doi: 10.1007/s11663-021-02303-6.

[61] K. Gu, N. Dogan, and K. S. Coley, “Dephosphorization Kinetics between Bloated Metal Droplets and Slag Containing FeO: The Influence of CO Bubbles on the Mass Transfer of Phosphorus in the Metal,” Metall. Mater. Trans. B Process Metall. Mater. Process. Sci., vol. 48, no. 6, pp. 2984–3001, 2017, doi: 10.1007/s11663-017-1070-1.

[62] C. L. Molloseau and R. J. Fruehan, “The reaction behavior of Fe-C-S droplets in CaO-SiO2-MgO-FeO slags,” Metall. Mater. Trans. B Process Metall. Mater. Process. Sci., vol. 33, no. 3, pp. 335–344, 2002, doi: 10.1007/s11663-002-0045-y.

[63] M. Barati and K. S. Coley, “A comprehensive kinetic model for the CO-CO2 reaction with iron oxide-containing slags,” Metall. Mater. Trans. B Process Metall. Mater. Process. Sci., vol. 37, no. 1, pp. 61–69, 2006, doi: 10.1007/s11663-006-0086-8.

[64] M. Barati and K. S. Coley, “Kinetics of CO-CO 2 Reaction with CaO-SiO 2 - FeOx Melts,” Metall. Mater. Trans. B, vol. 36B, p. 169, 2004.

[65] M. Barati, E. Chen, and K. Coley, “A comparison of the kinetics of the CO-CO 2 reaction with steelmaking and copper making slags,” 7th Int. Conf. Molten Slags, Fluxes Salts, pp. 393–398, 2004.

[66] I. A. Moore, “Direct Observation of Swelling Coal Particles,” wrap, Warwick, no. October, 2018.

[67] S. B. Liaw and H. Wu, “A New Method for Direct Determination of Char Yield during Solid Fuel Pyrolysis in Drop-Tube Furnace at High Temperature and Its Comparison with Ash Tracer Method,” Energy and Fuels, vol. 33, no. 2, pp. 1509–1517, 2019, doi: 10.1021/acs.energyfuels.8b03161.

[68] W. H. Chen, S. W. Du, C. H. Tsai, and Z. Y. Wang, “Torrefied biomasses in a drop tube furnace to evaluate their utility in blast furnaces,” Bioresour. Technol., vol. 111, pp. 433–438, 2012, doi: 10.1016/j.biortech.2012.01.163.

[69] W. H. Chen and J. S. Wu, “An evaluation on rice husks and pulverized coal blends using a drop tube furnace and a thermogravimetric analyzer for application to a blast furnace,” Energy, vol. 34, no. 10, pp. 1458–1466, 2009, doi: 10.1016/j.energy.2009.06.033.

[70] E. Biagini, M. Simone, and L. Tognotti, “Characterization of high heating rate chars of biomass fuels,” Proc. Combust. Inst., vol. 32 II, no. 2, pp. 2043–2050, 2009, doi: 10.1016/j.proci.2008.06.076.

[71] K. Zhang, Z. Wang, W. Fang, Y. He, E. Hsu, Q. Li, J. Gul-e-Rana, and K. Cen, “High-temperature pyrolysis behavior of a bituminous coal in a drop tube furnace and further characterization of the resultant char,” J. Anal. Appl. Pyrolysis, vol. 137, no. August 2018, pp. 163–170, 2019, doi: 10.1016/j.jaap.2018.11.022.

[72] J. Yu, J. Lucas, V. Strezov, and T. Wall, “Swelling and char structures from density fractions of pulverized coal,” Energy and Fuels, vol. 17, no. 5, pp. 1160–1174, 2003, doi: 10.1021/ef030022h.

[73] J. Tanner and S. Bhattacharya, “Kinetics of CO2 and steam gasification of Victorian brown coal chars,” Chem. Eng. J., vol. 285, pp. 331–340, 2016, doi: 10.1016/j.cej.2015.09.106.

[74] P. McNamee, L. I. Darvell, J. M. Jones, and A. Williams, “The combustion characteristics of high-heating-rate chars from untreated and torrefied biomass fuels,” Biomass and Bioenergy, vol. 82, pp. 63–72, 2015, doi: 10.1016/j.biombioe.2015.05.016.

[75] L. Shan, M. Kong, T. D. Bennet, A. C. Sarroza, C. Eastwick, D. Sun, G. Lu, Y. Yan, and H. Liu, “Studies on combustion behaviours of single biomass particles using a visualization method,” Biomass and Bioenergy, vol. 109, no. September 2017, pp. 54–60, 2018, doi: 10.1016/j.biombioe.2017.12.008.

[76] J. M. Steer, R. Marsh, D. Sexton, and M. Greenslade, “A comparison of partially burnt coal chars and the implications of their properties on the blast furnace process,” Fuel Process. Technol., vol. 176, no. March, pp. 230–239, 2018, doi: 10.1016/j.fuproc.2018.03.027.

[77] F. Ji, M. Barati, K. Coley, and G. A. Irons, “A kinetic study of carbon injection

into electric arc furnace slags," 7th Int. Conf. Molten Slags, Fluxes Salts, vol. Jonhannesb, no. January 2014, p. 1, 2004, [Online]. Available: http://www.saimm.co.za/Conferences/Slags2004/056_Ji.pdf

[78] M. P. King, F. Z. Ji, G. A. Irons, and K. S. Coley, "Kinetics of carbon reaction with electric Arc furnace slags during slag foaming," AISTech - Iron Steel Technol. Conf. Proc., vol. 1, no. February 2015, pp. 617–626, 2009.

[79] C. Gero, Schematic of Vertical tube furnace, drawn by Carbolite Gero, vol. 1. 2018, p. 86763.

[80] U. Manual, "Analytical QIC Capillary Inlet User Manual, Hiden Analytical," vol. 44, no. 0, 1925.

[81] NETZSCH, "NETZSCH STA 449 F1 Jupiter," pp. 1–9. [Online]. Available: https://d2brmtk65c6tyc.cloudfront.net/media/thermal-analysis/brochures/STA_449_F1_Jupiter_en_web.pdf?1557132264&Policy=eyJTdGF0ZW1lbnQiOlt7IlJlc291cmNlIjoiaHR0cHM6XC9cL2QyYnJtdGs2NWM2dHljLmNsb3VkZnJvbnQubmV0XC9tZWRpYVwvdGhlcm1hbC1hbmFseXNpc1wvYnJvY2h1cmVz

[82] J. Yu, J. A. Lucas, and T. F. Wall, "Formation of the structure of chars during devolatilization of pulverized coal and its thermoproperties: A review," Prog. Energy Combust. Sci., vol. 33, no. 2, pp. 135–170, 2007, doi: 10.1016/j.pecs.2006.07.003.

[83] L. Chen et al., "Gas evolution kinetics of two coal samples during rapid pyrolysis," Fuel Process. Technol., vol. 91, no. 8, pp. 848–852, 2010, doi: 10.1016/j.fuproc.2010.02.010.

[84] K. Slopiecka, P. Bartocci, and F. Fantozzi, "Thermogravimetric analysis and kinetic study of poplar wood pyrolysis," Appl. Energy, vol. 97, pp. 491–497, 2012, doi: 10.1016/j.apenergy.2011.12.056.

[85] Ľ. J. Lukáš Gašparovič, Zuzana Koreňová, "Kinetic study of wood chips decomposition by TGA," Direct, no. Slovak Society of Chemical Engineering Institute of Chemical and Environmental Engineering Slovak Universi36th International Conference of Slovak Society of Chemical Engineering, pp. 1407–1412, 2010, doi: 10.1007/s10924-010-0258-0.

[86] K. H. van Heek and W. Hodek, “Structure and pyrolysis behaviour of different coals and relevant model substances,” Fuel, vol. 73, no. 6, pp. 886–896, 1994, doi: 10.1016/0016-2361(94)90283-6.

[87] A. Anca-Couce and I. Obernberger, “Application of a detailed biomass pyrolysis kinetic scheme to hardwood and softwood torrefaction,” Fuel, vol. 167, pp. 158–167, 2016, doi: 10.1016/j.fuel.2015.11.062.

[88] K. K. Dwivedi, P. K. Chatterjee, M. K. Karmakar, and A. K. Pramanick, “Pyrolysis characteristics and kinetics of Indian low rank coal using thermogravimetric analysis,” Int. J. Coal Sci. Technol., vol. 6, no. 1, pp. 102–112, 2019, doi: 10.1007/s40789-019-0236-7.

[89] S. Ren, H. Lei, L. Wang, Q. Bu, S. Chen, and J. Wu, “Thermal behaviour and kinetic study for woody biomass torrefaction and torrefied biomass pyrolysis by TGA,” Biosyst. Eng., vol. 116, no. 4, pp. 420–426, 2013, doi: 10.1016/j.biosystemseng.2013.10.003.

[90] J. Liu, X. Jiang, J. Shen, and H. Zhang, “Pyrolysis of superfine pulverized coal. Part 1. Mechanisms of methane formation,” Energy Convers. Manag., vol. 87, pp. 1027–1038, 2014, doi: 10.1016/j.enconman.2014.07.053.

[91] D. Ferdous, A. K. Dalai, S. K. Bej, R. W. Thring, and N. N. Bakhshi, “Production of H2 and medium Btu gas via pyrolysis of lignins in a fixed-bed reactor,” Fuel Process. Technol., vol. 70, no. 1, pp. 9–26, 2001, doi: 10.1016/S0378-3820(00)00147-8.

[92] X. Yan, D. Che, and T. Xu, “Effect of rank, temperatures and inherent minerals on nitrogen emissions during coal pyrolysis in a fixed bed reactor,” Fuel Process. Technol., vol. 86, no. 7, pp. 739–756, 2005, doi: 10.1016/j.fuproc.2004.08.005.

[93] A. Heidari, R. Stahl, H. Younesi, A. Rashidi, N. Troeger, and A. A. Ghoreyshi, “Effect of process conditions on product yield and composition of fast pyrolysis of Eucalyptus grandis in fluidized bed reactor,” J. Ind. Eng. Chem., vol. 20, no. 4, pp. 2594–2602, 2014, doi: 10.1016/j.jiec.2013.10.046.

[94] X. Zhang, L. Dong, J. Zhang, Y. Tian, and G. Xu, “Coal pyrolysis in a fluidized bed reactor simulating the process conditions of coal topping in CFB boiler,” J.

Anal. Appl. Pyrolysis, vol. 91, no. 1, pp. 241–250, 2011, doi: 10.1016/j.jaap.2011.02.013.

[95] E. Biagini, F. Barontini, and L. Tognotti, “Devolatilization of biomass fuels and biomass components studied by TG/FTIR technique,” Ind. Eng. Chem. Res., vol. 45, no. 13, pp. 4486–4493, 2006, doi: 10.1021/ie0514049.

[96] R. Xu, J. Zhang, G. Wang, H. Zuo, Z. Liu, K. Jiao, Y. Liu, and K. Li, “Devolatilization Characteristics and Kinetic Analysis of Lump Coal from China COREX3000 Under High Temperature,” Metall. Mater. Trans. B Process Metall. Mater. Process. Sci., vol. 47, no. 4, pp. 2535–2548, 2016, doi: 10.1007/s11663-016-0708-8.

[97] D. Chen, D. Liu, H. Zhang, Y. Chen, and Q. Li, “Bamboo pyrolysis using TG-FTIR and a lab-scale reactor: Analysis of pyrolysis behavior, product properties, and carbon and energy yields,” Fuel, vol. 148, pp. 79–86, 2015, doi: 10.1016/j.fuel.2015.01.092.

[98] R. Bassilakis, R. M. Carangelo, and M. A. Wójtowicz, “TG-FTIR analysis of biomass pyrolysis,” Fuel, vol. 80, no. 12, pp. 1765–1786, 2001, doi: 10.1016/S0016-2361(01)00061-8.

[99] F. Han, A. Meng, Q. Li, and Y. Zhang, “Thermal decomposition and evolved gas analysis (TG-MS) of lignite coals from Southwest China,” J. Energy Inst., vol. 89, no. 1, pp. 94–100, 2016, doi: 10.1016/j.joei.2015.01.007.

[100] X. Li, G. Matuschek, M. Herrera, H. Wang, and A. Kettrup, “Investigation of pyrolysis of Chinese coals using thermal analysis/mass spectrometry,” J. Therm. Anal. Calorim., vol. 71, no. 2, pp. 601–612, 2003, doi: 10.1016/s0140-6701(04)90448-1.

[101] A. Arenillas, F. Rubiera, and J. J. Pis, “Simultaneous thermogravimetric-mass spectrometric study on the pyrolysis behaviour of different rank coals,” J. Anal. Appl. Pyrolysis, vol. 50, no. 1, pp. 31–46, 1999, doi: 10.1016/S0165-2370(99)00024-8.

[102] J. Wannapeera, B. Fungtammasan, and N. Worasuwannarak, “Effects of temperature and holding time during torrefaction on the pyrolysis behaviors of woody biomass,” J. Anal. Appl. Pyrolysis, vol. 92, no. 1, pp. 99–105, 2011, doi:

10.1016/j.jaap.2011.04.010.

[103] K. Jayaraman, M. V. Kok, and I. Gokalp, “Thermogravimetric and mass spectrometric (TG-MS) analysis and kinetics of coal-biomass blends,” Renew. Energy, vol. 101, pp. 293–300, 2017, doi: 10.1016/j.renene.2016.08.072.

[104] A. A. El-Tawil, L. S. Ökvist, H. M. Ahmed, and B. Björkman, “Devolatilization kinetics of different types of bio-coals using thermogravimetric analysis,” Metals (Basel)., vol. 9, no. 2, pp. 1–13, 2019, doi: 10.3390/met9020168.

[105] Y. Qiao, S. Chen, Y. Liu, H. Sun, S. Jia, J. Shi, C. M. Pedersen, Y. Wang, and X. Hou, “Pyrolysis of chitin biomass: TG-MS analysis and solid char residue characterization,” Carbohydr. Polym., vol. 133, pp. 163–170, 2015, doi: 10.1016/j.carbpol.2015.07.005.

[106] P. G. and P. G. R. Ramesh C. Borah, “A review on devolatilization of coal in fluidized bed,” Int. J. energy Res., vol. 31, no. August 2011, pp. 929–963, 2011, doi: 10.1002/er.

[107] H. Yang, R. Yan, H. Chen, C. Zheng, D. H. Lee, and D. T. Liang, “In-depth investigation of biomass pyrolysis based on three major components: Hemicellulose, cellulose and lignin,” Energy and Fuels, vol. 20, no. 1, pp. 388–393, 2006, doi: 10.1021/ef0580117.

[108] H. Yang, R. Yan, H. Chen, D. H. Lee, and C. Zheng, “Characteristics of hemicellulose, cellulose and lignin pyrolysis,” Fuel, vol. 86, no. 12–13, pp. 1781–1788, 2007, doi: 10.1016/j.fuel.2006.12.013.

[109] Q. Zhu, “Coal sampling and analysis standards,” IEA Clean Coal Cent., no. 2014, p. 123, 2010, [Online]. Available: https://www.usea.org/sites/default/files/042014_Coal sampling and analysis standards_ccc235.pdf

[110] K. Werner, L. Pommer, and M. Broström, “Thermal decomposition of hemicelluloses,” J. Anal. Appl. Pyrolysis, vol. 110, no. 1, pp. 130–137, 2014, doi: 10.1016/j.jaap.2014.08.013.

[111] H. Yang, R. Yan, H. Chen, D. H. Lee, D. T. Liang, and C. Zheng, “Mechanism of palm oil waste pyrolysis in a packed bed,” Energy and Fuels, vol. 20, no. 3, pp. 1321–1328, 2006, doi: 10.1021/ef0600311.

[112] M. M. Halmann, Chemical Fixation of Carbon DioxideMethods for Recycling CO2 into Useful Products. 2018. doi: 10.1201/9781315139098.

[113] A. Basile, G. Centi, M. De Falco, and G. Iaquaniello, “The vision of future sustainable energy, catalyst, and chemistry: Opportunities for innovation and business,” Studies in Surface Science and Catalysis. 2019. doi: 10.1016/B978-0-444-64337-7.00001-X.

[114] H. E. K. In, “Variation of peak temperature with heating rate in differential thermal analysis,” J. 0 f Res. Natl. Bur. Stand., vol. 57, no. 4, p. 2712, 2012, doi: 10.1002/9781119959809.ch9.

[115] Y. C. Bin-Hang Yan, Chen-Xi Cao, Yan Cheng, Yong Jin, “Experimental investigation on coal devolatilization at high temperatures with different heating rates,” Fuel, vol. 117, no. PARTB, pp. 1215–1222, 2014, doi: 10.1016/j.fuel.2013.08.016.

[116] Y. Qu, Experimental Study of the Melting and Reduction Behaviour of Ore Used in the HIsarna Process PhD thesis Yingxia Qu. 2013.

[117] Z. Chen, Y. Qu, C. Zeilstra, J. van der Stel, J. Sietsma, and Y. Yang, “Thermodynamic evaluation for reduction of iron oxide ore particles in a high temperature drop tube furnace,” Ironmak. Steelmak., vol. 47, no. 2, pp. 173–177, 2020, doi: 10.1080/03019233.2018.1498762.

[118] Y. Qu, Y. Yang, Z. Zou, C. Zeilstra, K. Meijer, and R. Boom, “Melting and reduction behaviour of individual fine hematite ore particles,” ISIJ Int., vol. 55, no. 1, pp. 149–157, 2015, doi: 10.2355/isijinternational.55.149.

[119] G. Di Nola, W. de Jong, and H. Spliethoff, “The fate of main gaseous and nitrogen species during fast heating rate devolatilization of coal and secondary fuels using a heated wire mesh reactor,” Fuel Process. Technol., vol. 90, no. 3, pp. 388–395, 2009, doi: 10.1016/j.fuproc.2008.10.009.

[120] E. Biagini, P. Narducci, and L. Tognotti, “Size and structural characterization of lignin-cellulosic fuels after the rapid devolatilization,” Fuel, vol. 87, no. 2, pp. 177–186, 2008, doi: 10.1016/j.fuel.2007.04.010.

[121] J. Li, G. Bonvicini, L. Tognotti, W. Yang, and W. Blasiak, “High-temperature rapid devolatilization of biomasses with varying degrees of torrefaction,” Fuel,

vol. 122, pp. 261–269, 2014, doi: 10.1016/j.fuel.2014.01.012.

[122] S. F. Zhang, F. Zhu, G. Bai, L. Y. Wen, and H. J. Peng, “High temperature pyrolysis behaviour and kinetics of lump coal in COREX melter gasifier,” Ironmak. Steelmak., vol. 41, no. 3, pp. 219–228, 2014, doi: 10.1179/1743281213Y.0000000122.

[123] W. H. Chen, S. W. Du, and T. H. Yang, “Volatile release and particle formation characteristics of injected pulverized coal in blast furnaces,” Energy Convers. Manag., vol. 48, no. 7, pp. 2025–2033, 2007, doi: 10.1016/j.enconman.2007.01.001.

[124] G. Wang, J. Zhang, G. Zhang, X. Ning, X. Li, Z. Liu, and J. Guo, “Experimental and kinetic studies on co-gasification of petroleum coke and biomass char blends,” Energy, vol. 131, pp. 27–40, 2017, doi: 10.1016/j.energy.2017.05.023.

[125] D. Khasraw, S. Spooner, H. Hage, K. Meijer, and Z. Li, “Devolatilisation characteristics of coal and biomass with respect to temperature and heating rate foontent along with two biomass samples sourcr HIsarna alternative ironmaking process,” Fuel, vol. 284, no. July 2020, p. 119101, 2021, doi: 10.1016/j.fuel.2020.119101.

[126] V. Krishnamoorthy, Y. D. Yeboah, and S. V. Pisupati, “Influence of pyrolysis gas on volatile yield and co 2 reaction kinetics of the char samples generated in a high-pressure, high-temperature flow reactor,” Energies, vol. 12, no. 1, 2019, doi: 10.3390/en12010107.

[127] X. Huang, D. Kocaefe, and Y. Kocaefe, “Utilization of Biocoke as a Raw Material for Carbon Anode Production,” Energy and Fuels, vol. 32, no. 8, pp. 8537–8544, 2018, doi: 10.1021/acs.energyfuels.8b01832.

[128] G. Wang, J. Zhang, X. Hou, J. Shao, and W. Geng, “Study on CO2 gasification properties and kinetics of biomass chars and anthracite char,” Bioresour. Technol., vol. 177, pp. 66–73, 2015, doi: 10.1016/j.biortech.2014.11.063.

[129] A. Abánades, C. Rubbia, and D. Salmieri, “Thermal cracking of methane into Hydrogen for a CO2-free utilization of natural gas,” Int. J. Hydrogen Energy, vol. 38, no. 20, pp. 8491–8496, 2013, doi: 10.1016/j.ijhydene.2012.08.138.

[130] M. Fraga, B. Flores, E. Osório, and A. Vilela, “Evaluation of the thermoplastic

behavior of charcoal, coal tar and coking coal blends," J. Mater. Res. Technol., vol. 9, no. 3, pp. 3406–3410, 2020, doi: 10.1016/j.jmrt.2020.01.076.

[131] J. Wu, Q. Liu, R. Wang, W. He, L. Shi, X. Guo, Z. Chen, L. Ji, and Z. Liu, "Coke formation during thermal reaction of tar from pyrolysis of a subbituminous coal," Fuel Process. Technol., 2017, doi: 10.1016/j.fuproc.2016.03.022.

[132] J. Leppälahti and T. Koljonen, "Nitrogen evolution from coal, peat and wood during gasification: Literature review," Fuel Process. Technol., vol. 43, no. 1, pp. 1–45, 1995, doi: 10.1016/0378-3820(94)00123-B.

[133] E. Biagini, A. Fantei, and L. Tognotti, "Effect of the heating rate on the devolatilization of biomass residues," Thermochim. Acta, vol. 472, no. 1–2, pp. 55–63, 2008, doi: 10.1016/j.tca.2008.03.015.

[134] J. K. Wright and B. R. Baldock, "Dissolution kinetics of particulate graphite injected into iron/carbon melts," Metall. Trans. B, vol. 19, no. 2, pp. 375–382, 1988, doi: 10.1007/BF02657735.

[135] R. Khanna, F. McCarthy, H. Sun, N. Simento, and V. Sahajwalla, "Dissolution of carbon from coal-chars into liquid iron at 1550°C," Metall. Mater. Trans. B Process Metall. Mater. Process. Sci., vol. 36, no. 6, pp. 719–729, 2005, doi: 10.1007/s11663-005-0075-3.

[136] S. Tsuey Cham, "Investigating Factors that Influence Carbon Dissolution from Coke into Molten Iron," no. February, 2007, [Online]. Available: internal-pdf:/S. Tsuey Cham_02whole_encrpt.pdf

[137] E. Biagini, S. Pintus, and L. Tognotti, "Characterization of high heating-rate chars from alternative fuels using an electrodynamic balance," Proc. Combust. Inst., vol. 30 II, no. 2, pp. 2205–2212, 2005, doi: 10.1016/j.proci.2004.07.005.

[138] A. Smolínski and N. Howaniec, "Analysis of porous structure parameters of biomass chars versus bituminous coal and lignite carbonized at high pressure and temperature-A chemometric study," Energies, vol. 10, no. 10, pp. 28–30, 2017, doi: 10.3390/en10101457.

[139] O. Karlström, A. Brink, E. Biagini, M. Hupa, and L. Tognotti, "Comparing reaction orders of anthracite chars with bituminous coal chars at high

temperature oxidation conditions," Proc. Combust. Inst., vol. 34, no. 2, pp. 2427–2434, 2013, doi: 10.1016/j.proci.2012.07.011.

[140] G. Newalkar, K. Iisa, A. D. Damico, C. Sievers, and P. Agrawal, "Effect of temperature, pressure, and residence time on pyrolysis of pine in an entrained flow reactor," Energy and Fuels, vol. 28, no. 8, pp. 5144–5157, 2014, doi: 10.1021/ef5009715.

[141] Z. H. Wang, K. Zhang, Y. Li, Y. He, M. Kuang, Q. Li, and K. F. Cen, "Gasification characteristics of different rank coals at H2O and CO2 atmospheres," J. Anal. Appl. Pyrolysis, vol. 122, pp. 76–83, 2016, doi: 10.1016/j.jaap.2016.10.019.

[142] S. Dong, P. Alvarez, N. Paterson, D. R. Dugwell, and R. Kandiyoti, "Study on the effect of heat treatment and gasification on the carbon structure of coal chars and metallurgical cokes using fourier transform raman spectroscopy," Energy and Fuels, vol. 23, no. 3, pp. 1651–1661, 2009, doi: 10.1021/ef800961g.

[143] T. J. Morgan, S. Q. Turn, A. George, and J. Aburto, "Fast pyrolysis behavior of banagrass as a function of temperature and volatiles residence time in a fluidized bed reactor," PLoS One, vol. 10, no. 8, 2015, doi: 10.1371/journal.pone.0136511.

[144] M. Thommes, K. Kaneko, A. V. Neimark, J. P. Olivier, F. Rodriguez-Reinoso, J. Rouquerol, and K. S. W. Sing, "Physisorption of gases, with special reference to the evaluation of surface area and pore size distribution (IUPAC Technical Report)," Pure Appl. Chem., vol. 87, no. 9–10, pp. 1051–1069, 2015, doi: 10.1515/pac-2014-1117.

[145] V. Gargiulo, A. Gomis-Berenguer, P. Giudicianni, C. O. Ania, R. Ragucci, and M. Alfè, "Assessing the Potential of Biochars Prepared by Steam-Assisted Slow Pyrolysis for CO2 Adsorption and Separation," Energy and Fuels, vol. 32, no. 10, pp. 10218–10227, 2018, doi: 10.1021/acs.energyfuels.8b01058.

[146] N. I. A. Ghani, N. Y. M. Yusuf, W. N. R. W. Isahak, and M. S. Masdar, "Modification of activated carbon from biomass nypa and amine functional groups as carbon dioxide adsorbent," J. Phys. Sci., vol. 28, no. February, pp. 227–240, 2017, doi: 10.21315/jps2017.28.s1.15.

[147] T. Theint, Z. Yan, S. Spooner, V. Degirmenci, and K. Meijer, “Gasification and physical-chemical characteristics of carbonaceous materials in relation to HIsarna ironmaking process,” Fuel, vol. 289, no. November 2020, p. 119890, 2021, doi: 10.1016/j.fuel.2020.119890.

[148] Z. Wang, Y. Cheng, Y. Qi, R. Wang, L. Wang, and J. Jiang, “Experimental study of pore structure and fractal characteristics of pulverized intact coal and tectonic coal by low temperature nitrogen adsorption,” Powder Technol., vol. 350, pp. 15–25, 2019, doi: 10.1016/j.powtec.2019.03.030.

[149] Y. Sun, Y. Han, P. Gao, X. Wei, and G. Li, “Thermogravimetric study of coal-based reduction of oolitic iron ore: Kinetics and mechanisms,” Int. J. Miner. Process., vol. 143, pp. 87–97, 2015, doi: 10.1016/j.minpro.2015.09.005.

[150] H. Sun and W. Easman, “Interfacial phenomena and reaction kinetics between the carbon and slag in the ironmaking process,” Energy and Fuels, vol. 21, no. 2, pp. 413–418, 2007, doi: 10.1021/ef060402d.

[151] D. Khasraw, T. Theint, X. Yang, V. Degirmenci, H. Hage, and K. Meijer, “Gasification and structural behaviour of different carbon sources and resultant chars from rapid devolatilization for HIsarna alternative ironmaking process Abstract :,” Fuel, vol. 309, no. September 2021, p. 122210, 2021, doi: 10.1016/j.fuel.2021.122210.

[152] L. Zhang, Y. Zhu, W. Yin, B. Guo, F. Rao, and J. Ku, “Isothermal Coal-Based Reduction Kinetics of Fayalite in Copper Slag,” ACS Omega, vol. 5, no. 15, pp. 8605–8612, 2020, doi: 10.1021/acsomega.9b04497.

[153] C. F. Dickinson and G. R. Heal, “A review of the ICTAC Kinetics Project, 2000. Part 1. Isothermal results,” Thermochim. Acta, vol. 494, no. 1–2, pp. 1–14, 2009, doi: 10.1016/j.tca.2009.05.003.

[154] Y. S. Sun, Y. X. Han, P. Gao, and G. F. Li, “Investigation of kinetics of coal based reduction of oolitic iron ore,” Ironmak. Steelmak., vol. 41, no. 10, pp. 763–768, 2014, doi: 10.1179/1743281214Y.0000000196.

[155] Y. Zhang, J. Zhao, X. Ma, M. Li, Y. Lv, and X. Gao, “Isothermal reduction kinetics and mechanism of pre-oxidized ilmenite,” Min. Eng., vol. 71, no. 9, pp. 53–54, 2019.

[156] Y. D. Wang, X. N. Hua, C. C. Zhao, T. T. Fu, W. Li, and W. Wang, “Step-wise reduction kinetics of Fe2O3 by CO/CO2 mixtures for chemical looping hydrogen generation,” Int. J. Hydrogen Energy, vol. 42, no. 9, pp. 5667–5675, 2017, doi: 10.1016/j.ijhydene.2017.01.159.

[157] A. Khawam and D. R. Flanagan, “Solid-state kinetic models: Basics and mathematical fundamentals,” J. Phys. Chem. B, vol. 110, no. 35, pp. 17315–17328, 2006, doi: 10.1021/jp062746a.

[158] Y. Man, J. X. Feng, F. J. Li, Q. Ge, Y. M. Chen, and J. Z. Zhou, “Influence of temperature and time on reduction behavior in iron ore-coal composite pellets,” Powder Technol., vol. 256, pp. 361–366, 2014, doi: 10.1016/j.powtec.2014.02.039.

[159] W. Lv, X. Lv, Y. Zhang, S. Li, K. Tang, and B. Song, “Isothermal oxidation kinetics of ilmenite concentrate powder from Panzhihua in air,” Powder Technol., vol. 320, no. May 2018, pp. 239–248, 2017, doi: 10.1016/j.powtec.2017.07.058.

[160] C. Li, X. Lv, J. Chen, X. Liu, and C. Bai, “Kinetics of titanium nitride synthesized with Ti and N2,” Int. J. Refract. Met. Hard Mater., vol. 52, pp. 165–170, 2015, doi: 10.1016/j.ijrmhm.2015.06.009.

[161] R. Vanparys, G. Brooks, M. A. Rhamdhani, and T. Crivits, “Slag-Coke Interactions in the Lead Blast Furnace,” Proc. EMC 2019, no. July, pp. 181–196, 2019.